

Deformability of Shredded Tires



Minnesota Local Road
Research Board

Research

FUNDING ACKNOWLEDGEMENT

This project was conducted with funding provided by the Minnesota Local Road Research Board (LRRB). The LRRB's purpose is to develop and manage a program of research for county and municipal state aid road improvements. Funding for LRRB research projects comes from a designated fund equivalent to $\frac{1}{2}$ of one percent of the annual state aid for county and city roads.

Technical Report Documentation Page

1. Report No. MN/RC - 1999-13	2.	3. Recipient's Accession No.	
4. Title and Subtitle DEFORMABILITY OF SHREDDED TIRES		5. Report Date January 1999	
		6.	
7. Author(s) Andrew Drescher David Newcomb Thor Heimdahl		8. Performing Organization Report No.	
9. Performing Organization Name and Address University of Minnesota Department of Civil Engineering 500 Pillsbury Drive, S.E. Minneapolis, MN 55455		10. Project/Task/Work Unit No.	
		11. Contract (C) or Grant (G) No. (C) 73595 TOC # 190	
12. Sponsoring Organization Name and Address Minnesota Department of Transportation 395 John Ireland Boulevard Mail Stop 330 St. Paul, Minnesota 55155		13. Type of Report and Period Covered Final Report - 1996 -1998	
		14. Sponsoring Agency Code	
15. Supplementary Notes			
16. Abstract (Limit: 200 words) This report describes three separate studies that examine the deformability of shredded tire fill material: <ul style="list-style-type: none"> ▪ The first study determined the response of shredded tires to cyclic loading. These tests were conducted in a load frame on both constrained and unconstrained samples and showed that the material became stiffer with increasing load. ▪ The second study focused on the long-term creep settlements of constrained and unconstrained samples. The results indicate that creep exists for a period of up to two years after loading. ▪ The third study investigated the possible anisotropic properties of the material. A larger modulus of elasticity was found in directions parallel to the layers than in the direction perpendicular to the layers. However, settlements computed using a representative anisotropic shredded tire fill material indicate that the current settlement analysis, based on isotropic shredded tire layers, predicts maximum settlements conservatively. 			
17. Document Analysis/Descriptors anisotropy shredded tires		18. Availability Statement No restrictions. Document available from: National Technical Information Services, Springfield, Virginia 22161	
19. Security Class (this report)	20. Security Class (this page)	21. No. of Pages	22. Price
Unclassified	Unclassified	145	

DEFORMABILITY OF SHREDDED TIRES

Final Report

Prepared by

Andrew Drescher
David Newcomb
Thor Heimdahl

University of Minnesota
Department of Civil Engineering
122 CivE Building
500 Pillsbury Dr. S.E.
Minneapolis, MN 55455-0220

January 1999

Published by

Minnesota Department of Transportation
Office of Research Services
First Floor
395 John Ireland Boulevard, MS 330
St. Paul, Minnesota 55155

The contents of this report reflect the views of the authors who are responsible for the facts and accuracy of the data presented herein. The contents do not necessarily reflect the views or policies of the Minnesota Department of Transportation at the time of publication. This report does not constitute a standard, specification, or regulation.

CONTENTS

CHAPTER 1 - INTRODUCTION

Background and Literature Review	1
Engineering Properties of Shredded tires	5
Aim and Scope	9

CHAPTER 2 - SHREDDED TIRES CHARACTERIZATION

Source of Shredded Tires	13
Geometric Characterization	15
Physical Characterization	21

CHAPTER 3 - BEHAVIOR UNDER REPEATED LOAD

Introduction	23
Testing Apparatus	25
Material and Test Program	27
Test Results	32
Analysis of Results	49

CHAPTER 4 - BEHAVIOR UNDER CONSTANT LOAD

Introduction	59
Testing Apparatus	60

Material and Test Program	65
Test Results	67
Application of Results	77
CHAPTER 5 - ANISOTROPIC PROPERTIES	
Introduction	83
Testing Apparatus	85
Material and Test Program	94
Test Results	99
Application of Results	116
CHAPTER 6 - CONCLUSIONS	127
- RECOMMENDATIONS	131
REFERENCES	133

LIST OF FIGURES

Schematics of subgrade shredded tire fill on the Esker Trail Project	4
Shredded tire pieces	14
Measurements for grain-size analysis	16
Grain-size distribution according to dimensions	18
Distribution according to aspect ratio	19
Cross-section of a tire	20
Repeated load experiments	24
MTS load frame setup	26
Vertical stresses in a shredded tire fill	30
Stress-strain curves for first load cycle	37
Stress-strain curves for slow and fast loading rates – Constrained	38
Stress-strain curves for slow and fast loading rates – Unconstrained	39
Stress-strain curve for constrained compression	40
Accumulated plastic strain per cycle, constrained case	42
Unconstrained compression	43
Accumulated plastic strain per cycle	44
Schematic of loading, unloading, and reloading subsets	46
Loading subset for constrained compression tests	47
Loading subset for unconstrained compression tests	48
Plots of constant strain, loading subset, constrained case	50
Stress vs. sample ht., loading subset, constrained case	51

Master curve for loading subset, constrained case	52
Plots of constant strain, loading subset, unconstrained case	53
Stress vs. sample ht., loading subset, unconstrained case	54
Master curve for loading subset, unconstrained case	56
Complete master curve for constrained compression test	57
Complete master curve for unconstrained compression test	58
Creep test loading system schematics	61
Apparatus for constrained compression tests	63
Apparatus for unconstrained compression tests	64
Load cell	66
Strain versus time (time referenced to time of load application)	70
Strain versus time (time referenced to one day after loading)	72
Strain versus time – Log plot - Constrained test (time referenced to one day after loading)	74
Strain versus time – Log plot - Unconstrained test (time referenced to one day after loading)	75
Strain-rate vs. time for 30-day intervals	76
Stress distribution in embankment	78
Strain-rate as a function of stress for material in center of embankment	80
Flattening of shredded tire pieces	84
Overlapping layers in shredded tire material	84
Plywood	86
Layered material	86

Schematic of Biaxial Apparatus	88
Biaxial Apparatus Schematic	90
Bar/gap-stacked arrangement	90
Bar/gap-stacked arrangement: intersection of moving walls and frame	92
Stacking shredded tire pieces with alternating curvature	95
Target stress path for test with vertical compaction	98
Stress paths from typical anisotropy test	107
Vertical stress versus vertical strain	108
Horizontal stress versus horizontal strain	109
Vertical stress versus horizontal stress	110
Test-cases	117
Settlement as a function of G'	122
Settlement isolines – vertical component of displacement	124

LIST OF TABLES

Properties of Shredded Tire Material	22
Repeated Load Test Matrix	28
Creep Test Matrix	68-69
Application of Results Summary	81
Biaxial Loading/Unloading Test Matrix	100
Experimental Anisotropic Parameters	111
Elastic Constants	115
Material and Layer Characteristics for Study Cases	118
Results of Settlement Analysis, Anisotropic Material	120
Results of Settlement Analysis, Isotropic Material	123

EXECUTIVE SUMMARY

Shredded tires have been successfully used as a lightweight subgrade fill in many civil engineering applications. When replacing conventional fill in road and underground construction, shredded tire material has been shown to reduce problems arising from overburden stress and capillary rise.

Compressibility, shear strength, permeability, and short-term creep characteristics of shredded tires have been investigated in the past. This report describes the research conducted at the University of Minnesota, where three separate studies on shredded tire material were completed. In the first study, tests to determine the response of shredded tires to cyclic loading were conducted in a load frame on both constrained and unconstrained samples. Non-linear behavior was observed, such that the material became stiffer with increasing load. The second study focused on long-term creep settlements of shredded tires. Constrained and unconstrained samples were subjected to constant load for several months, and results indicate that creep occurs up to two years of loading. Shredded tires were examined for possible anisotropy in the third study, where large-size pieces were stacked in overlapping layers and loaded in two directions. It was found that the modulus of the material is higher in directions parallel to the layers than in the direction perpendicular to the layers. A numerical code was used to compute settlements of a representative anisotropic shredded tire fill, and compare them to settlements of a fill regarded as isotropic. Results imply that the current settlement analysis, which is based on isotropic shredded tire layers, predicts maximum settlements conservatively.

CHAPTER 1

INTRODUCTION

BACKGROUND AND LITERATURE REVIEW

There are more than 2 billion scrap tires stockpiled in the United States, and each year another 240 million tires are discarded nationwide (NAPA, 1993). The storage of these tires is undesirable for many reasons. Exposed scrap tire stockpiles are unsightly, and they tend to resurface if buried under a thin layer of soil (Manion and Humphrey, 1992). Also, fires that start in piles of tires are difficult to extinguish. Furthermore, mosquitoes flourish in water trapped in the inner portions of the tires, posing the threat of encephalitis (Manion and Humphrey, 1992).

The reuse and disposal of scrap tires has taken many forms. With a heating value of 15,000 Btu per pound, better than for most coals, the rubber from tires is burned as fuel in places such as electric utility boilers and cement kilns, making tires a good energy source (NAPA, 1993). This action is a means of disposal, however, and the valuable durability properties for which the tires are designed are not recovered.

Scrap tires are also used in the production of paving material called rubber modified asphalt. The hot mix of this asphalt includes shredded tire material in the form of crumb rubber modifier (CRM), which consists of rubber pieces 1 mm (0.04 in.) in size or less (NAPA, 1993). Typically, 8.9 kN (1 ton) of hot rubber modified asphalt mix contains about 89 N (20 lbs.) of crumb rubber.

A third use for scrap tires is in civil engineering applications. In California, whole tires were stacked to form retaining walls to reinforce a highway shoulder and an embankment subject to soil erosion (NAPA, 1993). A Minnesota forest road built over weak organic deposits was upgraded by placing a soil cover over tire mats that were formed by tying whole tires together. Settlement was “significantly lower than that expected on conventional road sections” (Drescher and Newcomb, 1994). However, tying the mats together was highly labor-intensive.

In more recent civil engineering applications, tires were shredded into smaller pieces and the resulting bulk material was used as subgrade fill, replacing heavier conventional fill material such as gravel. Vertical stresses in fills are thereby reduced. In a highway embankment in southern Oregon, an ancient landslide was re-mobilized after the embankment was raised and widened as part of an improvement project (Read, et al, 1991). To decrease load on the embankment, and to reduce slide movement, 580,000 shredded tires were used as subgrade fill in place of existing soil. Subsequent observation and testing indicates that the embankment is performing adequately. Upton et al. (1992), commenting on the condition of the above road, stated that “tests indicate the pavement section over the shredded tire fill meets 20-year design life criteria [for pavements]”, demonstrating the integrity of roads constructed over shredded tire fills. Edil and Bosscher (1992) reported similar findings for a test embankment in Wisconsin that was constructed using sand/gravel and shredded tire layers of varying thickness, and subjected to low-volume truck traffic for several months. The predicted design life of asphalt

concrete paved sections, were they placed over the shredded tire embankment, was 12-13 years.

Another example of slope stabilization is given by the construction of a subgrade fill for a highway exit ramp embankment in Minnesota, which included the placement of an estimated one million shredded scrap tires to depths of up to 4.6 m (15 ft.) (NAPA, 1993). At this site, a weak layer of plastic silty loam beneath 7.6 m (25 feet) of conventional fill was causing instability of the embankment in the form of a rotational failure. Were shredded tires not used, the excavation of an additional 10 m (33 feet) of material would have been necessary to stabilize the slope from further damage, a more costly alternative. This illustrates that the use of shredded tires in civil engineering applications may be an economical method of controlling the number of stockpiled scrap tires. In the same project, a concrete pavement was placed over the fill, and has performed well over a period of several years [B. Nelson, personal communication, Feb. 26, 1998], showing the potential use of rigid pavements for low-volume roads.

Besides increasing slope stability, the use of shredded tires in subgrade fills reduces settlements over soft soil. This is evidenced by Minnesota's Esker Trail project, where the settlements resulting from the placement of light shredded tire material over a layer of peat 1.5 m (5 ft.) deep were approximately 40 – 50% less than what was anticipated with heavier granular subgrade (Drescher and Newcomb, 1994). Figure 1.1 depicts the Esker Trail fill schematically, and shows how a common shredded tire fill is layered.

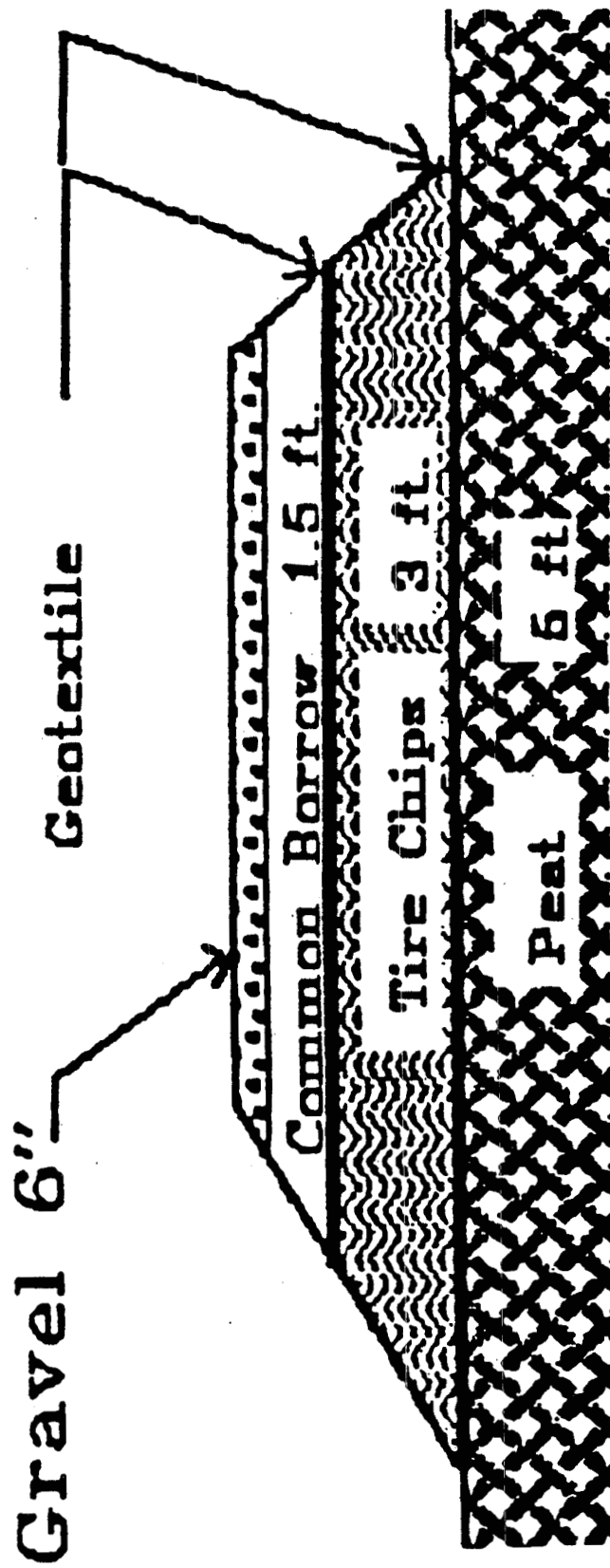


Fig. 1.1. Schematic of subgrade shredded tire fill on the Esker Trail Project

Replacing conventional subgrade fill material with lightweight shredded tires may also result in the decrease of lateral pressure on retaining walls and bridge abutments (Humphrey and Sandford, 1993; Soupir, 1998), yet another possible advantage of using the material.

In addition to providing benefits related to the decrease of vertical stresses in fills, the use of shredded tires in road construction has been shown to reduce capillary rise, thereby providing resistance against frost heave occurring in cold weather climates. This would prolong the life of gravel- or asphalt-surfaced roads. (Humphrey and Nickels, 1994).

ENGINEERING PROPERTIES OF SHREDDED TIRES

The results of past research have provided estimates for several engineering properties of shredded tire material. Newcomb and Drescher (1994) have reported the bulk unit weight of small-size (30 mm mean size) shredded tire pieces to be 4.9 kN/m^3 (31 pcf). Unit weights in other studies ranged from 3.1 to 5.2 kN/m^3 (20 pcf to 33 pcf) for uncompacted shredded tire material and from 5.3 to 7.4 kN/m^3 (34 to 47 pcf) for compacted material (Humphrey et al., 1992; NAPA, 1993). This implies that conventional granular fill has a bulk unit weight about 3 times that of shredded tires (Das, 1995), demonstrating the lightweight properties of shredded tires when used in a fill. Also, by comparison, the unit weight of water is 9.81 kN/m^3 (62.4 pcf), about twice the value for shredded tires.

Within the study by Newcomb and Drescher (1994), a specific gravity of 1.08 was found for the small-size tire pieces. The corresponding porosity was 57% and thus the void ratio was 1.32. Large-size pieces had a lower density, and therefore a higher porosity and void ratio.

The compressibility of shredded tire material has been extensively studied. Tests were performed by Edil and Bosscher (1992) in which material 50-75 mm (2-3 in.) in size was placed in a 152-mm (6 in.) diameter cylindrical mold and subjected to compression along the axis of the mold. A typical sample had an initial porosity of about 67% and a unit weight of approximately 4 kN/m^3 (25.5 lb/ft^3). Under a 690 kPa (100 psi) stress, the porosity was about 50% and the sample had compressed 36% of its original height. Edil and Bosscher also demonstrated that by mixing 40% sand by weight in a shredded tire material matrix, compression was reduced by as much as 50%. They found that pure sand compressed about one seventh as much as pure shredded tires. Humphrey et al. (1992) conducted similar one-dimensional compression tests on compacted samples with pieces 25 to 38 mm (1 to 1.5 in.) in size. Test results indicated average vertical strains of 26.5% and 39.5% at vertical stresses of 69 kPa (10 psi) and 276 kPa (40 psi), respectively.

Newcomb and Drescher (1994) calculated a value of Young's modulus for shredded tire material based on experimental constrained modulus and coefficient of lateral earth pressure values from tests on laterally-constrained samples. For pieces 50 mm (2 in.) in size, an average Young's modulus of 780 kPa (113 psi) was determined for the reloading region for material under repeated load (stress at ultimate load was about

400kPa (58 psi)). The value for wood chips in that study was about 100 times greater. In triaxial compression tests, Wu et al. (1997) found Young's modulus of shredded tires to range from 580 to 690 kPa (84 to 100 psi) for shredded tires 1.5 in. in size.

As an illustration of the compressibility characteristics of shredded tires in an applied use, a field study on the settlement of an Oregon shredded tire fill revealed that a compacted layer of shredded tires 3.8 m (12.5 ft.) thick settled approximately 46 cm (18 in.) during the placement of 91 cm (36 in.) of soil cap and 58 cm (23 in.) of aggregate base. The layer settled another 5.1 cm (2 in.) during 3 months of traffic and due to the placement of 15 cm (6 in.) of asphalt concrete (Read, et al, 1991).

In an experiment by Edil and Bosscher (1992) to determine a Poisson's ratio value for shredded tires, a compacted sample of shredded tires was enclosed in a cylindrical PVC membrane that was split into four identical panels by making cuts parallel to the axis of the cylinder. The panels were joined at the cuts by a number of latex strips that allowed the cylinder form to expand easily while retaining its prismatic shape. Due to the small amount of confinement, it was assumed that by subjecting the sample to axial load, the material was under uniaxial compression. To calculate Poisson's ratio of the material, lateral expansion was measured and compared to axial strain. With axial loading of the cylindrical mold up to a stress level of up to 18.1 kPa (2.63 psi), Poisson's ratio was found to be 0.27 for the initial loading, 0.3 for the second cycle of loading, and 0.17 for the third cycle of loading. Manion and Humphrey (1992) performed one-dimensional compression tests on compacted shredded tire material that was about 25 to 38 mm (1 to 1.5 in.) in dimension and confined in PVC pipe 30 cm (12 in.) in

diameter. By finding hoop stresses acting in the cylinder, they calculated a coefficient of lateral earth pressure of $K = 0.44$ for vertical stresses less than 159 kPa (23 psi). Using the expression

$$v = \frac{K}{1 + K} \quad (1.1)$$

an average Poisson's ratio of 0.3 was calculated for the same stress range. In similar tests, Drescher and Newcomb (1994) reported an average K value of 0.4 for vertical stresses below about 172 kPa (25 psi). Using (1.1), this gives a Poisson's ratio of 0.29 for the same stress range.

Humphrey et al. (1992) investigated the time dependent settlement, or creep, of shredded tires in laboratory tests. Material 25 to 38 mm (1 to 1.5 in.) in size was placed in a laterally constraining cylinder and subjected to a constant vertical stress of 1.0 kPa (7.0 psi) for a period of about one month. The vertical strain occurring between 1 and 31 days after loading was about 1%, indicating that the viscoelastic properties of the material would have an effect on settlements of a fill.

Tests to determine the shear strength of shredded tire material were performed by Humphrey and Sandford (1993) on pieces that were 76 mm (3 in.) or less in dimension. Using a direct shear apparatus, an angle of friction of about 23° was found and the cohesion of the material was about 55 kPa (8 psi). Wu et al. (1997) reported significantly higher friction angles from the results of triaxial compression tests, with values ranging from 45° to 60° . Five sizes of pieces were tested, with maximum size tire shreds ranging

from 2 mm to 38 mm for the different sizes, and no correlation between size and friction angle was found.

In tests by Humphrey et al. (1992), a constant head apparatus was used to determine the permeability of shredded tire material. For samples that had been compressed to less than 80% of their original height, the permeability coefficient was about 3 cm/s (1.2 in./s). This is a value comparable with that found for clean gravel or coarse sand (Das, 1994), demonstrating the desirable drainage characteristics of the material. Edil and Bosscher (1992) reported that the coefficient of permeability of 50 mm (4 in.) pieces in tests was about 0.5 cm/s for axial stresses up to 103 kPa (15 psi). This value was reduced to about 0.1 cm/s with the inclusion of 30% sand by weight.

AIM AND SCOPE

Since the relatively high compressibility of shredded tires is a concern in the construction of subgrade fills, many laboratory tests have been aimed at determining the response of the material to cyclic loading (Edil and Bosscher, 1992; Humphrey et al., 1992; Newcomb and Drescher, 1994). However, the vertical stresses used in these tests are beyond those found in actual shredded tire fills. The behavior of the material may be different if it is loaded within a lower range of stresses. Also, in previous cyclic loading tests, most shredded tire specimens were confined laterally by a rigid container. No direct comparison was made between the behavior of material that is laterally constrained and material that is laterally unconstrained. To further investigate the response of shredded tire material to repeated load, and to present results for a more suitable range of stresses,

cyclic loading tests were conducted at the University of Minnesota. Using a load frame, samples of small-size (50 mm) shredded tires were subjected to load in both confined and unconfined conditions, and differences in resulting settlements were noted.

Creep tests lasting up to about one month have been performed on shredded tires in the past by Humphrey et al. (1992). Knowledge of creep characteristics for a greater duration of loading would be beneficial in the design of fills, since settlement over a long period of time is a concern in fills covered by rigid pavements. To investigate the viscoelastic behavior of shredded tire material for loading periods longer than a year, long-term creep tests on small-size (50 mm) shredded tire pieces have been undertaken in this project. These include constrained creep tests in cylindrical containers, and unconstrained creep of shredded tire piles. Several test apparatus were constructed, and using dead weights, levers, and pulleys, constant load has been applied to shredded tire samples for periods up to two years.

During the construction of fills with large-size shredded tire pieces, it has been noted that masses of the material display a layered structure when compacted. Like other layered materials, the deformability parameters in the vertical and in the horizontal direction may differ. This possible material anisotropy may lead to errors in the settlement analysis of fills under traffic loading, which is currently performed with the assumption of material isotropy. In tests conducted at the University of Minnesota, the mechanical anisotropy found in masses of shredded tires was assessed by laboratory experiments. Tests were performed in a biaxial apparatus developed specifically for the

project in which samples of large-size (200 mm) shredded tire pieces were compressed in two directions.

To familiarize the reader with the material used in the project, Chapter 2 explains how shredded tire pieces are manufactured and what their approximate sizes and shapes are. Also, bulk properties such as unit weight and void ratio are discussed. In Chapter 3, the repeated load tests are described, the results of which are presented and analyzed to indicate the cyclic loading behavior of the material. Chapter 4 deals with the creep or constant load experiments. Results are used to determine the long-term settlement characteristics of shredded tires. Anisotropy of shredded tire material is the subject of Chapter 5, which includes a description of the tests performed in the biaxial apparatus. Anisotropic parameters are calculated, and these are used in a numerical analysis to compare settlements of fills with an anisotropic shredded tire layer with those for a fill with shredded tire material regarded as isotropic.

CHAPTER 2

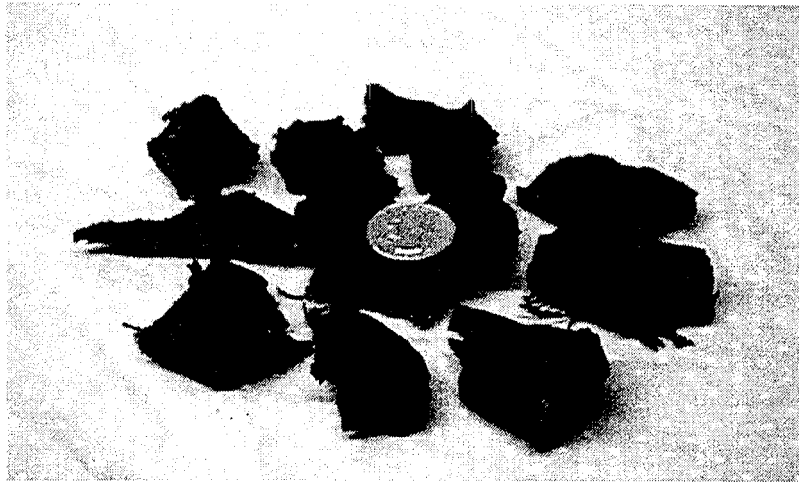
SHREDDED TIRES CHARACTERIZATION

SOURCE OF SHREDDED TIRES

Shredded tire material comes from whole scrap tires that have been cut into much smaller pieces by shredders. Pieces used in this project with an average size of about 55 mm by 25 mm by 10 mm (2.2 in. by 1.0 in. by 0.4 in.) have passed through six separate shredders, arranged in a sequence that causes successively smaller pieces to be generated. Steel wires are present in many shredded tire pieces. For the removal of pieces with excessive amounts of protruding steel wires, many tire shredding facilities have conveyor belts, which carry the shredded tire material under magnets.

Figure 2.1a and 2.1b are photographs of typical shredded tire pieces. The shearing and tearing during shredding produces pieces that are highly irregular in shape. The cross-section of an individual piece varies along its length. Small-size pieces, in general, are flat due to the thin-wall construction of whole tires. Also, the curvature of whole tires is reflected by the surfaces of most large-size pieces.

The shredded tire pieces for this project were obtained from Monitor Tire Disposal in St. Marten, Minnesota. The original waste-product material was screened by



a)



b)

Fig. 2.1. Shredded tire pieces

a) small-size pieces (quarter is shown for scale)

b) large-size pieces (quarter is shown for scale)

removing pieces with an excessive amount of protruding wires, according to the guidelines of the Minnesota Department of Natural Resources and used by the Oregon DOT (Read, et al, 1991). The lightweight fill specifications of that department dictate that "... metal fragments shall be firmly attached and 98% embedded in the tire sections from which they were cut out." Also, small fragments of rubber and other debris were discarded.

Two sizes of shredded tire pieces were used. The smaller pieces are of size no greater than 90 mm (3.5 in.) in length, with average size piece of about 53 mm by 25 mm by 11 mm (2.1 in. by 1.0 in. by 0.4 in.), Fig. 2.1a. These will be referred to as 50-mm pieces. The smallest pieces of the 50-mm variety have a maximum length no less than 30 mm (1.2 in.). Among the larger size pieces, none are more than 400 mm (16 in.) in length and the average size piece is about 200 mm by 125 mm by 19 mm (8 in by 5 in. by 0.75 in.), Fig. 2.1b. The larger-size pieces will be referred to as 200-mm pieces. The smallest of the 200-mm pieces have a maximum length no less than 100 mm (4 in.).

GEOMETRIC CHARACTERIZATION

As most tests in the project were carried out using small size pieces, a representative sample was randomly chosen from the 50-mm shredded tire pieces for detailed size analysis. Hand measurements taken of the shredded tire pieces are referred to as greatest dimension, conjugate average width, and conjugate average depth, Fig. 2.2. The greatest dimension of a shredded tire piece is the distance between the points furthest apart from each other. The terms conjugate average width and conjugate average depth

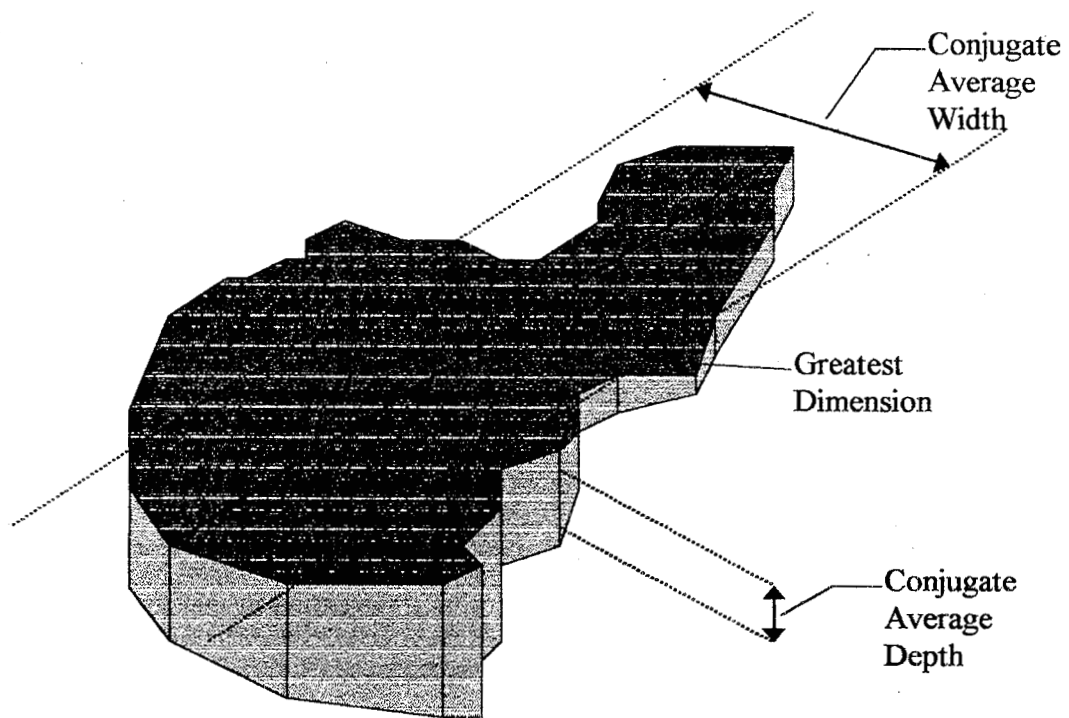


Fig. 2.3. Measurements for grain-size analysis

characterize a shredded tire piece by giving its average dimensions in directions perpendicular to the greatest dimension. Next, the aspect ratio of a shredded tire piece was found by dividing the greatest dimension by the conjugate average width. It was found that the width of the 50-mm pieces is greater than their depth, which indicates that the pieces are somewhat flat, and that their length is significantly greater than their width and depth, which indicates that the pieces are elongated, Fig. 2.3. The aspect ratios range from 1 to about 6, Fig. 2.4. The size tendencies of shredded tire pieces are largely due to the thin-wall construction of whole tires.

Besides being long and flat, shredded tire pieces have surfaces that represent the curvature of whole tires. Due to their toroidal geometry, whole tires have circumferential curvature. Also, curvature in another direction is shown by the U-shaped cross-section of a hollow tire carcass, Fig. 2.5, particularly noticeable along the inner wall. Both sidewall and tread portions of tires produce shredded tire pieces with curvature. The curvature of whole tires is most prominent in dome-shaped larger pieces, which comprise the majority of the 200-mm samples. The curvature in 50-mm pieces is less pronounced due to their smaller size. Also, the shredders often cut the 50-mm pieces into wedges whose surface area does not include a significant portion of the curved surfaces of the inner and outer walls of the whole tires.

A detailed size analysis of the 200-mm pieces was not performed. However, as stated, the average size piece is about 200 mm by 125 mm by 19 mm (8 in by 4 in. by 0.75 in.). Using a calculation similar to that for the 50-mm pieces, the typical aspect ratio of a

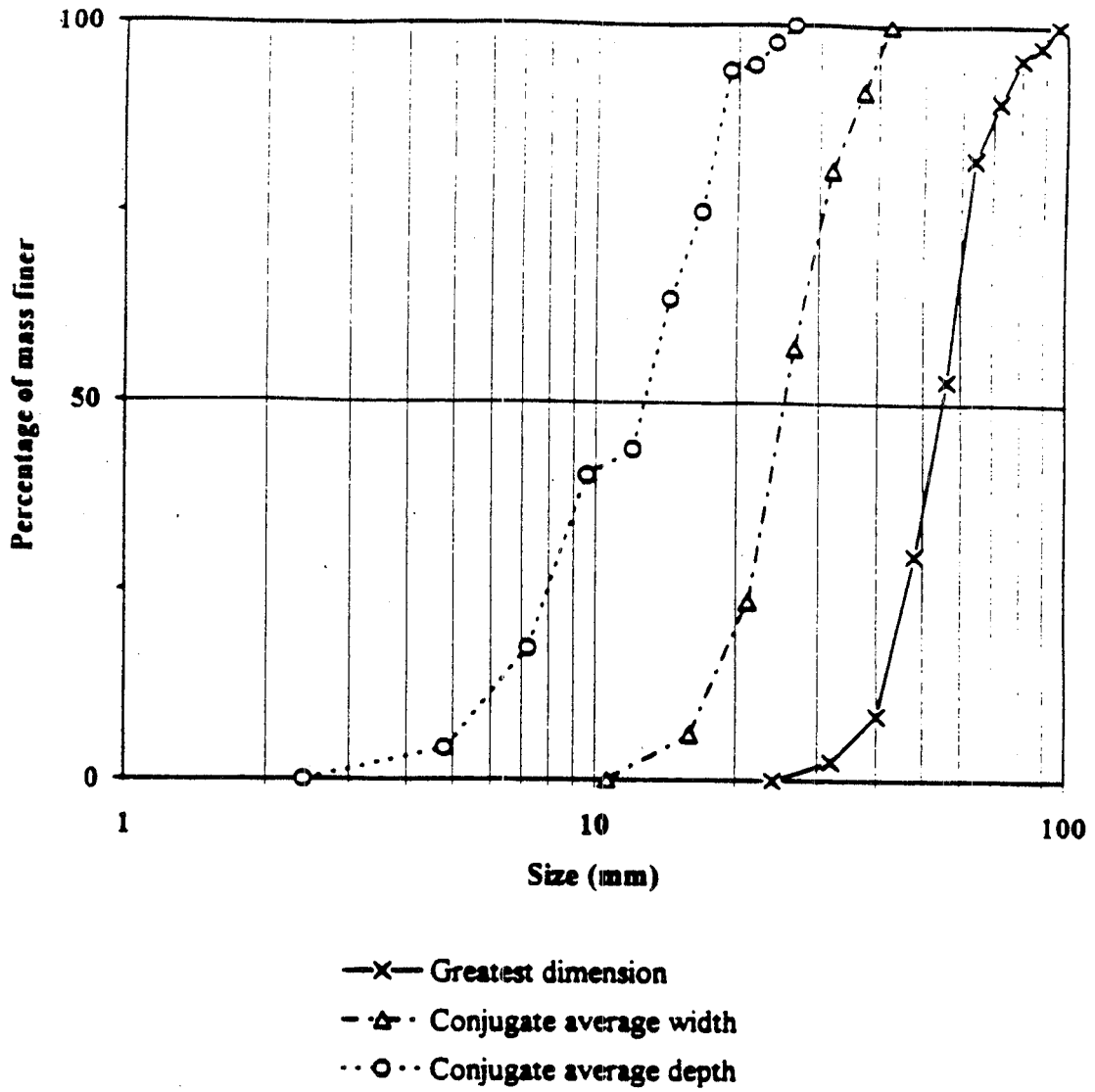


Fig. 2.3 Grain-size distribution according to dimensions (50 mm) pieces

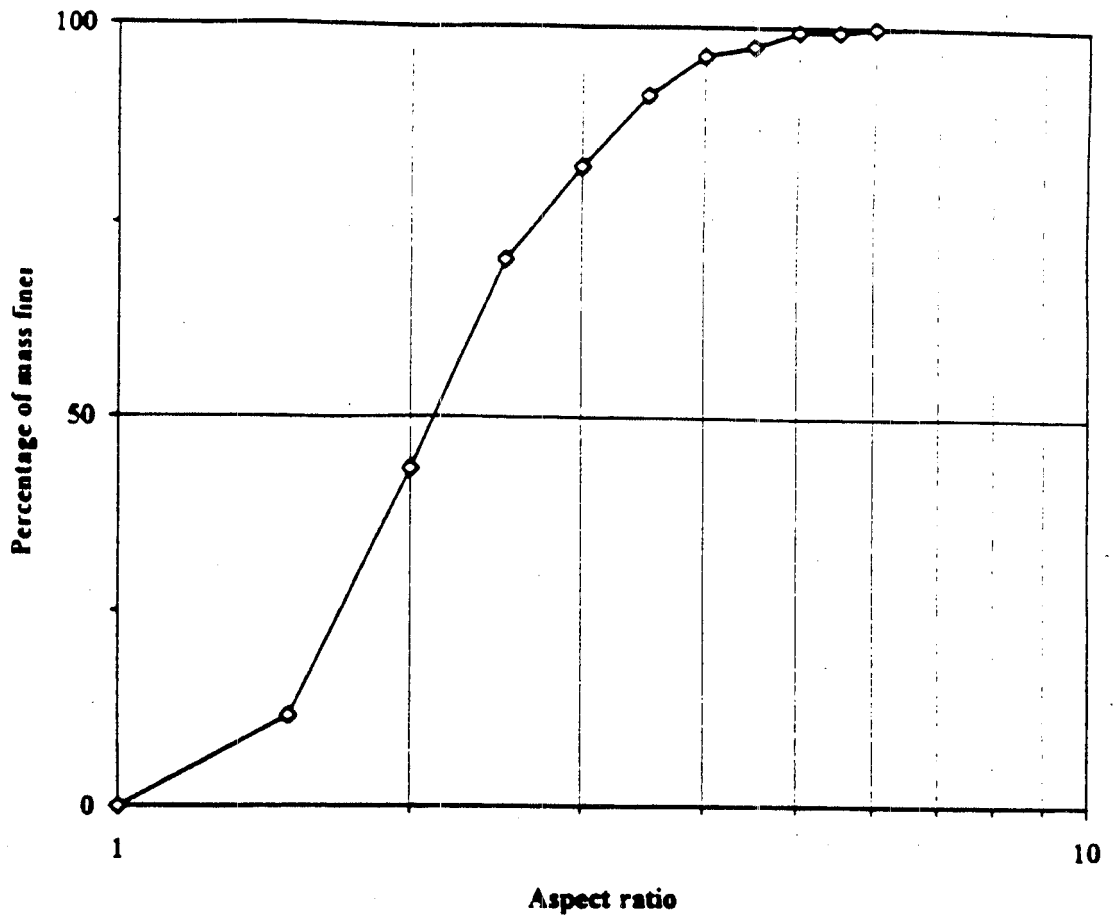


Fig. 2.4 Distribution according to aspect ratio (50 mm) pieces

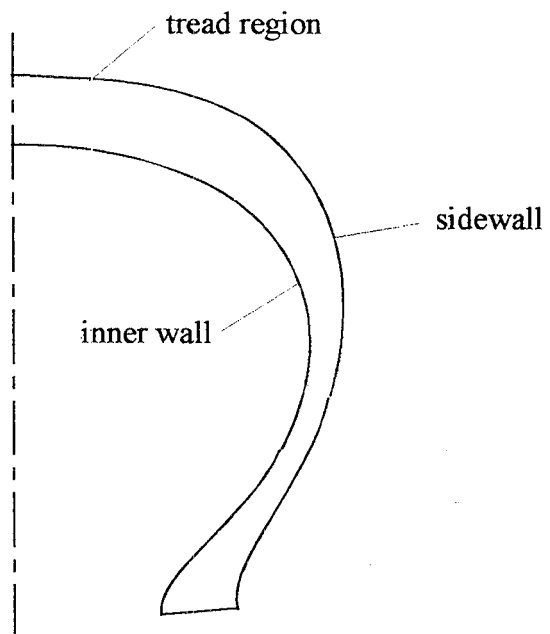


Fig. 2.5. Cross-section of a tire

200-mm piece is about 2. A visual comparison of the length and width dimensions of the 200-mm pieces to the thickness dimension revealed that they are much thinner than the 50-mm pieces. This thickness differential arises because the 50-mm pieces tend to be cut from the thicker tread region, whereas the 200-mm pieces tend to include significant portions of the sidewall region.

PHYSICAL CHARACTERIZATION

In engineering applications, the physical characterization of shredded tire material is of primary importance. More specifically, the bulk unit weight, γ , and the porosity, n , or void ratio, e , are of interest. From laboratory tests, the bulk unit weight of uncompacted 50-mm pieces in a cylindrical vessel ranged from 3.5 to 4.3 kN/m³ (22 to 27 lbs/ft³). When compacted, the bulk unit weight ranged from 4.2 to 5.1 kN/m³ (27 to 32 lbs/ft³). The specific gravity of shredded tire pieces was found to be 1.11.

An estimate of the porosity was found from

$$n = \frac{G_s \gamma_w - \gamma_{st}}{G_s \gamma_w} \quad (2.1)$$

where G_s is the specific gravity of the shredded tire pieces, γ_w is the unit weight of water, and γ_{st} is the bulk unit weight of shredded tires.

Upon calculating the porosity, the void ratio, e , was calculated from

$$e = \frac{n}{1-n} \quad (2.2)$$

The results are shown in the Table 2.1.

Table 2.1. Properties of Shredded Tire Material

Condition	Bulk unit weight (kN/m ³)	Porosity	Void ratio
Uncompacted	3.5 to 4.3	0.64	1.78
Compacted	4.2 to 5.1	0.57	1.33

CHAPTER 3

BEHAVIOR UNDER REPEATED LOAD

INTRODUCTION

In the design and construction of shredded tire fills, it is important to know how shredded tire material deforms in response to various levels of load. Loads from compaction, weight of overburden material, and traffic, all induce settlement. With repeated applications of these loads, the ability of the material to rebound (resilience) is also a concern. In order to address these issues, cyclic loading-unloading tests were performed on shredded tire material.

Two types of experiments were conducted: a) constrained compression, and b) unconstrained compression. The first type refers to compression with no lateral strain, the so-called one-dimensional compression test often carried out for soils (oedometer test), Fig. 3.1a. In application to shredded tire material, this test was used by Humphrey (1993), Drescher and Newcomb (1996), and Edil and Bosscher (1997), and provides information for directly evaluating the so-called compression index and swell index commonly used in predicting settlements of shallow foundations (Das, 1995). If lateral stresses are measured, and linear elastic response is assumed, Young's modulus, E , and Poisson's ratio, ν , can be determined from this test, as shown by Drescher and Newcomb (1996) and Edil and Bosscher (1997).

In the second type of experiment, a laterally unconstrained and flattened heap of shredded tires, resembling a truncated cone, was axially loaded by a plate, Fig. 3.1b.

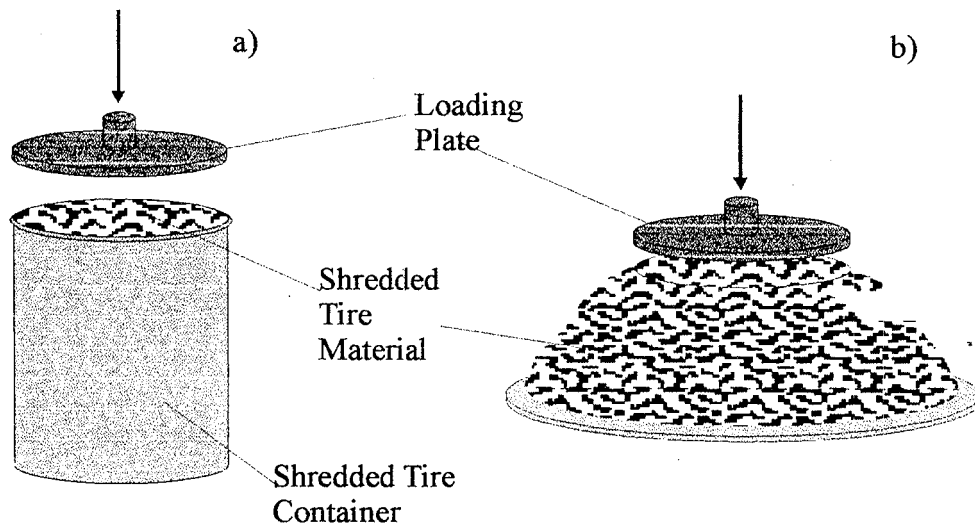


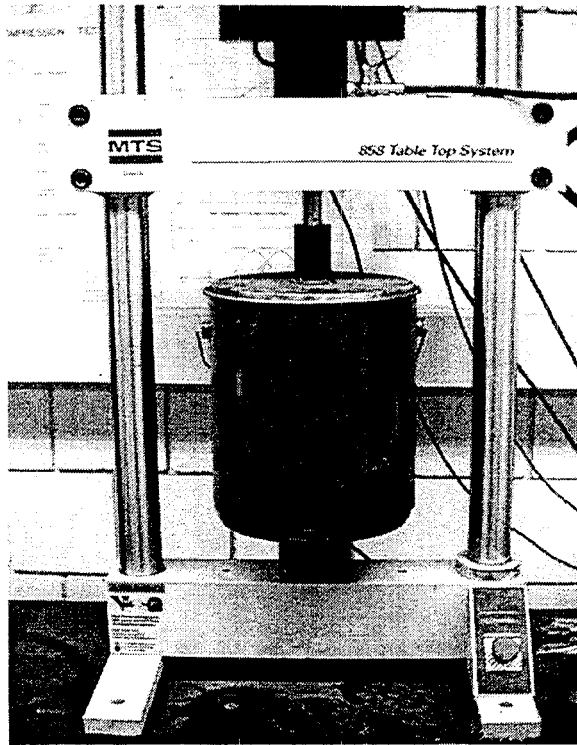
Fig. 3.1. Repeated load experiments
a) Constrained compression
b) Unconstrained compression

This test was selected to provide information about the response of the material to loading in conditions resembling those at the edge or near the edge of a road or embankment. It should be stressed here that due to the particulate nature of shredded tire material, standard uniaxial compression, being more adequate for material properties evaluation, cannot be performed, and triaxial compression would require very large and sophisticated testing equipment which is not commercially available. The advantage of the unconstrained compression test selected is that it provides an upper bound to settlements of a fill. The lower bound is provided by the constrained compression test. Actual settlement of in situ material can be expected to lie within these bounds, considering similar load history. Thus, conditions representing the extremes of confinement, constrained and unconstrained compression, were used.

TESTING APPARATUS

The constrained and unconstrained compression tests were performed with the help of an MTS 858 Table Top System load frame of 25-kN (5.5-kip) capacity, Fig. 3.2. The constrained tests were conducted in a 0.021 m³ (5 gal) straight wall cylindrical steel container, Fig. 3.2a. The inside dimensions of the container are 290 mm (11.25 in.) in diameter and 330 mm (13 in.) in height. The steel loading plate, which is 277 mm (10.9 in.) in diameter and 13 mm (0.5 in.) thick and attached to the actuator, is slightly smaller than the inside diameter of the container to prevent jamming. A separate 13 mm (0.5 in.)

a)



b)

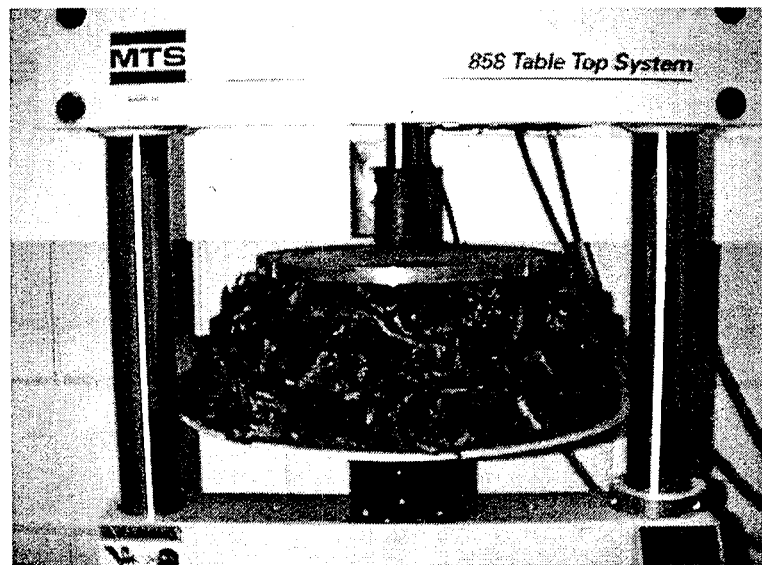


Fig. 3.2. MTS load frame setup
a) constrained compression
b) unconstrained compression

thick circular steel plate fits under the container for uniform support of the base. Material was loosely placed in the container to a depth of about 140 mm (5.5 in.).

In unconstrained tests, material was loosely piled to a height between 60 mm and 120 mm (2.5 and 5 in.) on an aluminum plate that is 3.5 mm (1/8 in.) thick and 460 mm (18 in.) in diameter and fully covered by shredded tire pieces, Fig. 3.2b. The top of the pile was formed into a more or less flat circular surface so that a load approximately uniform with radius could be applied by a steel plate of the same dimensions as in constrained tests.

For both types of tests, a computer directed the actuator to perform programmed test procedures using Testware-SX software included with the MTS Table Top System. Throughout the test, values of load and vertical displacement were collected continuously in a data file at each specified time increment.

MATERIAL AND TEST PROGRAM

The tests were performed on 50-mm shredded tire pieces. Once a sample of the material was placed in a container or piled on a plate, it was subjected to three compaction loads of 14 kPa (2 psi) before cyclic loading was performed.

The test matrix is shown in Table 3.1. The tests differed in loading rates, loading history, and number of cycles. The range of loads applied in tests was governed by the range of vertical stresses acting on shredded tire pieces in subgrade fills. For the purpose of estimating these stresses, the unit weight of soil, γ_s , was assumed to be 19.6 kN/m³ (125 lb/ft³) (Das, 1995) and the unit weight of compacted shredded tire pieces, γ_{st} , was assumed

Table 3.1. Repeated Load Test Matrix

Test Numbers	Type of Test	Maximum Stress (range 1 / range 2 / ...) kPa (psi)	Number of Cycles
1-1 to 1-3	Constrained compression	26.2/62.1/100.7 (3.8/9.0/14.6)	5/5/5
2-1 to 2-3	Constrained compression	62.7/102.0 (9.1/14.8)	5/5
3-1 to 3-3	Constrained compression	102.7 (14.9)	5
4-1 to 4-24	Unconstrained compression	56.5 to 89.6 (8.2 to 13.0)	1 to 15
5-1 to 5-4	Unconstrained compression	23.4/51.0/82.7/115.1 (3.4/7.4/12.0/16.7)	5/5/5/5
6-1 to 6-18	Constrained compression	131 (19.0)	15 to 100
7-1 to 7-12	Unconstrained compression	95 (13.8)	20
8-1 to 8-15	Unconstrained compression	26.2/56.5/88.9/120.7 (3.8/8.2/12.9/17.5)	5/5/5/5 to 20/20/20/20

to be 4.7 kN/m³ (30 lb/ft³) (See Chapter 2). Estimated vertical stresses within the shredded tire layer, σ_{st} , in fills were calculated from

$$\sigma_{st} = \gamma_s h_s + \gamma_{st} (z_r - h_s) \quad (3.1)$$

where h_s is the thickness of the soil covering the shredded tires and z_r is the depth within the road bed. Fig. 3.3 depicts vertical stress as it varies with the depth of a fill. In this plot, the depth is a combination of the thickness of the soil layer and the shredded tire layer, and the resulting value for vertical stress depends on the contribution of each of these layers. In light of typical overburden stresses, the stress levels in tests did not go beyond 138 kPa (20 psi).

As stated, tests were performed to study how changing the loading rate influences settlement. This allowed for examination of time-dependent settlement, or creep, for short-term loading. Creep has been shown to occur in shredded tire material, particularly noticeable during the period immediately after loading. (see Chapter 4). In the construction of fills, shredded tires are subject to load that slowly changes with time. Shredded tire material and soil are typically placed in a number of layers 0.3 m-thick or less (Newcomb and Drescher, 1994). In these layers, called lifts, the material is spread uniformly and compacted, which takes time, before the next layer is made. In the time it takes for a lift to be placed and the next one to follow, creep settlement occurs in the

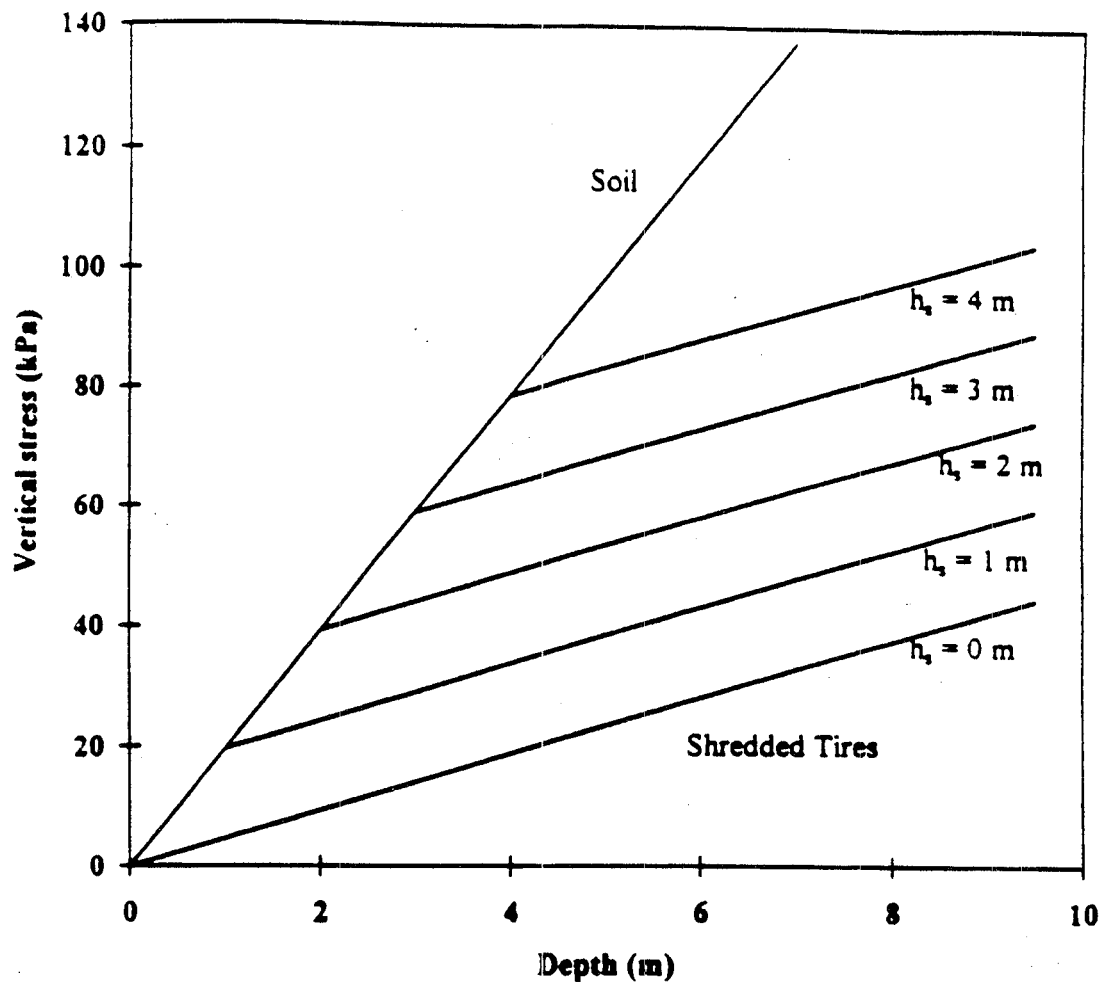


Fig. 3.3 Vertical stresses in a shredded tire fill

underlying shredded tires. As far as creep settlement is concerned, this stepwise loading can be approximated by a continuously increasing loading applied at a slow rate.

In Tests 6-17, 6-18, 7-11, and 7-12, a loading rate of 0.05 kN/sec. was used. Loading at this rate was intended to simulate the stepwise loading described above. This slow rate contrasted with the normal loading rate, which was 5 kN/sec. The normal loading rate was designed to simulate rapid loading, such as the dumping of overburden fill above a shredded tire layer or that caused by construction equipment or traffic vehicles. In Tests 6-7 to 6-16 and Tests 7-1 to 7-10, the normal rate was used, and by comparing the results of these tests with those of Tests 6-17, 6-18, Tests 7-11, and 7-12, the effects of creep on short-term settlement could be studied.

In Test Groups 6 and 7, shredded tire samples were subject to as many as 80 cycles of load. The variation of plastic strain with increasing number of cycles was investigated.

In unconstrained compression tests, settlement may be affected by the friction between the shredded tire material and the metal of the load and base plates. As vertical load is applied, the friction above and below the sample restricts lateral motion of the material near the plates, while material at the midheight of the sample is unaffected directly. Thus, by increasing sample height without changing the dimensions of the loading or support plates, the effects of boundary friction on settlement should become less pronounced. With decreased resistance to lateral movement per unit height, a sample greater in height will act like a sample with less lateral confinement, and will therefore

have less resistance to vertical movement and appear less stiff than a sample shorter in height.

In constrained compression tests, the friction between the shredded tires and the metal of the container influences the response of the material to vertical load. The friction along the vertical walls of the container absorbs part of the vertical load, and the resultant vertical force acting on the shredded tires is gradually reduced with depth. For this reason, vertical stresses decrease with depth in a sample. By increasing sample height, the effects of wall friction on vertical strain increase, and for a given load, the average vertical stress over the sample height decreases.

To study the effects of boundary friction in both the constrained and unconstrained compression tests, several heights of samples were used. For example, for Tests 7-1 to 7-10, compacted heights of samples ranged from 7.0 cm (2.8 in.) to 10 cm (3.9 in.).

TEST RESULTS

Data Evaluation

The Testware-SX computer application was used to collect load and vertical displacement measurements for each time increment. The axial force, P , was used in the calculation of vertical stress, and the change in height of the sample, Δh , was used in the calculation of vertical strain.

In the constrained compression tests, if the wall friction is negligible, it is reasonable to assume that the vertical stress and strain are uniformly distributed within the sample. Accordingly, the average vertical stress, σ , was calculated from

$$\sigma = \frac{P}{A_c} \quad (3.2)$$

where A_c is the cross-sectional area of the cylindrical container. The corresponding average vertical strain, ε , was calculated as

$$\varepsilon = -\frac{\Delta h}{h_0} \quad (3.3)$$

where h_0 is the height of the sample upon compaction.

In unconstrained compression tests, even if the effect of boundary-friction is eliminated, the assumption of stress and strain uniformity throughout the sample no longer holds true. As the width of the pile increases with depth, the stresses decrease, and they are higher in the middle than at the edges of any horizontal cross-section. To calculate representative vertical stresses, it was assumed that the external load is uniformly distributed over any cross-section, and decreases with depth from the loading plate in a 2:1 depth-to-width ratio. Also, the full radius of the plate was assumed to be in contact

with the material. Assuming the stress at midheight to represent average stress leads to the following expression for stress

$$\sigma = \frac{P}{A_p} \quad (3.4)$$

where A_p is given by

$$A_p = \frac{\pi}{16} (4r_0 + h_0 - \Delta h)^2 \quad (3.5)$$

where r_0 is the radius of the loading plate. The representative vertical strains were calculated as the average strain over the height. Thus, Eq. (3.3) was used.

The manual placement of the shredded tire material was slightly different in unconstrained tests than in constrained tests. In unconstrained tests, pieces were piled on the bottom plate when it was outside the load frame, and the pile was formed into the shape of a truncated cone with a relatively flat top. The pile was then slid into position under the loading plate. In an attempt to provide uniform support beneath the loading plate, pieces were added to the pile, primarily near the edges of the loading plate. Especially in samples greater in height, the angle of repose was such that added pieces caused material to fall down the side and off of the pile, leaving a space with little support for the loading plate. To reconstruct places where this was occurring, pieces were inserted

one-by-one until a stable slope to support the plate was recovered. In constrained tests, pieces were placed in the container without being rearranged.

In both tests, after the placement of pieces, the samples were subjected to 3 compaction load cycles. On average, the vertical strains due to compaction were about 14% and 21% in the constrained and unconstrained cases, respectively. The higher strain due to compaction in the unconstrained case, coupled with the rearrangement of pieces for loading plate support, may have caused the material in the unconstrained case to be more dense after compaction than in the constrained case. The unit weights of the material after compaction were estimated to be about 4.7 kN/m^3 (30 pcf) in the constrained case and 6.0 kN/m^3 (38 pcf) in the unconstrained case. Ideally, unit weights between cases should be the same. Were the unconstrained samples tested at the same unit weight as in the constrained samples, the unconstrained material would have appeared less stiff. In comparing the stress-strain relations between the two confinement cases, the difference in unit weight should be kept in mind.

RESULTS

The following figures show typical results from a total of 82 cyclic loading tests. It should be noted that the reference value of zero stress for each stress-strain curve corresponds to stress just before cyclic loading was performed. The actual vertical stresses were about 5.5 kPa (0.8 psi) and 6.9 kPa (1.0 psi) on average for the unconstrained and constrained compression tests, respectively. Although the stresses shown in the stress-

strain curves are reference vertical stresses, they will simply be referred to as vertical stresses.

Figure 3.4 depicts the variation of vertical stress with vertical strain for the first load cycle of Tests 6-16 and 7-4, which are constrained and unconstrained compression tests, respectively. The curvatures of the stress-strain plots indicate increasing stiffness of the material in both tests.

The loading rate for the tests shown in Fig. 3.4 was 5 kN/sec. To examine the effects of creep on short-term settlement, the plots in Fig. 3.4 can be compared to those for tests performed at a loading rate of 0.05 kN/sec. Fig. 3.5 shows the stress-strain curves for Tests 6-16 and 6-17, which correspond to the fast and slow rates, respectively, in the constrained compression case. Similarly, Tests 7-4 and 7-11 are compared in Fig. 3.6 for the unconstrained compression case. It is evident that greater strain occurs in tests with slow rates. In constrained tests, wall friction may have far less influence on settlement for the slow rate, since time is allowed for the resultant friction force to be transferred to vertical force on the shredded tires. This may be one reason that the effect of loading rate is much greater in the constrained case than in the unconstrained case. Also, due to this possible transfer of friction to vertical load with time in the constrained case, the strain exclusively due to creep may be less than it appears.

Figure 3.7 shows the results of a typical cyclic loading test for a sample in the constrained condition, Test 6-16. Eighty load cycles were applied, with an applied stress

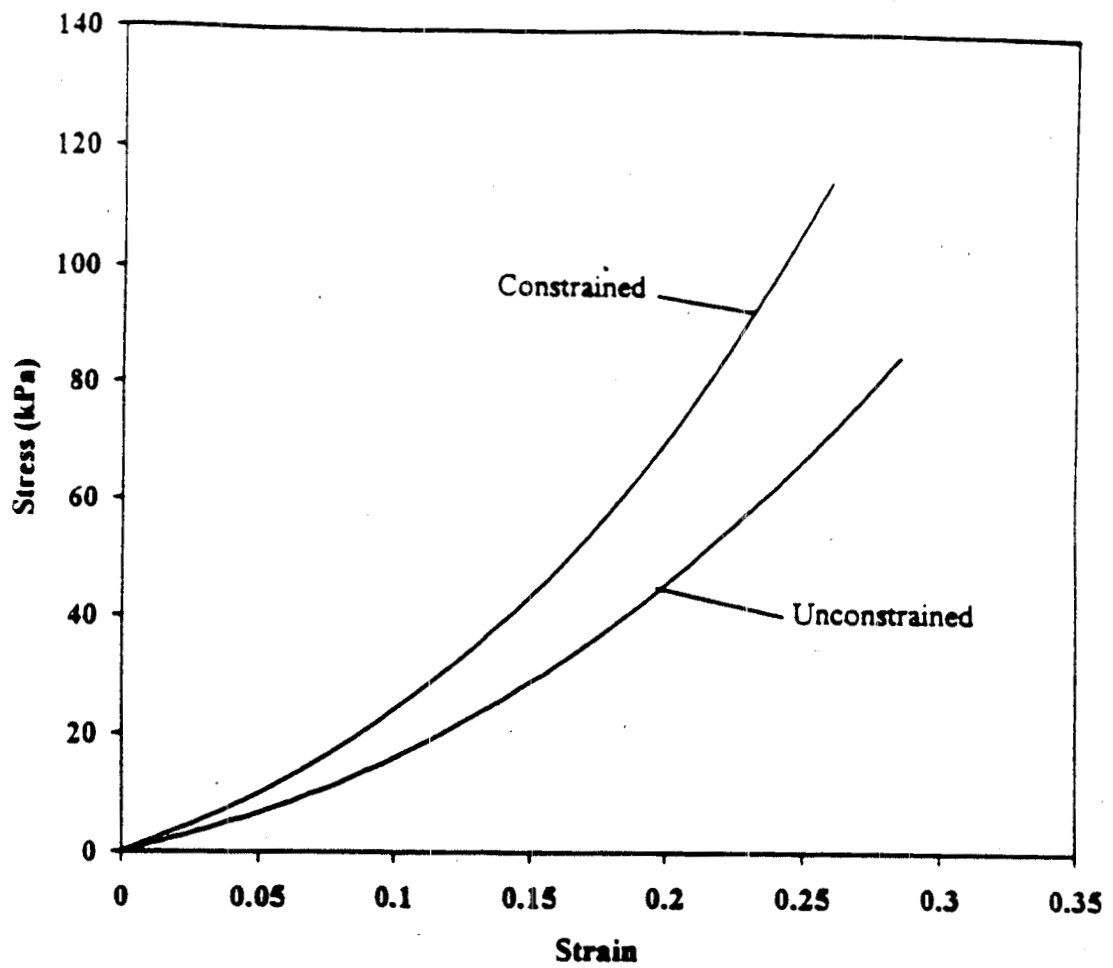


Fig. 3.4. Stress-strain curves for first load cycle

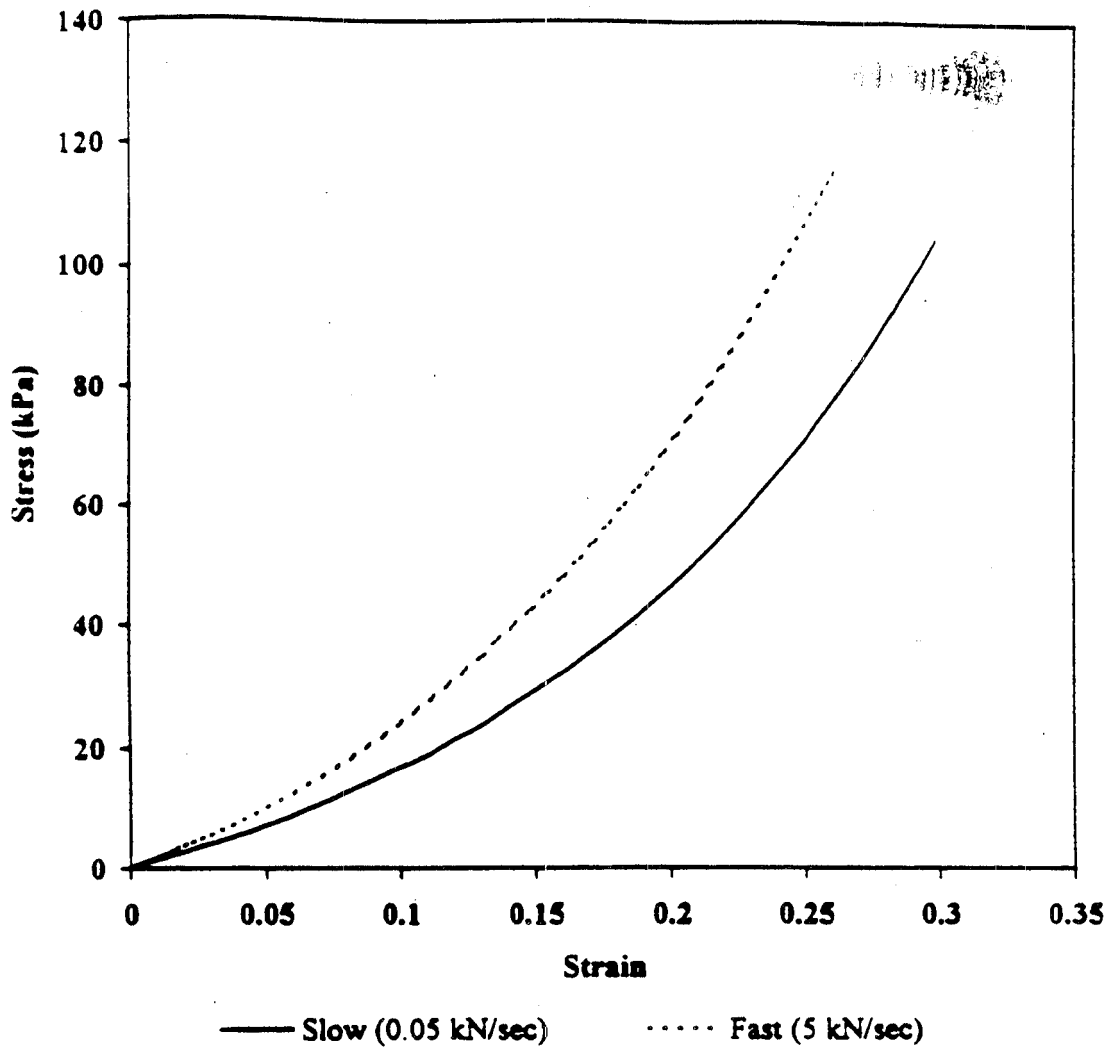


Fig. 3.5. Stress-strain curves for slow and fast loading rates - Constrained

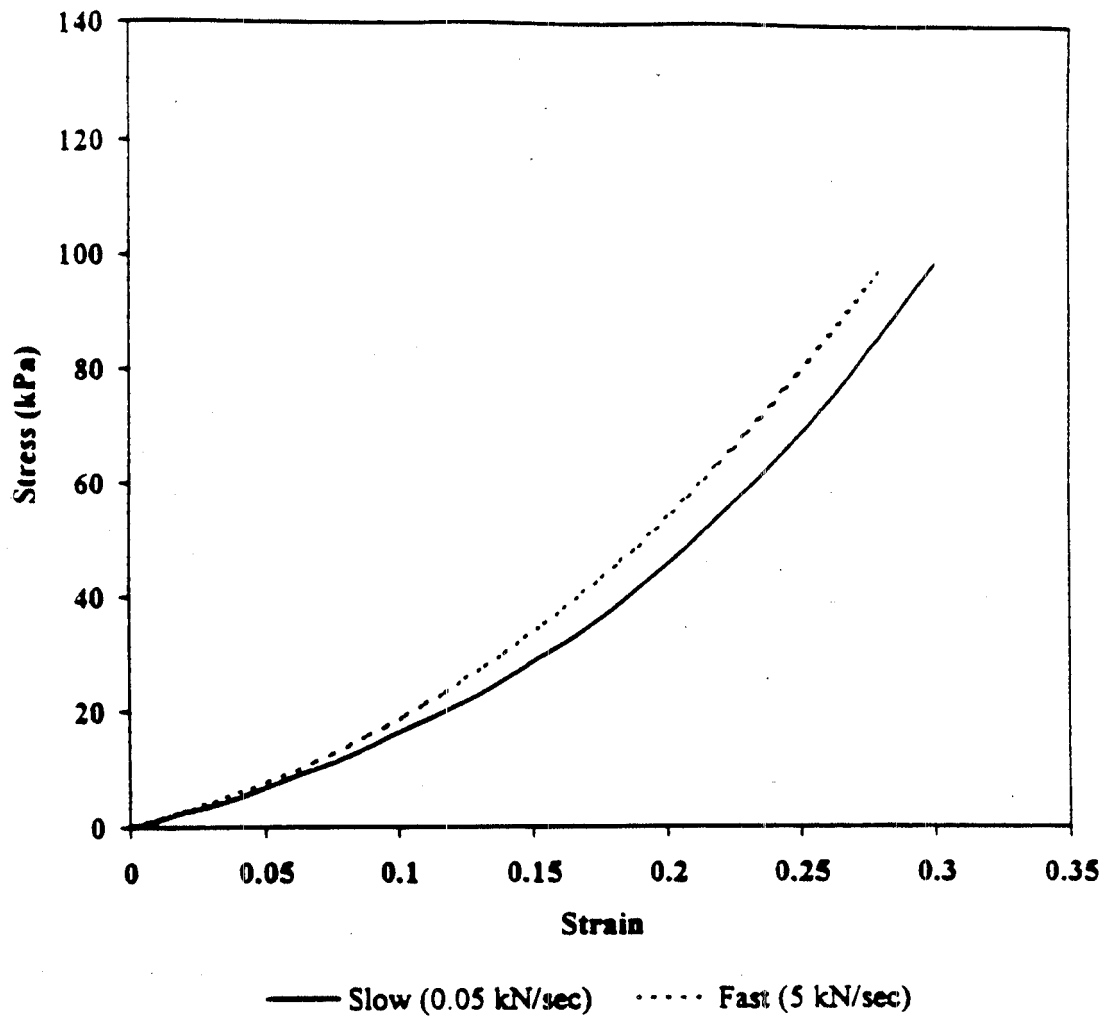


Fig. 3.6. Stress-strain curves for slow and fast loading rates - Unconstrained

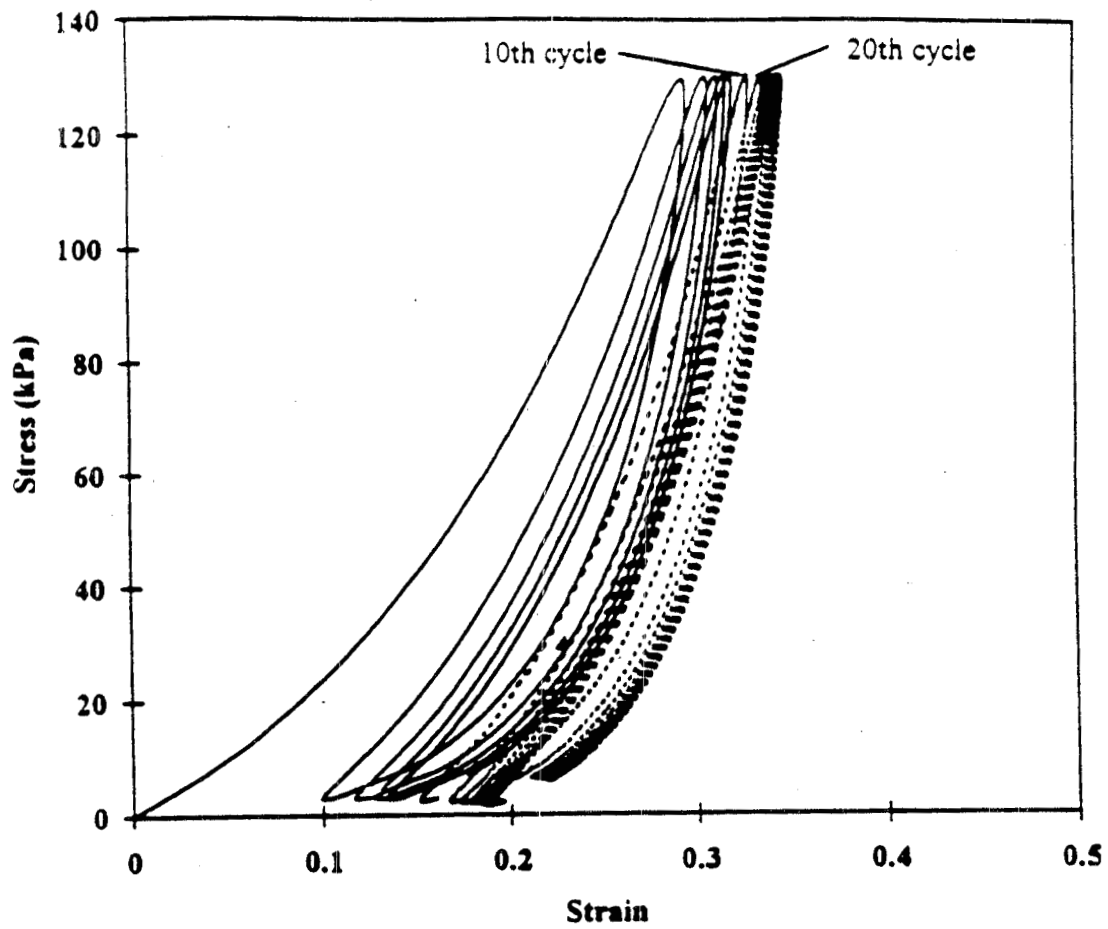


Fig. 3.7. Constrained compression

of 130 kPa (19 psi) per cycle. The plots of stress vs. strain are shown for the first five load cycles, the tenth load cycle, and for every ten load cycles thereafter. Plastic strain for a cycle may be defined as the difference in strain at a stress of 2.7 kPa (0.39 psi) between the start of the load cycle in question, and the start of the cycle that follows. When defined this way, plastic strain of about 8% occurred during the first load cycle. In subsequent load cycles, plastic strain was greatly reduced. This demonstrates the value of subjecting the material to several cycles of compaction load. In Fig. 3.8, the accumulated plastic strain is plotted against the number of cycles. The plastic strain decreases rapidly during the first few cycles. Beyond 20 load cycles, the accumulated strain per cycle is nearly constant at about 0.03% strain per cycle.

Repeated load tests using unconstrained samples were also performed, but after about 5 cycles, the material would move laterally to such an extent that the number of pieces still under compression was less than in the first load cycle. In other words, the apparent vertical strain was partially due to a cumulative amount of material being removed from the influence of the vertical load. Therefore, the amount of plastic strain exclusively due to material behavior is difficult to determine. A typical stress-strain plot for the unconstrained compression tests is shown in Fig. 3.9 for Test 7-4, where applied stress was about 120 kPa (17 psi) per cycle.

Figure 3.10 shows a comparison of the accumulated strain in Tests 6-16 and 7-4 for twenty load cycles. In general, plastic strain per cycle is greater in the unconstrained compression test than in the constrained compression test, even though applied stress in

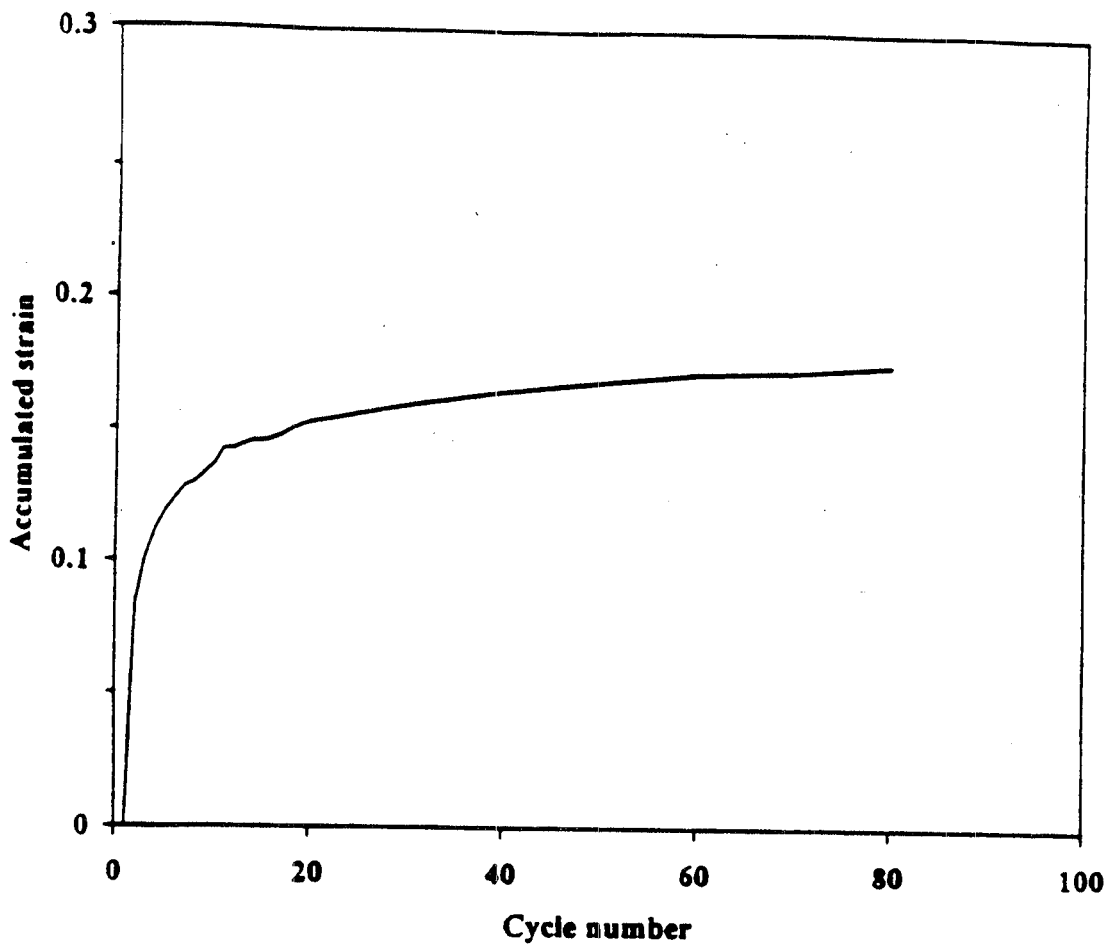


Fig. 3.8. Accumulated strain per cycle, constrained case

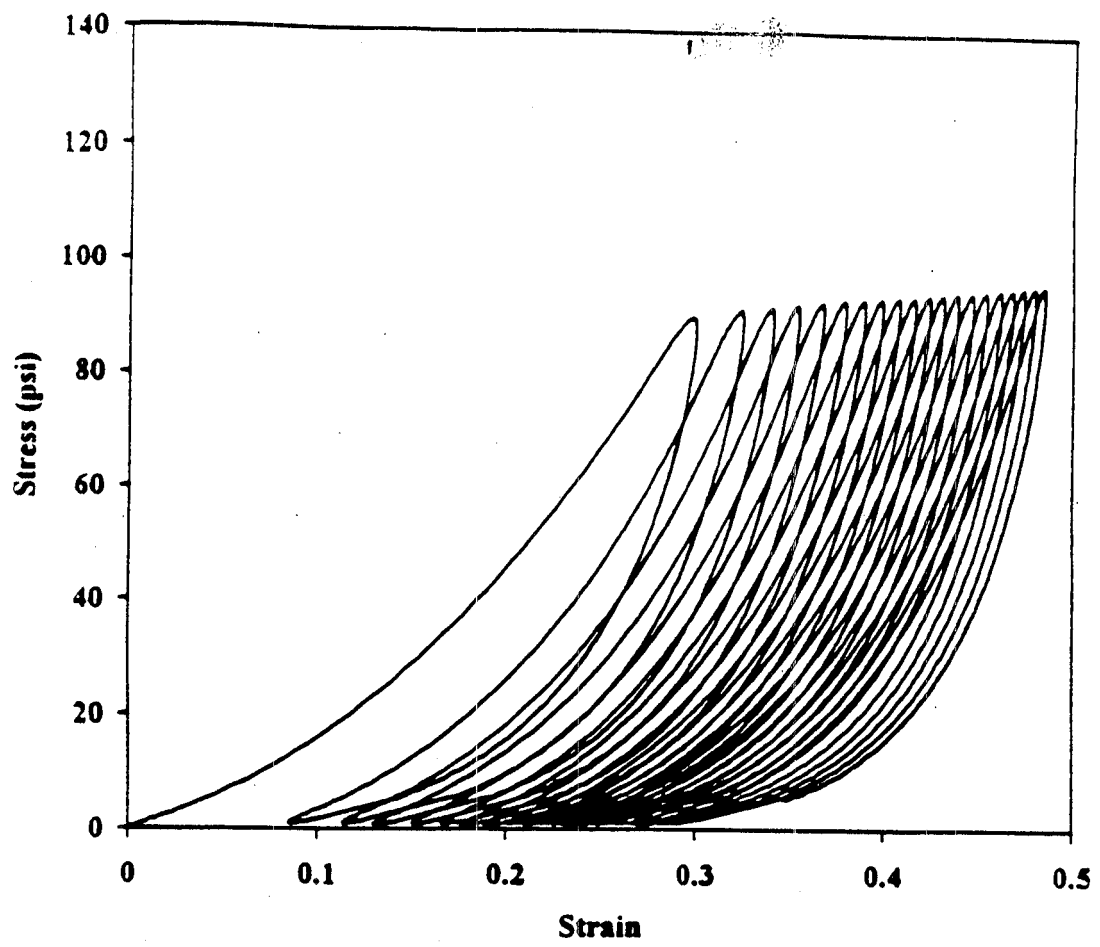


Fig. 3.9. Unstrained compression

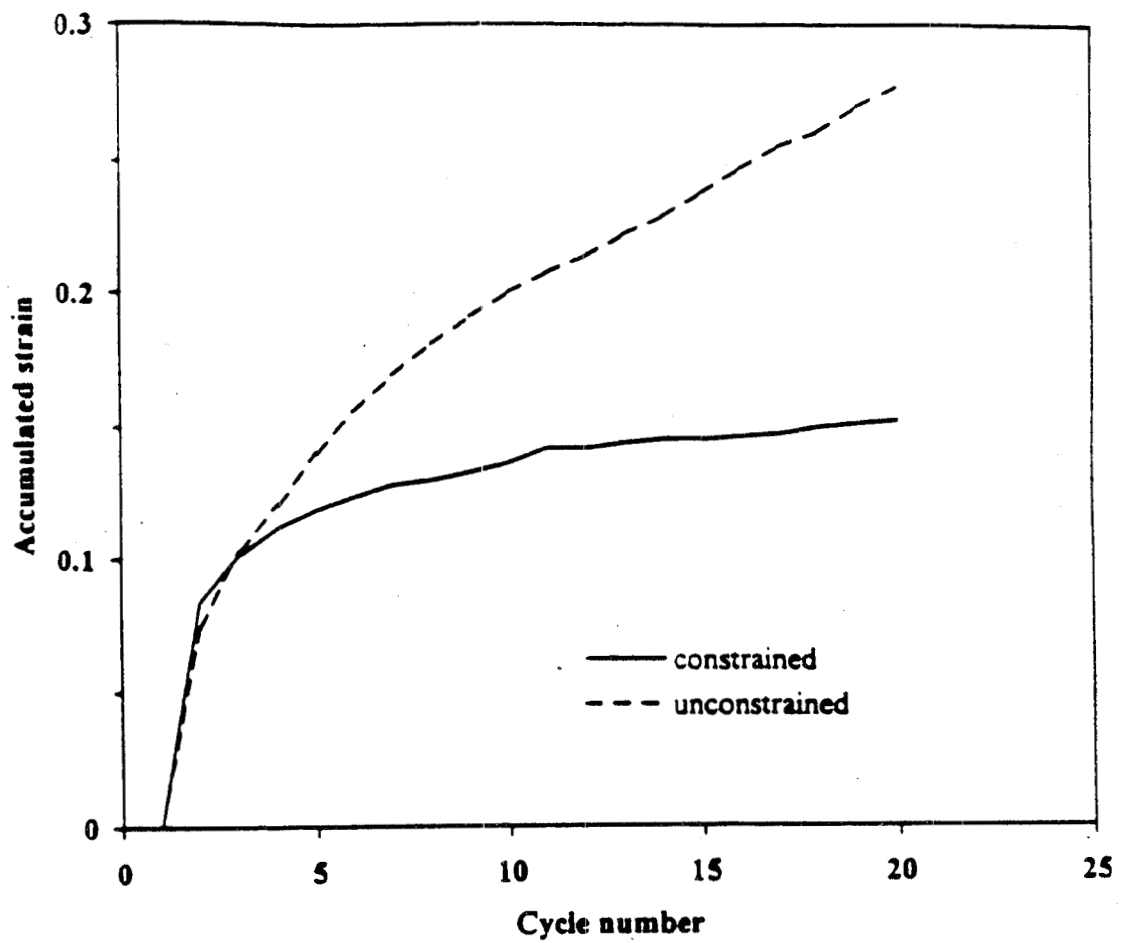


Fig. 3.10. Accumulated strain per cycle

the constrained compression test was slightly higher. For load cycles 12 through 20, the plastic strain per cycle was approximately constant at 0.13% for Test 6-16 and 0.80% for Test 7-4.

To analyze the effects of boundary friction on results tests were performed on samples of different height. Two sets of stress-strain curves were constructed a) one set for the constrained compression test results of Tests 6-7 to 6-16, and b) one for the unconstrained compression test results of Tests 7-1 to 7-10. Each curve in a set includes the loading and unloading for the first load cycle and the loading for the second load cycle. Each set of stress-strain curves is then divided into three subsets for analysis: a) a loading subset (first load cycle), b) an unloading subset (first load cycle), and c) a reloading subset (second load cycle). Figure 3.11 depicts the subsets schematically. Since there is always a transition region between unloading and loading and vice versa, upper and lower stress limits were set in the analysis of results to ensure accuracy. Later, as will be shown, extrapolations were made to recover stress-strain relations for stress values outside the set limits.

Examples of stress-strain curves for the loading subsets are shown in Figs. 3.12 and 3.13, where plots for several sample heights are included. As shown in Fig. 3.12, which corresponds to laterally constrained samples of Tests 6-7 to 6-16, samples greater in height appear stiffer, most likely due the effects of wall friction. In Fig. 3.13, where the stress-strain plots of three laterally unconstrained samples from Tests 7-1 to 7-10 are depicted, it is evident that plate friction causes shorter samples to appear stiffer.

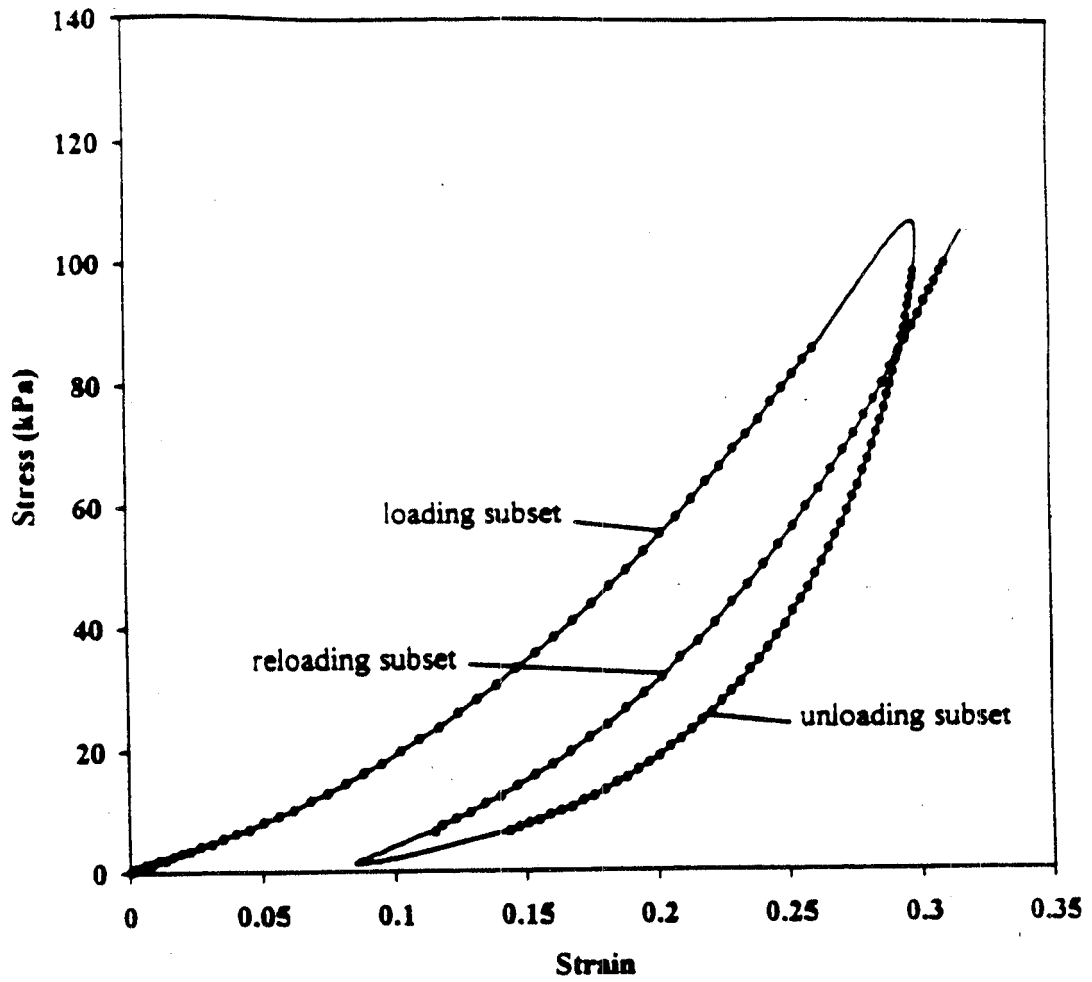


Fig. 3.11. Schematic of loading, unloading, and reloading subsets

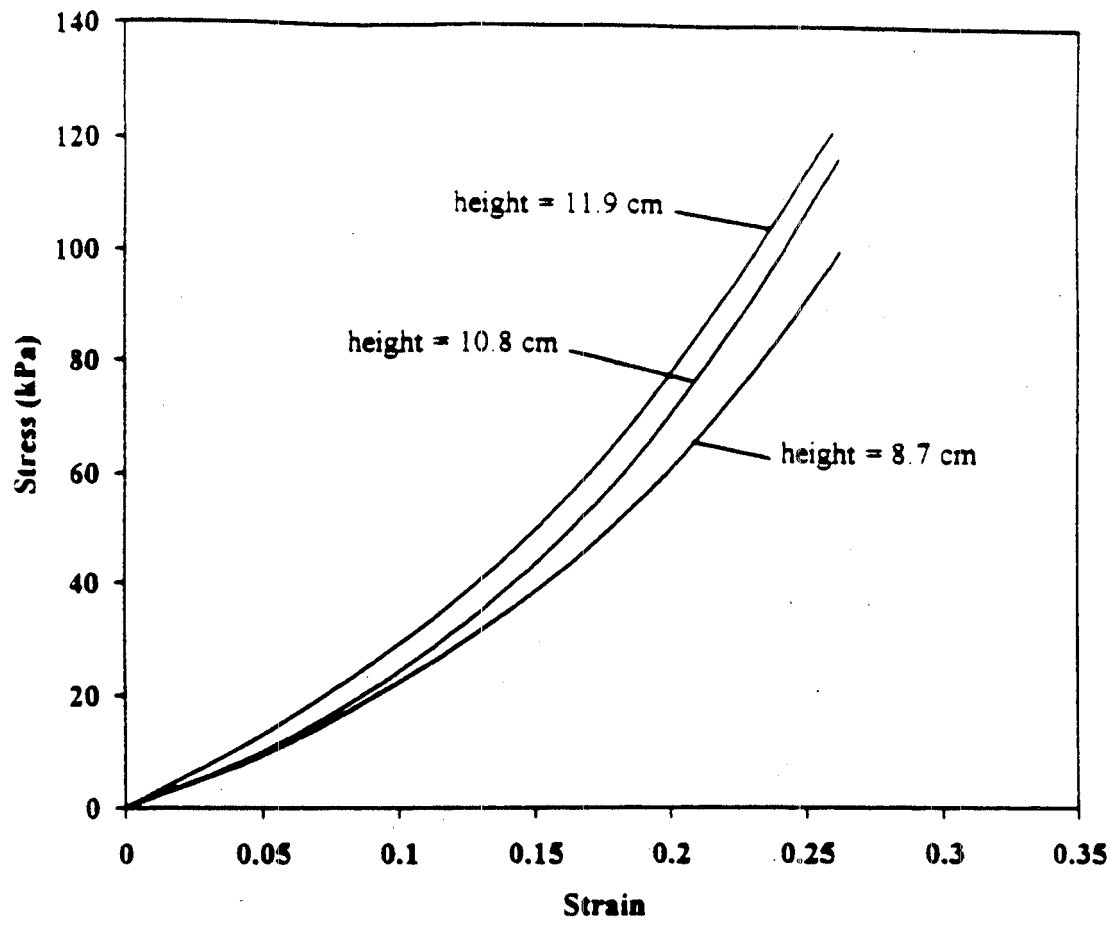


Fig. 3.12. Loading subset for constrained compression tests

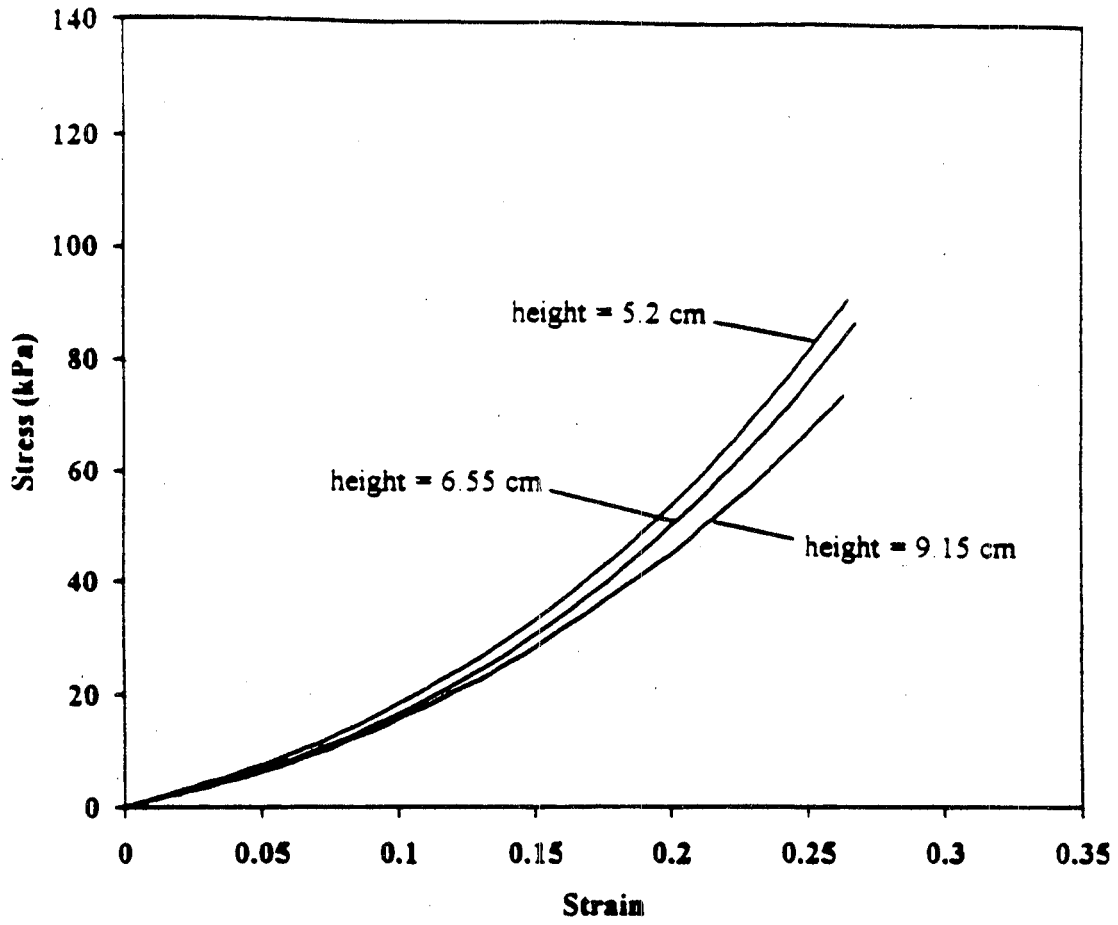


Fig. 3.13. Loading subset for unconstrained compression tests

ANALYSIS OF RESULTS

With the aim of obtaining stress-strain curves for shredded tire material that are adjusted for the effects of friction, master curves of stress vs. strain were made using the two sets of plots mentioned above.

The construction of master curves can be illustrated by considering the loading subset in the constrained compression tests, Fig. 3.12. A sequence of strain values is chosen, ascending as follows: 0.03, 0.06, ..., 0.24. For each strain value in this sequence, a plot of constant strain is superimposed on Fig. 3.12, as shown in Fig. 3.14 for four values of strain. From the intersection points of constant strain plots with the various stress-strain curves, collections of stress values are made for each strain value. Each stress value in a collection is referenced to a particular sample height. From these collections of stress values, plots of stress versus sample height may then be constructed for each strain value, and placed on a common graph, Fig. 3.15. Curves are then manually fit to the points, and extrapolated to zero-height. In these curves, these extrapolated stress values correspond theoretically to the case where no friction exists between the sample and the walls. The resulting master curve is shown in Fig. 3.16.

A plot similar to Fig. 3.15 may be constructed for the unconstrained compression tests by superimposing plots of constant strain onto Fig. 3.13, as shown in Fig. 3.17. By gathering plots of stress vs. sample height for each strain value, Fig. 3.18 is obtained. According to the earlier discussion, samples nearing infinite height in the unconstrained compression tests should have a material response almost free of the effects of boundary

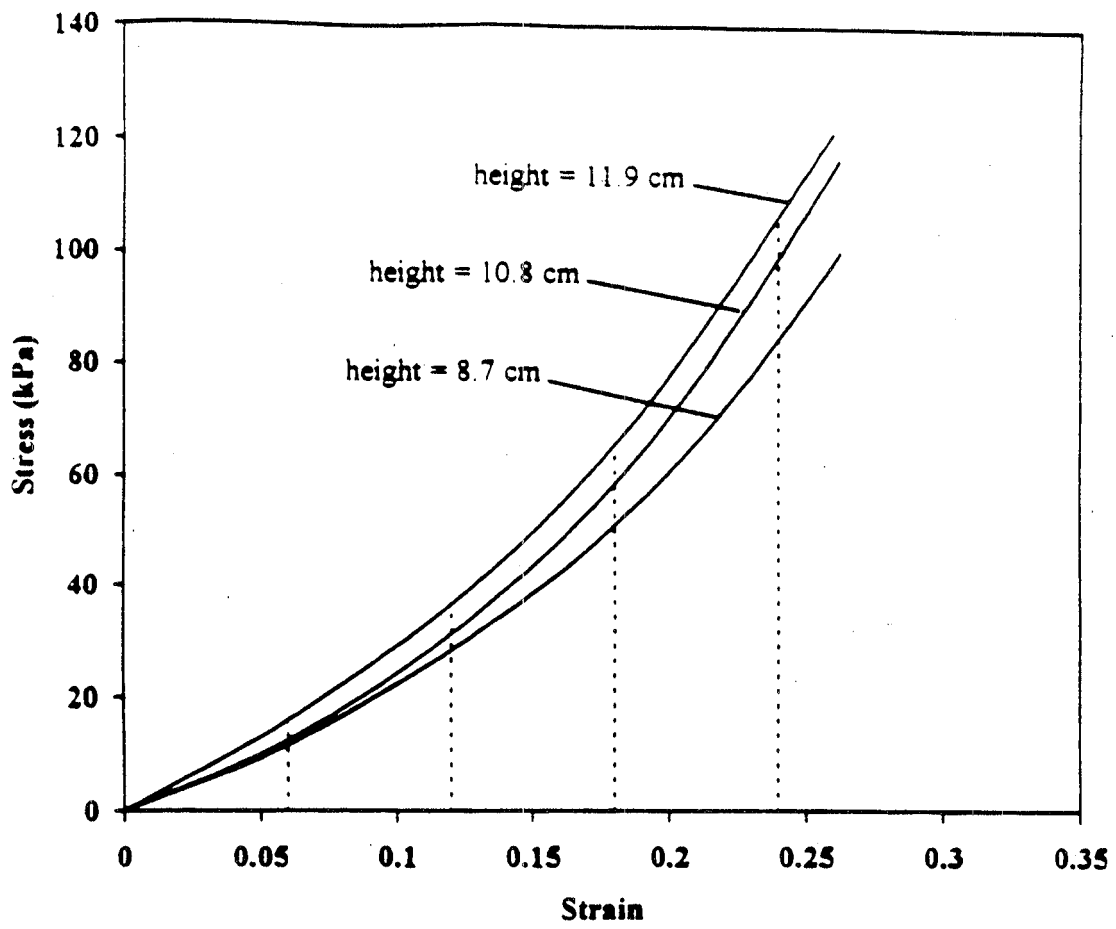


Fig. 3.14. Plots of constant strain, loading subset, constrained case

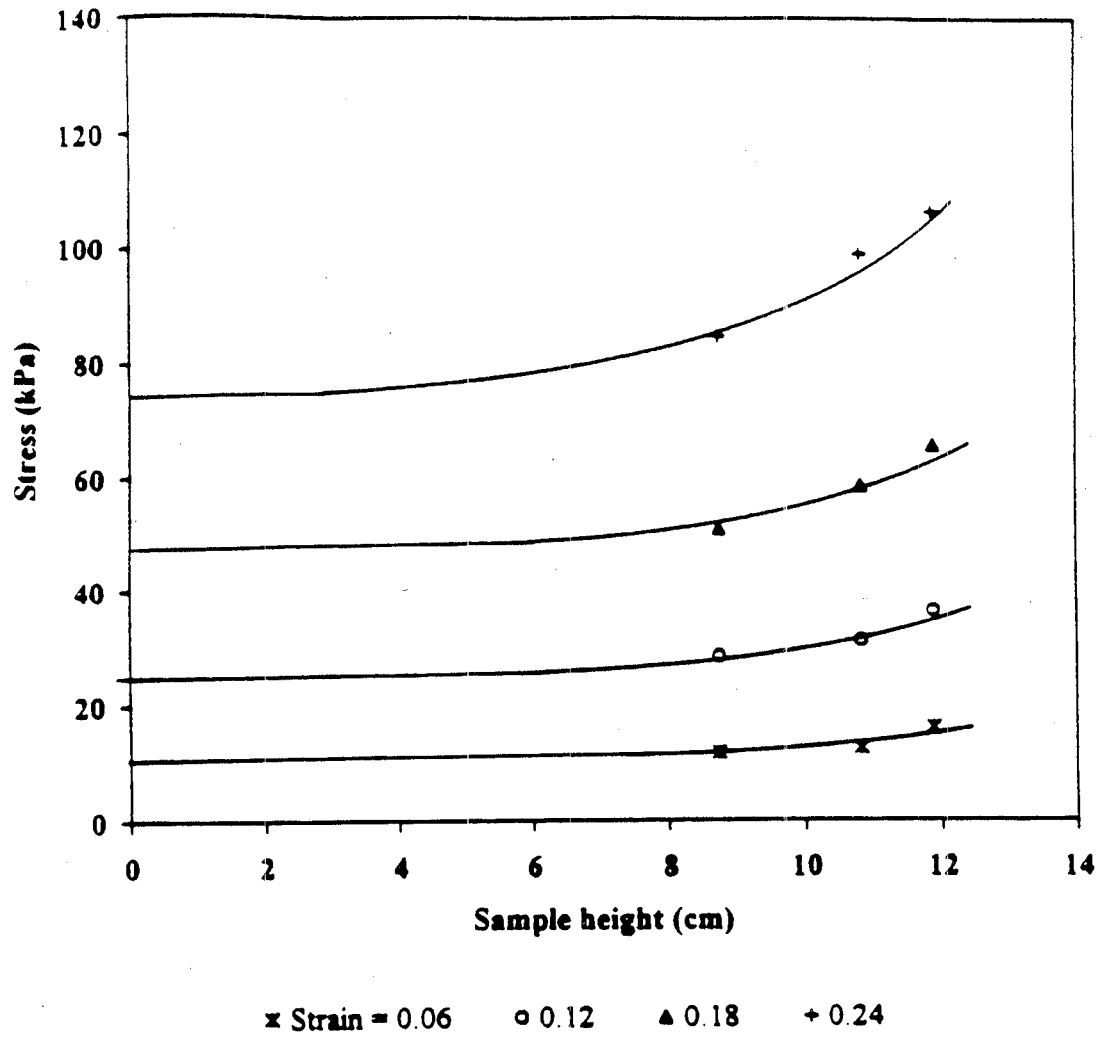


Fig. 3.15. Stress vs. sample ht., loading subset, constrained case

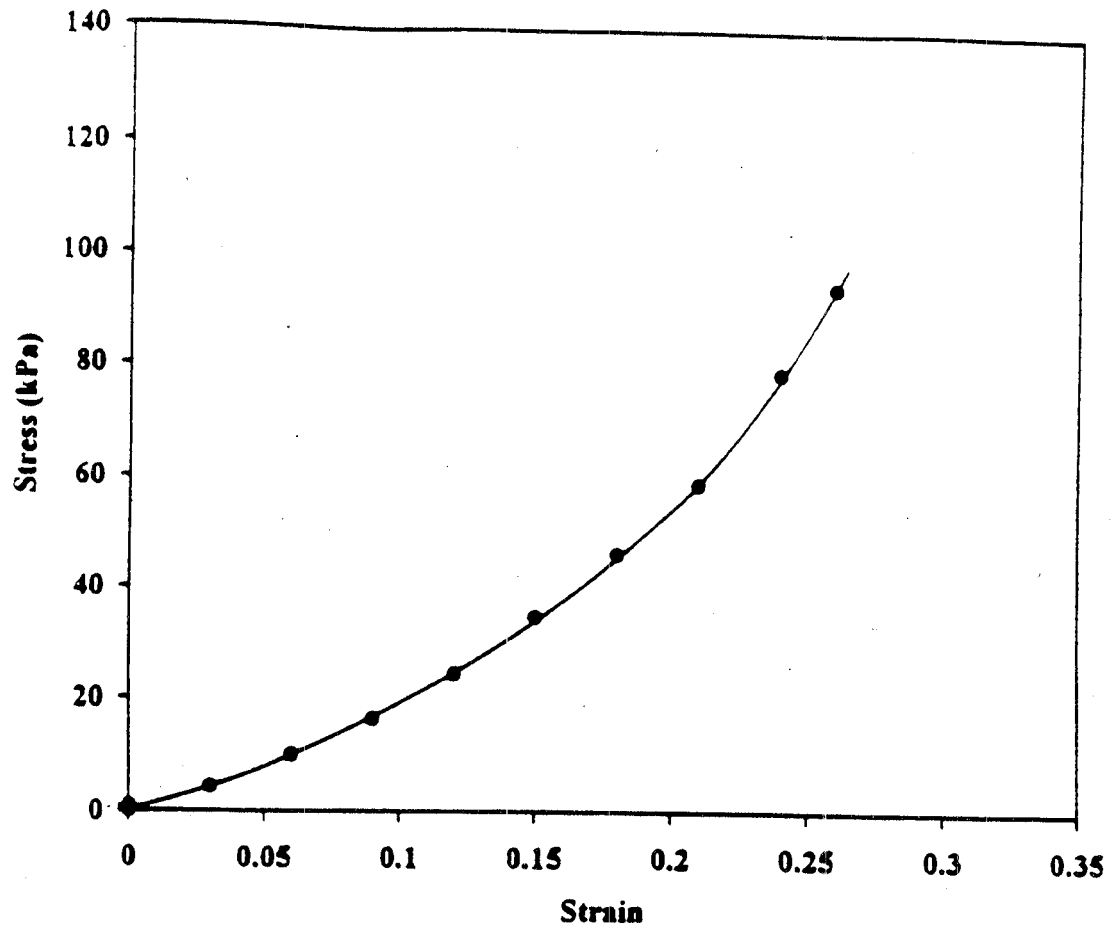


Fig. 3.16. Master curve for loading subset, constrained case

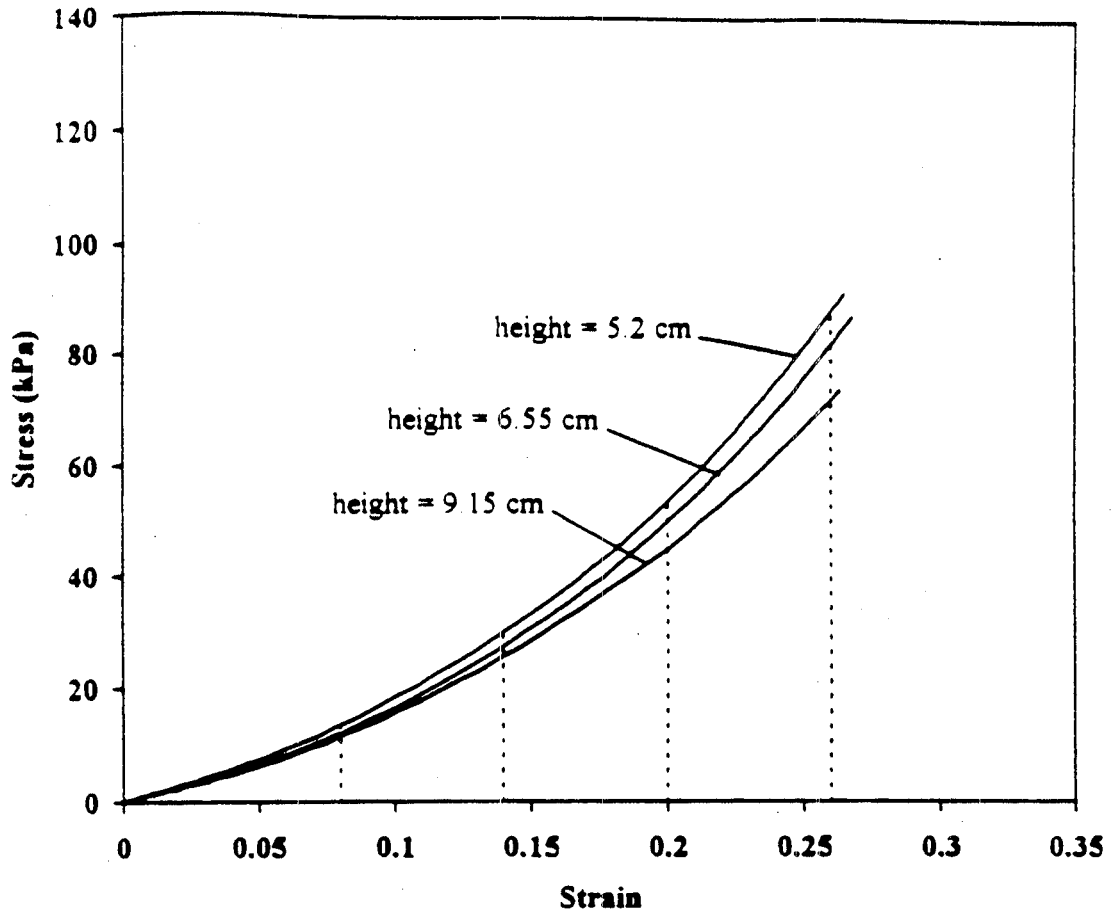


Fig. 3.17. Plots of constant strain, loading subset, unconstrained case

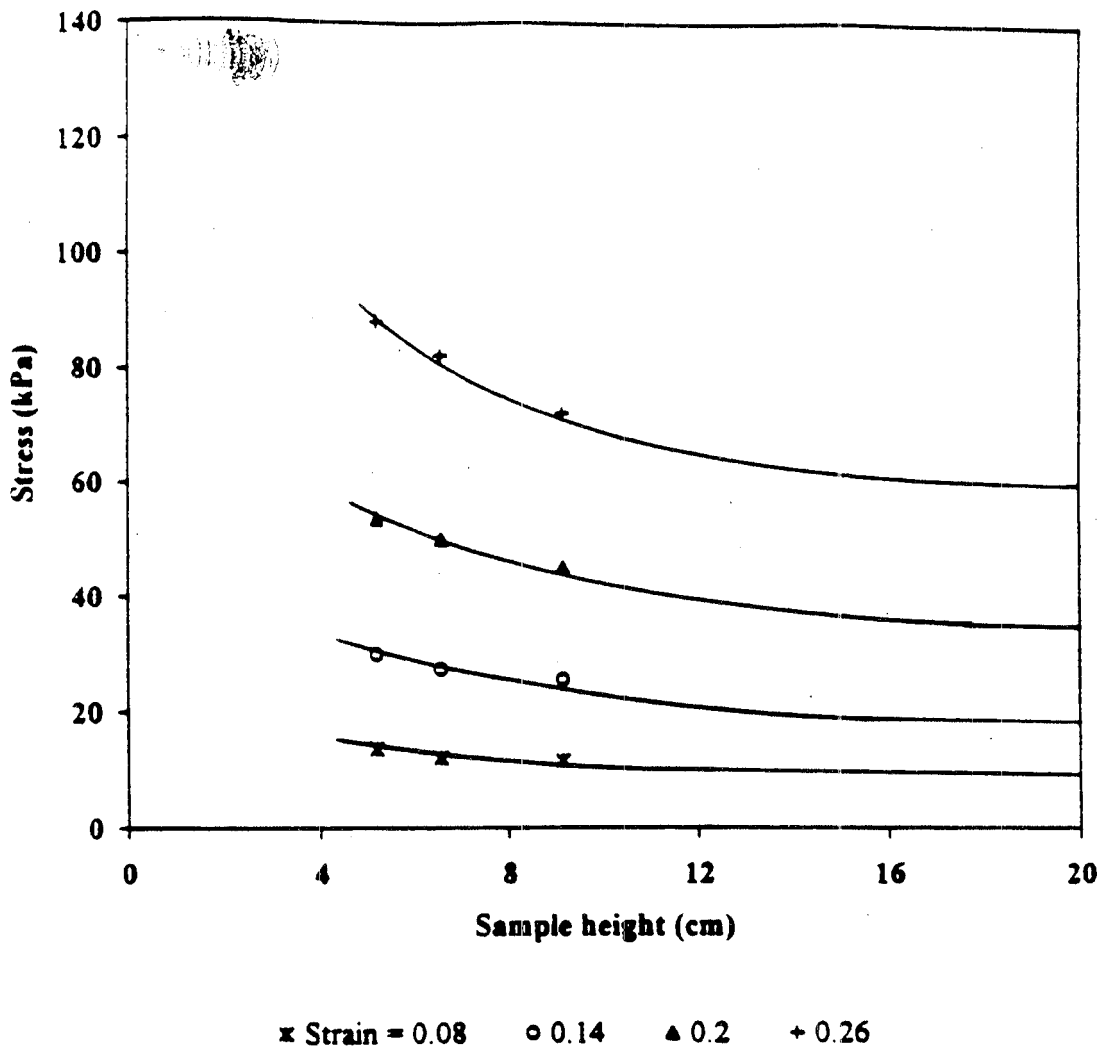


Fig. 3.18. Stress vs. sample ht., loading subset, unconstrained case

friction. This is reflected in Fig. 3.18, where, as the sample height increases, constant stress values are approached asymptotically. The so obtained master curve is shown in Fig. 3.19.

Master curves were similarly constructed for the unloading and reloading subsets of stress-strain curves for both the constrained and unconstrained compression tests. These curves are included in Figs. 3.20 and 3.21, which contain the complete master curves for the constrained and unconstrained compression tests, respectively. To connect the loading, unloading, and reloading curves together, extrapolations of the curves are shown by dotted lines. While both plots indicate stiffening with increasing stress, the constrained material appears stiffer in general than the unconstrained material. The difference in stiffness might be even more pronounced were the unconstrained samples tested at a lower density, comparable with that in the constrained compression tests.

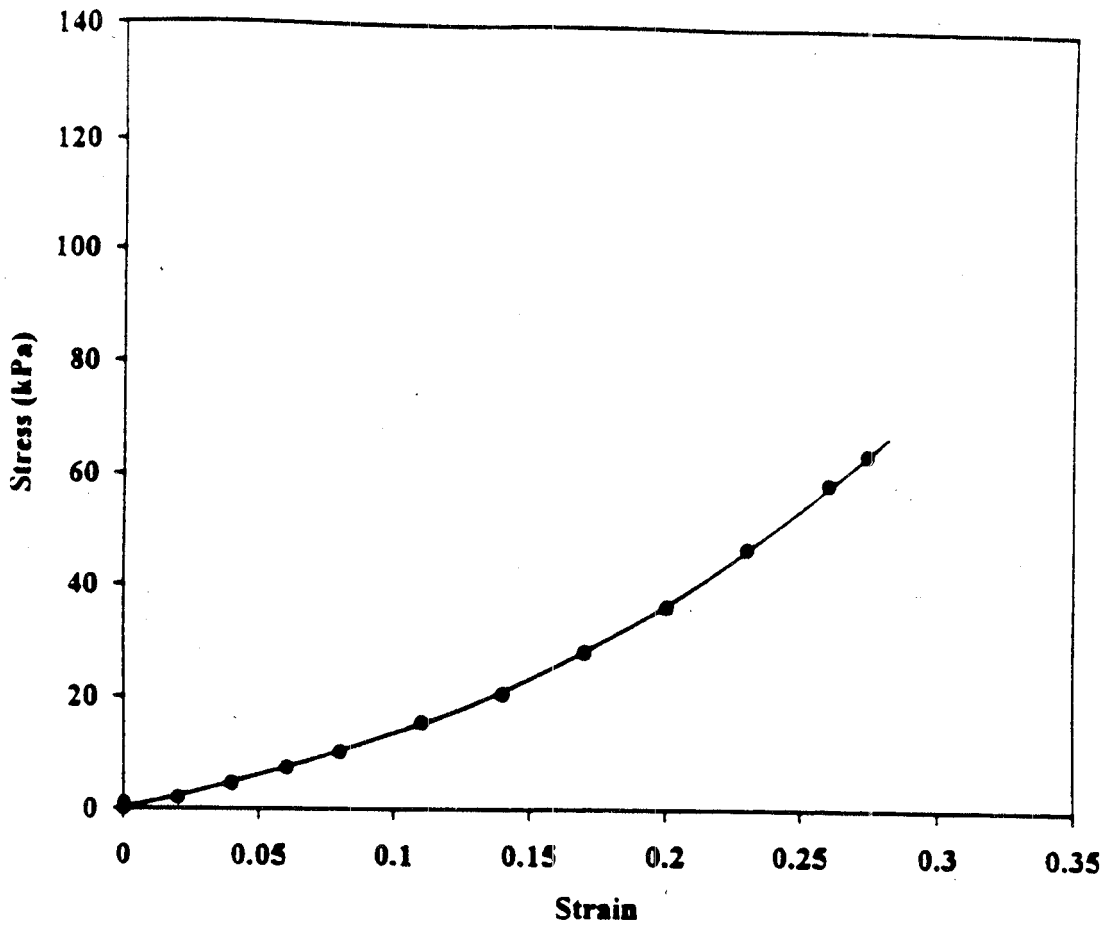


Fig. 3.19. Master curve for loading subset, unconstrained case

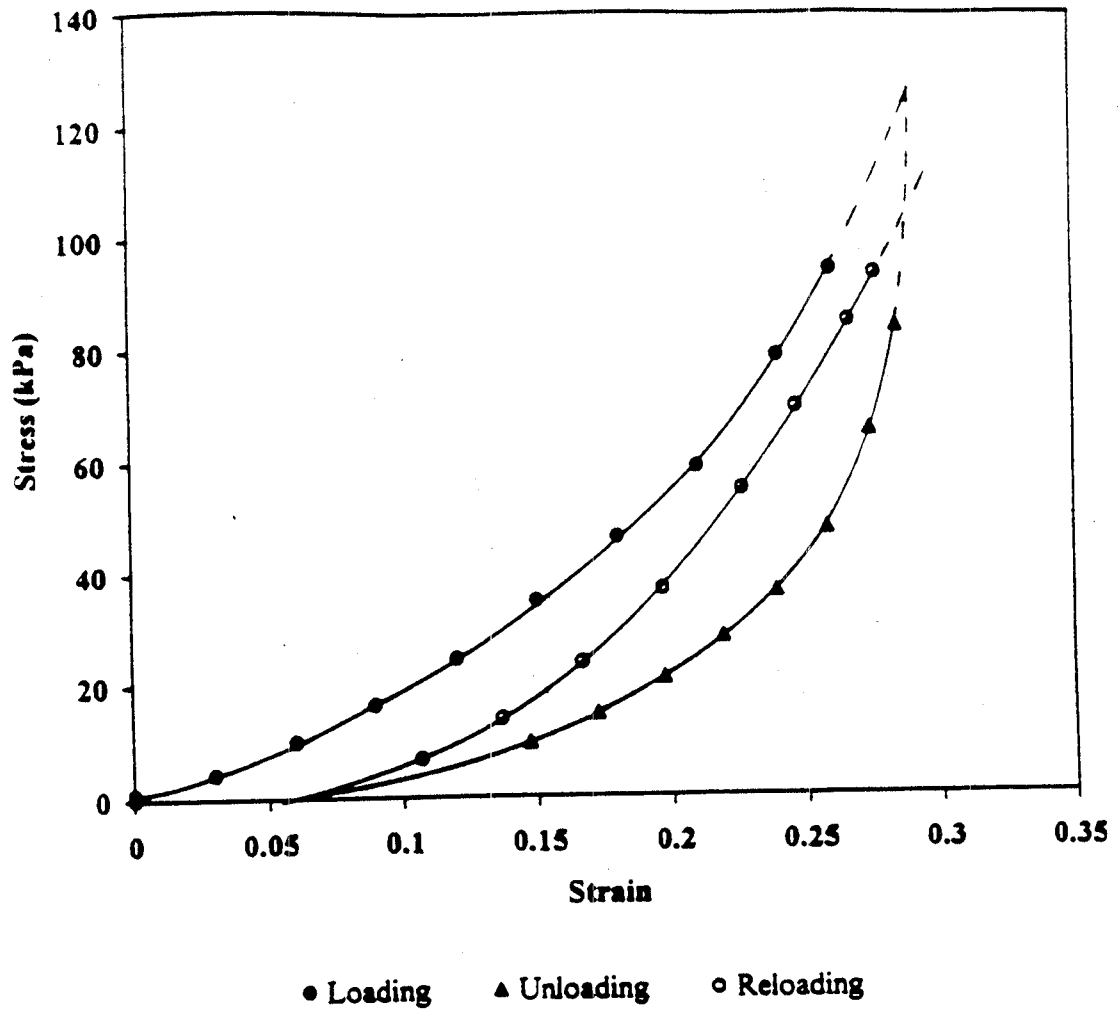


Fig. 3.20. Complete master curve for constrained compression test

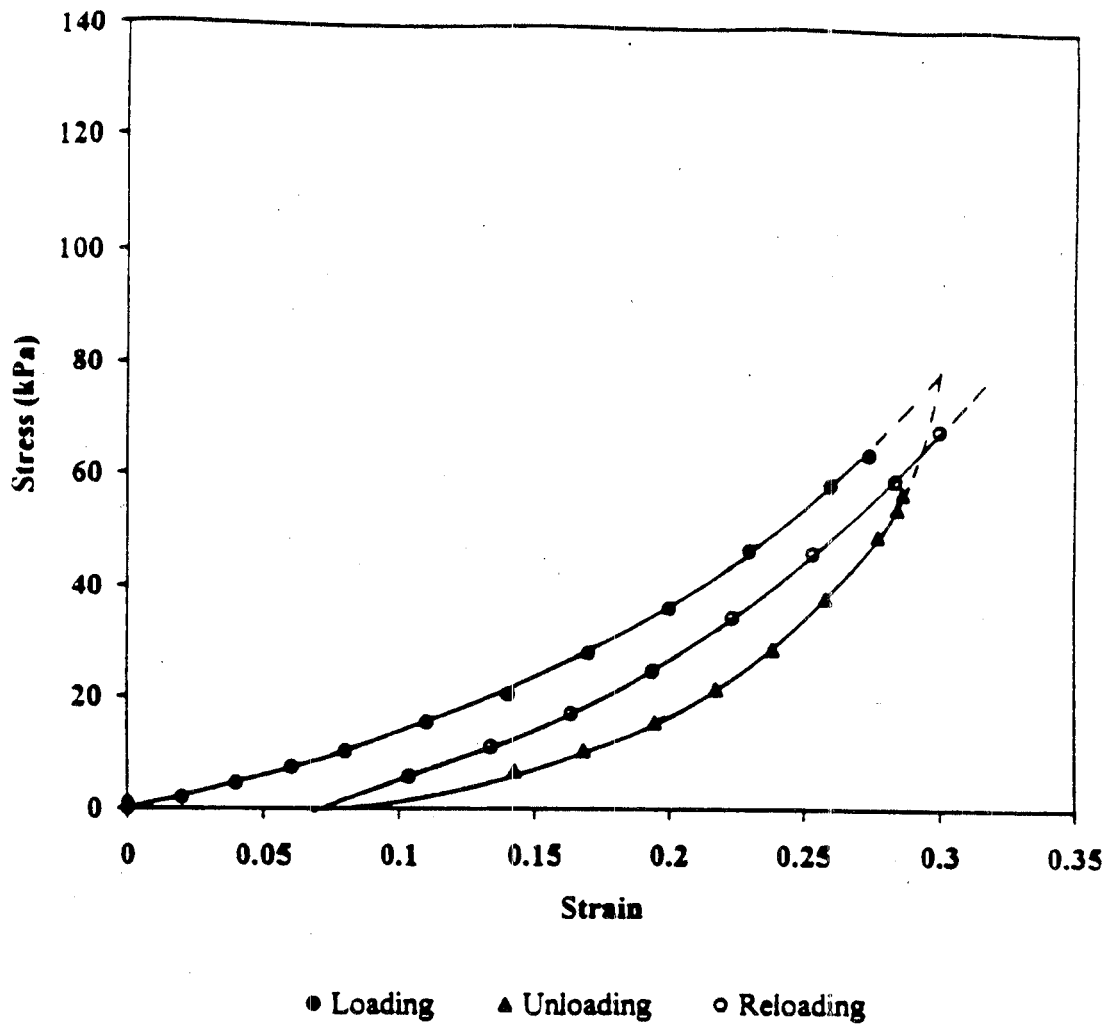


Fig. 3.21. Complete master curve for unconstrained compression test

CHAPTER 4

LONG TERM BEHAVIOR UNDER CONSTANT LOAD

INTRODUCTION

Long term settlements due to creep are a concern in the construction of shredded tire fills. Due to the viscoelastic nature of rubber, deformation of the material can be expected to increase over time. The rate with which the long term deformation occurs is important in predicting the increase of settlements and may influence the way a road is constructed. For example, after overburden material is placed above the shredded tire layer in a fill, some time is usually allowed to elapse before paving materials are applied. The length of this waiting period may be reconsidered if it is found that creep might occur at a rate detrimental to the integrity of the road.

In the past, research has mainly focused on approximating the immediate response of shredded tire material to compressive loads. Studies done for long periods of loading are scarce. A month-long constrained compression creep test was performed by Humphrey (1992), and the results indicate that creep was still occurring at a noticeable rate after 25 or more days. To obtain information on the rate of creep over a much longer period of time, tests have been conducted in this project with the aim of monitoring creep over more than one year. In the manner of the monotonic and repeated loading tests described in Chapter 3, constrained and unconstrained compression were selected as the types of tests. The experimental apparatus was different, however, as described in the following section.

TESTING APPARATUS

Principle of the Apparatus

In long-duration creep tests (up to several months or years), maintaining or controlling and correcting the applied constant load becomes a technically difficult task. Servo-controlled, motor driven screw-type, and pressure driven hydraulic-type loading frames are not suitable due to possible malfunctions. Dead-weight-type (gravity driven) loading systems are therefore superior. To apply high loads directly, high-volume weights are required, and the size of the system becomes excessively large. Weight-multiplying arrangements, which are based on the principles of levers, pulleys, and cables, are preferable.

Figure 4.1 presents the schematics of the loading system selected. It consists of a lever, fulcrum, a set of pulleys and a cable, load shaft, loading plate, and base. A dead-weight load is placed in the load box located at one end of the cable, and this force is transmitted through the cable onto the pulleys attached to the lever and base. Theoretically, the tension in each cable sector is equal to the dead weight applied. The force applied at each pulley's location is equal to the resultant of forces acting in each cable sector. The lever itself multiplies the forces acting at each pulley, which results in a force acting at the shaft that is much greater than the dead-weight at the end of the cable. The multiplication factor depends on the location of each pulley with respect to the fulcrum and the loading shaft. By adjusting the location of the pulleys, fulcrum, and the magnitude of the dead weight, a desired load on the loading shaft can easily be controlled.

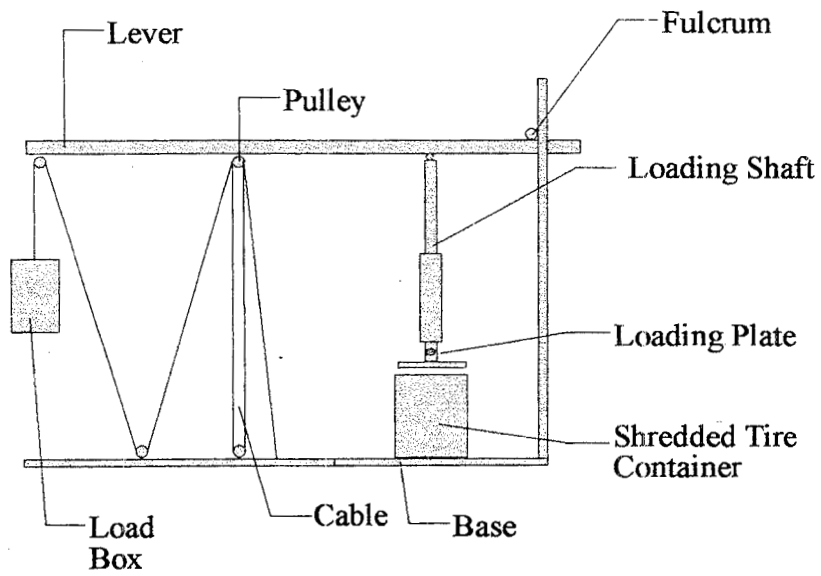


Fig. 4.1. Creep test loading system schematics

Apparatus Design

Figure 4.2 depicts the actual design of the apparatus for constrained compression, which consists of a base with a platform, one-sided lever, fulcrum, a set of pulleys and a cable, a vertical loading shaft, guide bushing, loading plate, and a load cell. Figure 4.3 shows the design of the apparatus for unconstrained compression. In this case, the applied load was designed to be less than in the constrained compression, and the pulleys and cable were not necessary. To induce force in the loading shaft, dead weights were hung by rope from the lever. Each apparatus is comprised of two identical loading units and is easily adapted for either constrained or unconstrained compression tests. For the constrained compression tests, both units were used simultaneously, whereas for unconstrained tests only one loading unit was used. The overall dimensions of the apparatus are 1.57 m (62 in.) height, 1.93 m (76 in.) length, and 0.81 m (32 in.) width, and the total weight is about 3.1 kN (700 lb.). The base, lever, and lever support are made of steel tubing. The shaft is made of steel rod, the bushing of steel pipe, and the loading plate and base platform of steel.

Full vertical transfer of load to the load shaft is not always possible if rotation of the lever about the fulcrum is allowed. With rotation, there is a component of force present that induces lateral force on the shaft. The bushing shown in Fig. 4.2 prevents this lateral force from affecting the shredded tire sample. The guide bushing is lubricated to eliminate friction. Rotation itself can be reduced by adjusting the turnbuckle at the top of the loading shaft. The turnbuckle, whose location is shown in Fig. 4.2, is threaded, and can be raised or lowered to keep the lever horizontal, thus limiting its rotation.

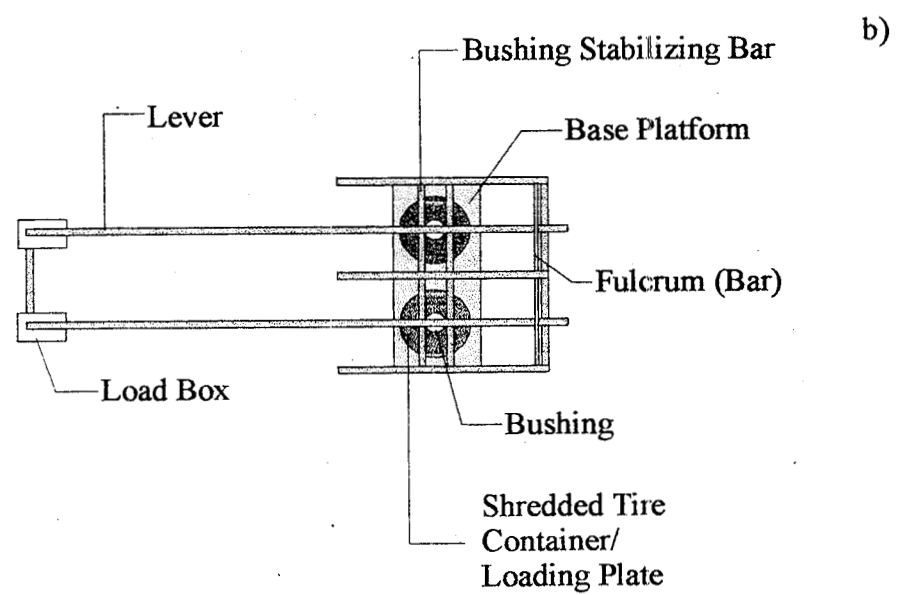
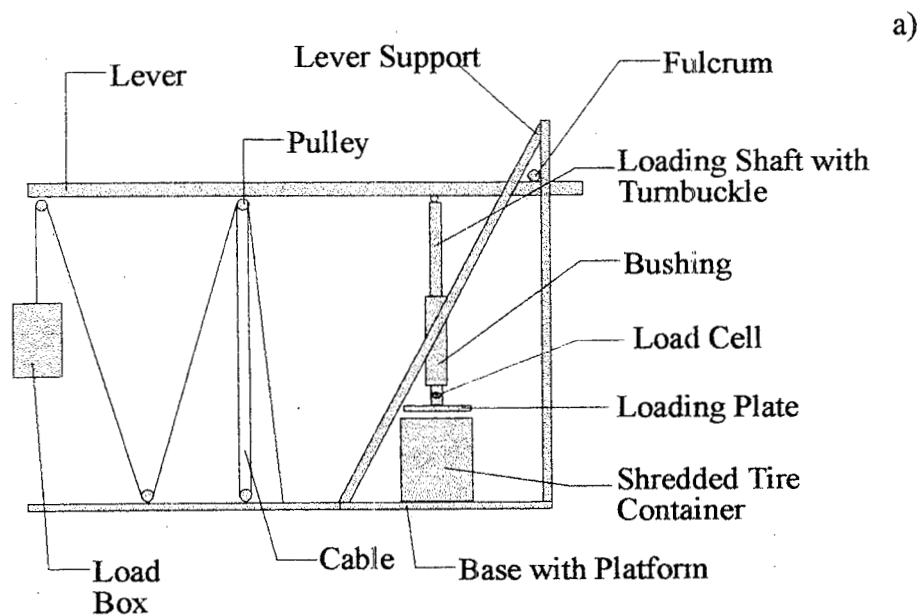


Fig. 4.2. Apparatus for constrained compression tests
 a) Elevation view
 b) Plan view

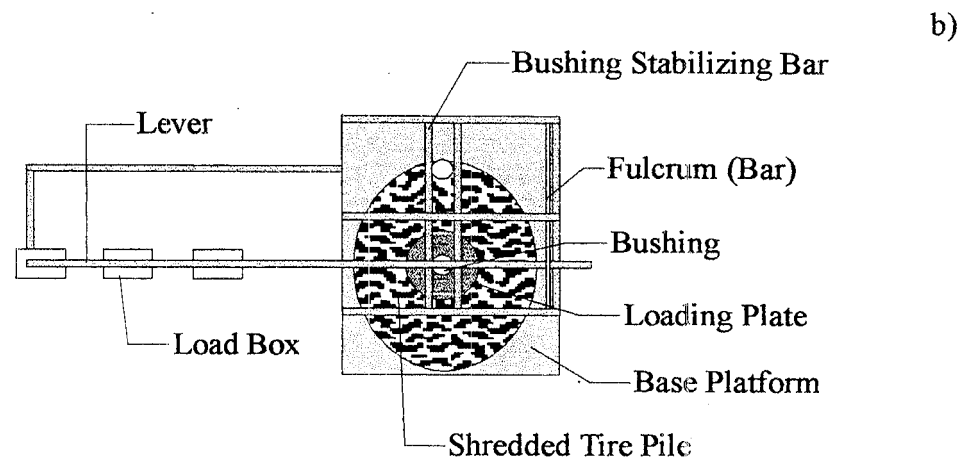
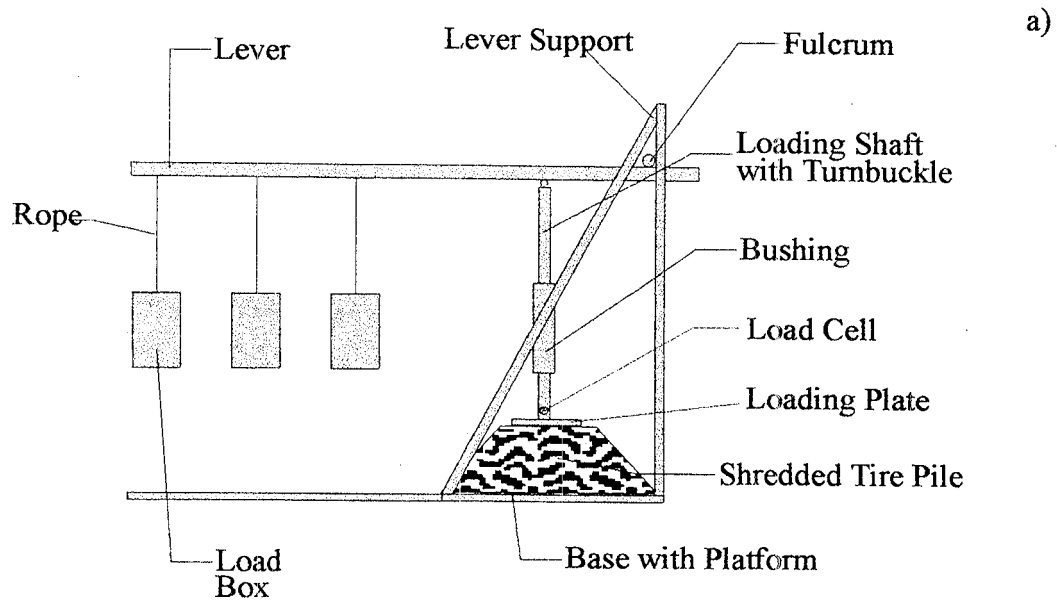


Fig. 4.3. Apparatus for unconstrained compression tests
 a) Elevation view
 b) Plan view

By using the pulley-and-cable loading system, the magnitude of the theoretically predicted force on the shaft is not guaranteed, nor does it necessarily remain constant while the shredded tire pieces creep. This is because friction in the load bearing axle of each pulley hinders the rotation of the pulley wheel. To monitor the actual load acting on the shredded tire pieces, an in-house developed load cell is placed in between the shaft and the loading plate in each loading unit.

The ring-type load cells, Fig. 4.4, have a capacity of 5000 lbs. and are instrumented with strain-gages, whose response is measured by means of a strain indicator. Calibration tests conducted using an MTS-858 Table Top System load frame indicated that the response of each load cell is linear.

MATERIAL AND TEST PROGRAM

The material used in the creep test was the 50-mm size shredded tire pieces. The constrained compression tests were conducted in the same steel container as described in Section 3.2, Fig. 3.1a. The initial heights of the samples were about 33 cm (13 in.). Similar to the repeated load tests of Chapter 3, the unconstrained compression tests were performed on a pile of shredded tires. However, the length and width of the pile was larger, namely 1.12 m (44 in.) and 0.76 m (30 in.), respectively, and the height was 0.28 m (11 in.).

The stress levels of the creep tests simulated stress levels encountered in shredded tire fills with typical overburden stress (see Fig. 3.3). Typically, material close to the edge

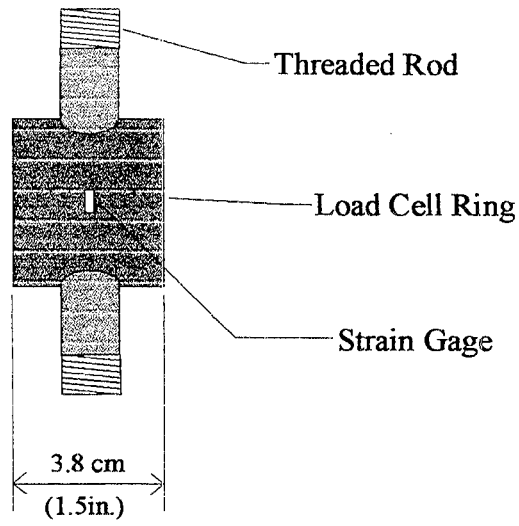
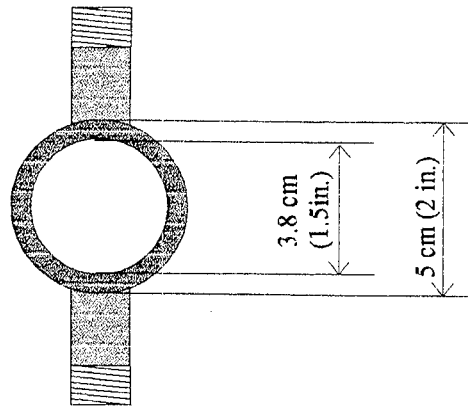


Fig. 4.4 Load Cell

of a shredded tire embankment is under less vertical stress than near the center. Also, lateral constraint becomes less with increasing distance from the center of the fill. Thus, in general, loads in unconstrained tests were conducted at lower levels of load than in constrained tests. The test matrix for the creep tests is presented in Table 4.1, and this shows the differences in stresses between constrained and unconstrained compression tests. Before the creep load was applied, the material was first compacted by subjecting it to three cycles of loading/unloading of about 15 kPa (2.2 psi).

TEST RESULTS

Data Evaluation

The axial load measured in tests, P , and the change in height of the sample, Δh , were used to calculate the average vertical stress, σ , and the average vertical strain, ϵ . For the constrained compression tests, these were calculated from equations identical to (3.2) and (3.3). The reference height h in Eq. (3.3) is the height of the sample after the completion of three compaction cycles.

For unconstrained tests, the representative vertical strains and stresses were also calculated from equations given in Chapter 3, i.e., Eqs. (3.3) and (3.4). The stress at mid-height was chosen as representative and the strains were averaged over the height.

Results

Figure 4.5 shows strain vs. time plots for typical constrained and unconstrained compression tests, where strain includes the immediate settlement due to the application of

Table 4.1. Creep Test Matrix

Test #	Type of Test	Constant Stress kPa (psi)	Test Dates	Remarks
1.	Constrained compression	84.1 (12.2)	8/26/96 - 12/2/96	*)
2.	Constrained compression	90.3 (13.1)	8/26/96 - 12/2/96	*)
3.	Unconstrained compression	41.4 (6.0)	11/2/96 - 12/2/96	*)
4.	Unconstrained compression	70.3 (10.2)	11/2/96 - 12/2/96	*)
5.	Constrained compression	48.3 (7.0)	10/16/97 - 9/30/98	
6.	Constrained compression	96.5 (14.0)	12/19/96 - 9/30/98	
7.	Constrained compression	82.7 (12.0)	12/19/96 - 9/30/98	
8.	Unconstrained compression	35.9 (5.2)	9/30/97 - 10/14/97	
9.	Unconstrained compression	42.1 (6.1)	12/19/96 - 9/24/97	
10.	Unconstrained compression	50.3 (7.3)	12/19/96 - 9/30/98	

(continued)

Table 4.1. Creep Test Matrix (continued)

Test #	Type of Test	Constant Stress kPa (psi)	Test Dates	Remarks
11.	Unconstrained compression	60.7 (8.8) 33.8 (4.9)	12/19/97 - 5/12/97 5/12/97 - 6/23/97	unloading
12.	Unconstrained compression	27.6 (4.0)	6/23/97 - 7/18/97	
13.	Unconstrained compression	31.7 (4.6)	7/22/97 - 8/1/97	
14.	Unconstrained compression	43.4 (6.3)	8/4/97 - 8/29/97	
15.	Unconstrained compression	47.6 (6.9)	9/2/97 - 9/12/97	
16.	Unconstrained compression	57.9 (8.4)	9/15/97 - 9/30/98	

*) Tests were terminated due to moistening of material as a result of a ceiling water leak.

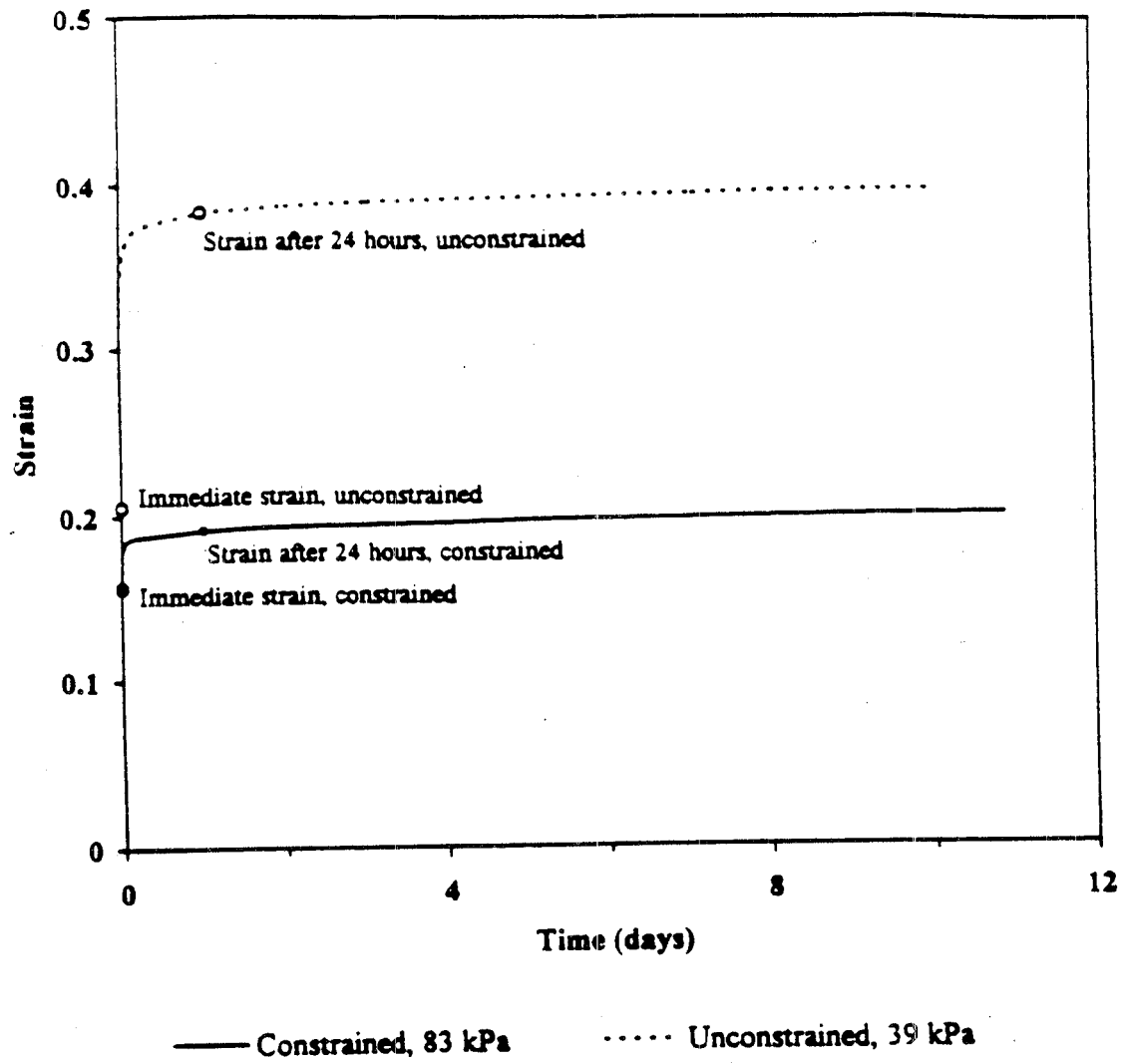


Fig. 4.5. Strain versus time (time referenced to time of load application)

load (elastic response), and the creep settlement that occurs thereafter. As the caliper and load cell readings took a short period of time to perform, the onset of creep always occurred before the first readings were taken. The first readings were taken at about 10 seconds upon loading, and the corresponding strains were considered as immediate. The creep strains were defined as strains above the value of the immediate strains. It was found from a total of eight tests conducted that the immediate strains in the constrained test were about 15%, whereas in the unconstrained test they were about 21%. This indicates clearly that the unconstrained samples underwent more immediate settlement than constrained samples even though, in general, the load was higher in the latter. In all tests, the creep settlement increased rapidly with time right after loading. The strain due to creep over the first 24 hours of loading was about 15% for unconstrained samples and about 2% for constrained samples.

Figure 4.6 shows the variation of the creep strain with time past 24 hours for the constrained and unconstrained tests. In general, creep strain in the unconstrained test was more than that for the constrained test. A pronounced decrease in strain-rate over the first few days is seen for both constrained and unconstrained tests. The strain-rate decreased sharply with time until about 30 days after loading, and fluctuated less with time thereafter. The increased rate of strain for the period from 150 to 250 days is possibly due to an increase in humidity during the summer months. A qualitatively similar increase is observed between 550 to 610 days. A temperature of about 20° C was kept constant over the entire course of the experiment, ruling out increased temperature as the cause of strain-rate fluctuations. Beyond about 250 days of loading, Fig. 4.6 indicates that the

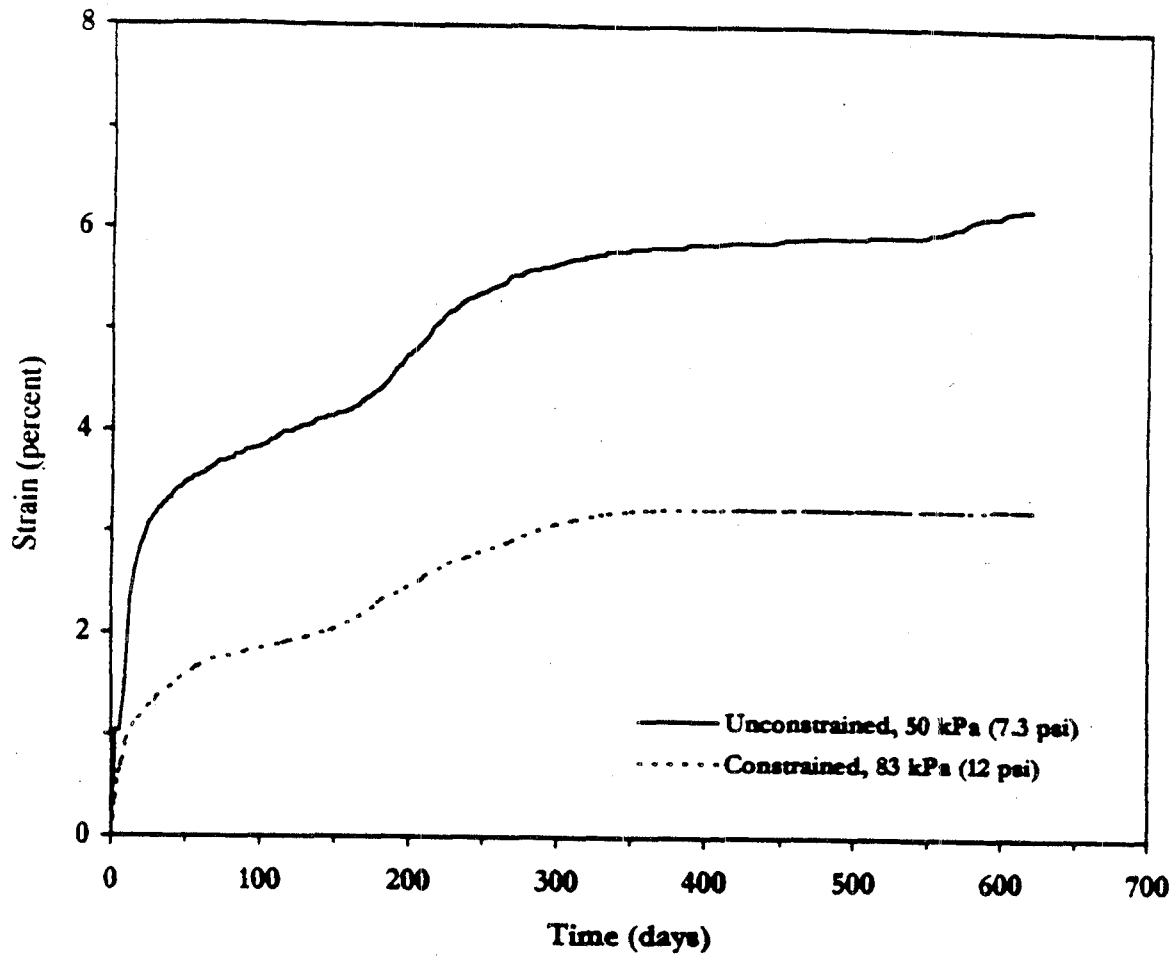


Fig 4.6 Strain vs. time (time referenced to one day after loading)

strain rates for the constrained and unconstrained tests appear to be of the same magnitude, although the rate of creep is slightly less for the unconstrained case. For the period 300 to 550 days beyond loading, the average strain-rates for the constrained and unconstrained tests were about 0.0044% and 0.0087% strain per week, respectively. Although the difference in strain-rates for this period is large, it may not be important for practical purposes because both values are small.

In Figures 4.7 and 4.8, the logarithmic plots shown depict the variation of creep strain with time beyond one day of loading. A linear regression was performed, and power law relations are shown in the figures. The corresponding equations are:

$$\text{Fig. 4.7 (constrained):} \quad \epsilon_c = 0.366t^{0.359} \quad (4.1)$$

$$\text{Fig. 4.8 (unconstrained):} \quad \epsilon_c = 1.11t^{0.278} \quad (4.2)$$

where ϵ_c is creep strain beyond 24 hours of loading, and t is time in days referenced to 24 hours after loading. It is seen that, for the first year of loading, the creep strain vs. time relation can be roughly approximated by a logarithmic relation.

Fig. 4.9 shows the average strain-rates for 30-day intervals of loading in selected unconstrained and constrained tests. The first value shown is at 30 days, which corresponds to the average daily strain rate during the period from 1 to 30 days after loading. The next value is at 60 days, which corresponds to the average daily strain rate

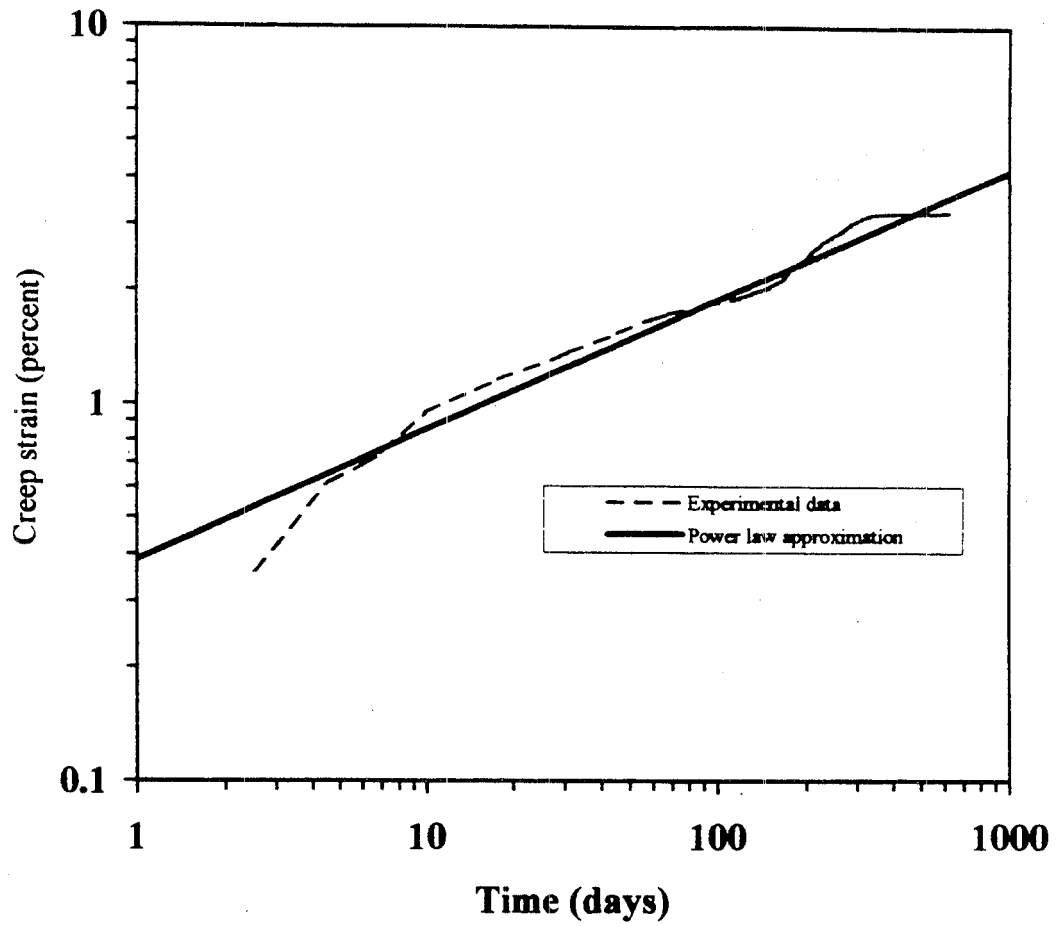


Fig. 4.7. Creep strain vs. time - Log plot - Constrained test
(time referenced to one day after loading)

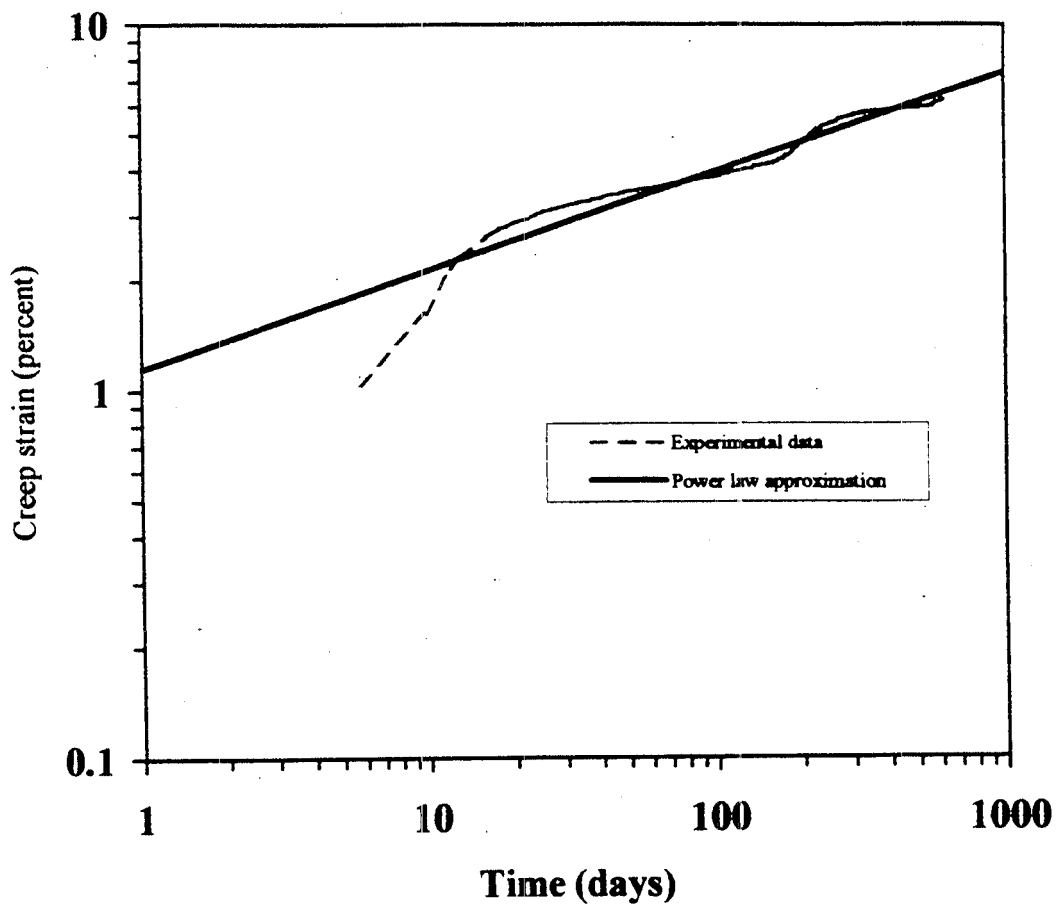


Fig. 4.8. Creep strain vs. time - Log plot - Unconstrained test (time referenced to one day after loading)

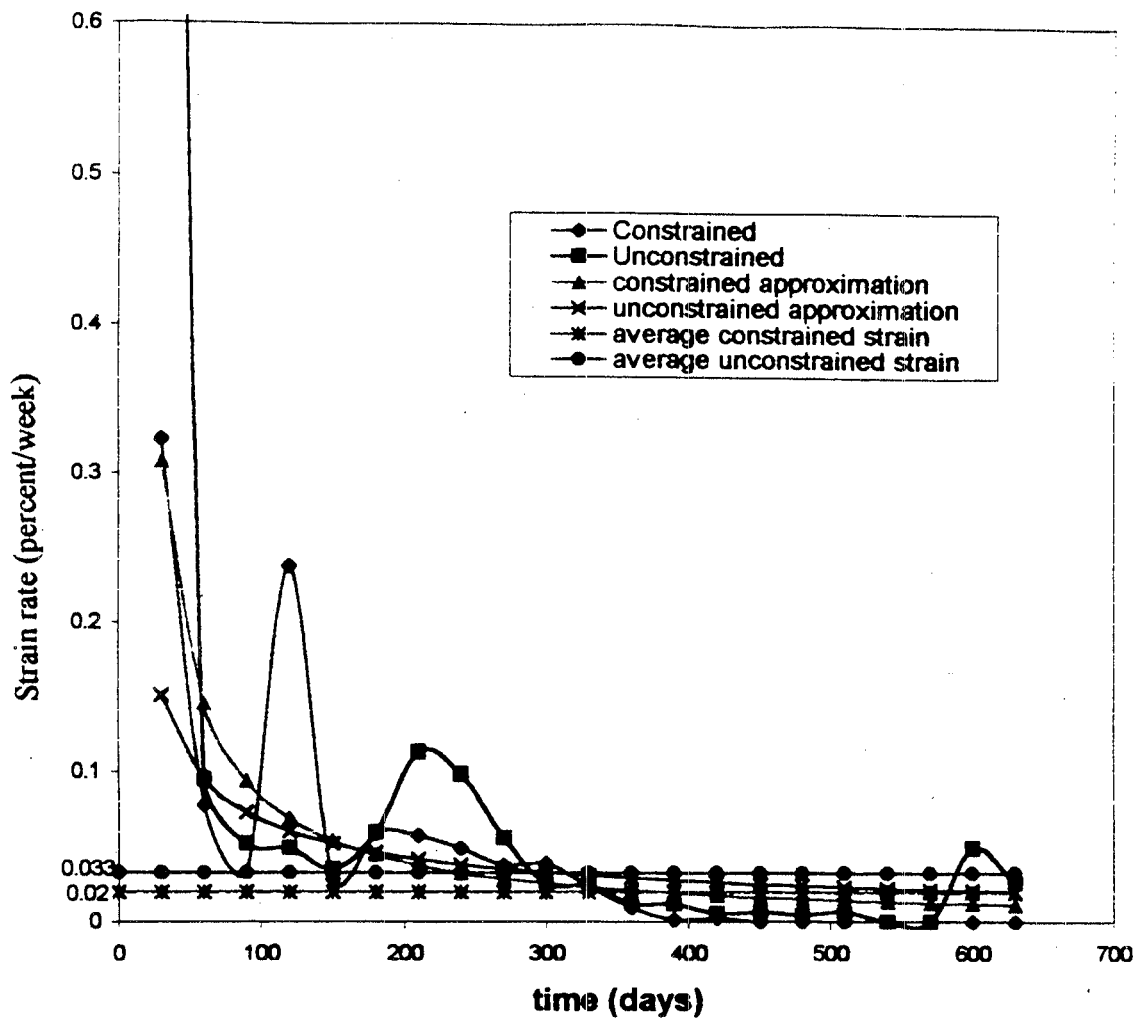


Fig. 4.9. Strain rate vs. time for 30-day intervals

during the period from 30 to 60 days after loading. The subsequent values are for similar 30-day intervals. Using a power law relation, a “best fit” line was approximated using a least-squares technique for the period from 30 to 630 days. The resulting equations are:

$$\text{Constrained} \quad \dot{\epsilon} = 12.06t^{-1.08} \quad (4.3)$$

$$\text{Unconstrained} \quad \dot{\epsilon} = 1.43t^{-3.17} \quad (4.4)$$

where $\dot{\epsilon}$ is the strain rate and t is time in days. The average strain-rate for the period from 60 to 630 days beyond loading was found to be 0.033% per week in the unconstrained creep test. In the constrained creep test, the average strain-rate for the same period was 0.02% per week. The average strain-rates for the period from 330 to 360 days beyond loading were 0.012% and 0.0093% per week for the unconstrained and constrained tests, respectively. This shows that creep was still occurring after a year of loading.

APPLICATION OF RESULTS

To illustrate the effect of creep on fill settlement, a fictitious but representative embankment can be considered, Fig. 4.10. In the middle and near the edge of the embankment, the material is assumed to behave like that in constrained and unconstrained creep tests, respectively. The stress of 83 kPa applied in the constrained tests corresponds to 3.2 m of soil over a 4.4 m layer of shredded tires in the middle of the embankment. An estimate of the creep settlement of the shredded tire layer at this location of the fill can be made by assuming that the measured average strain-rate is related to stress by

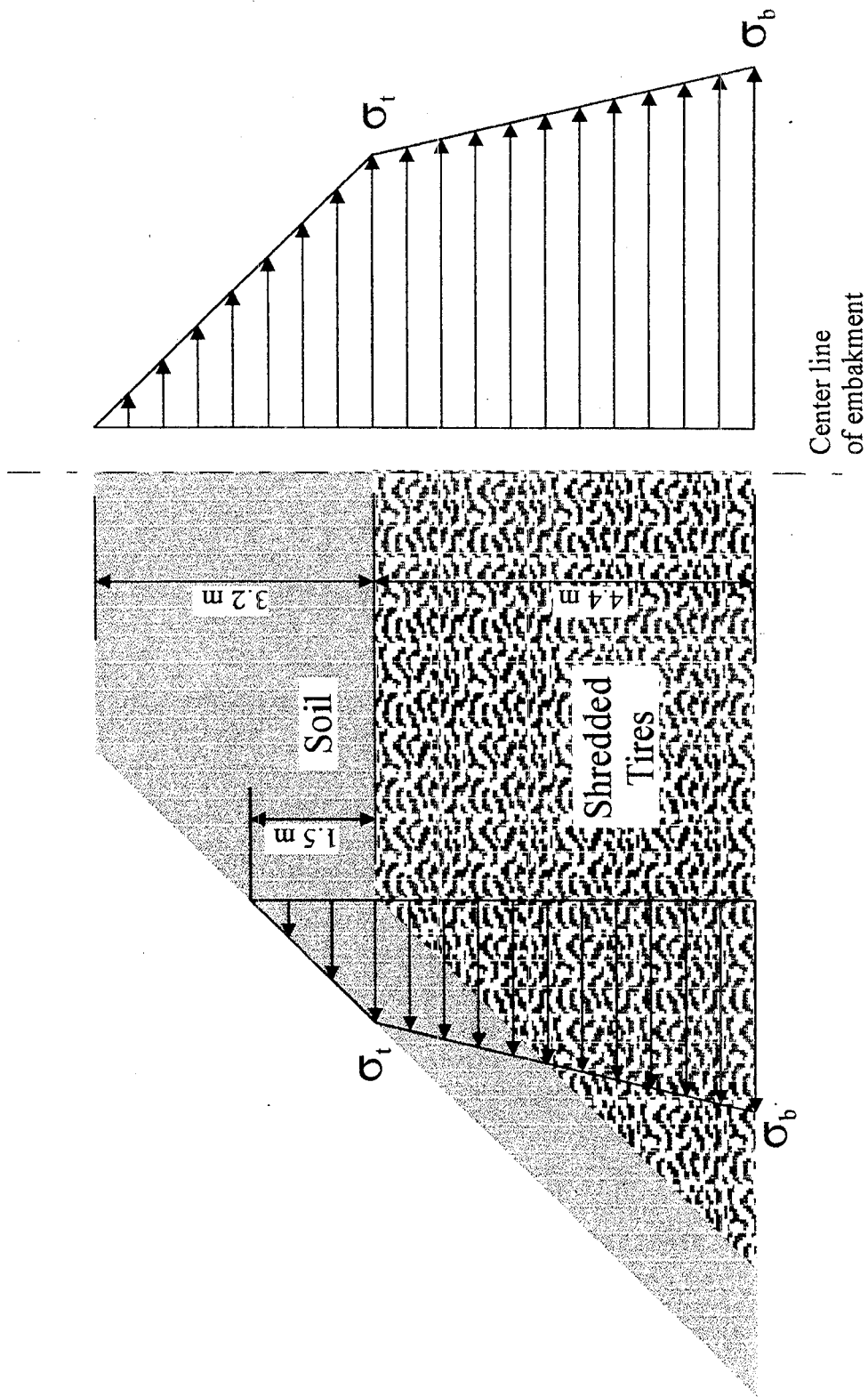


Fig. 4.10. Stress distribution in embankment

$$\dot{\epsilon} = B \sigma^m \quad (4.5)$$

where $\dot{\epsilon}$ is the strain rate for the period from 60 to 630 days beyond loading, B and m are constants, and σ is vertical stress. The vertical stress is approximated by Eq. (3.1), where stress varies linearly with depth within a layer of shredded tires, as depicted in Fig. 4.10. With the average value of strain rate (0.02% strain/week) at the bottom of the 4.4 m shredded tire layer corresponding to a stress of 83 kPa, and by assuming a value for the constant m in Eq. (4.5), the constant B is found. For instance, for $m = 0.5$, $B = 0.00219$, and for $m = 1.0$, $B = 0.00024$. Since the stress is assumed to vary linearly with depth, an average strain rate for the shredded tire layer, $\dot{\epsilon}_{av}$, can be found by

$$\dot{\epsilon}_{av} = \frac{\int_{\sigma_t}^{\sigma_b} B \sigma^m d\sigma}{\sigma_b - \sigma_t} \quad (4.6)$$

or

$$\dot{\epsilon}_{av} = \frac{B}{m+1} \frac{\sigma_b^{m+1} - \sigma_t^{m+1}}{\sigma_b - \sigma_t} \quad (4.7)$$

where σ_t and σ_b are the vertical stresses at the top and bottom of the shredded tire layer, respectively. In the center of the fill, $\sigma_t = 63$ kPa (9.1psi) and $\sigma_b = 83$ kPa (12psi). In Figure 4.11, strain rates calculated according to (4.5) are plotted as a function of stress for $m = 0.5$ and $m = 1$. If the average strain rate calculated in (4.7) is used for the whole

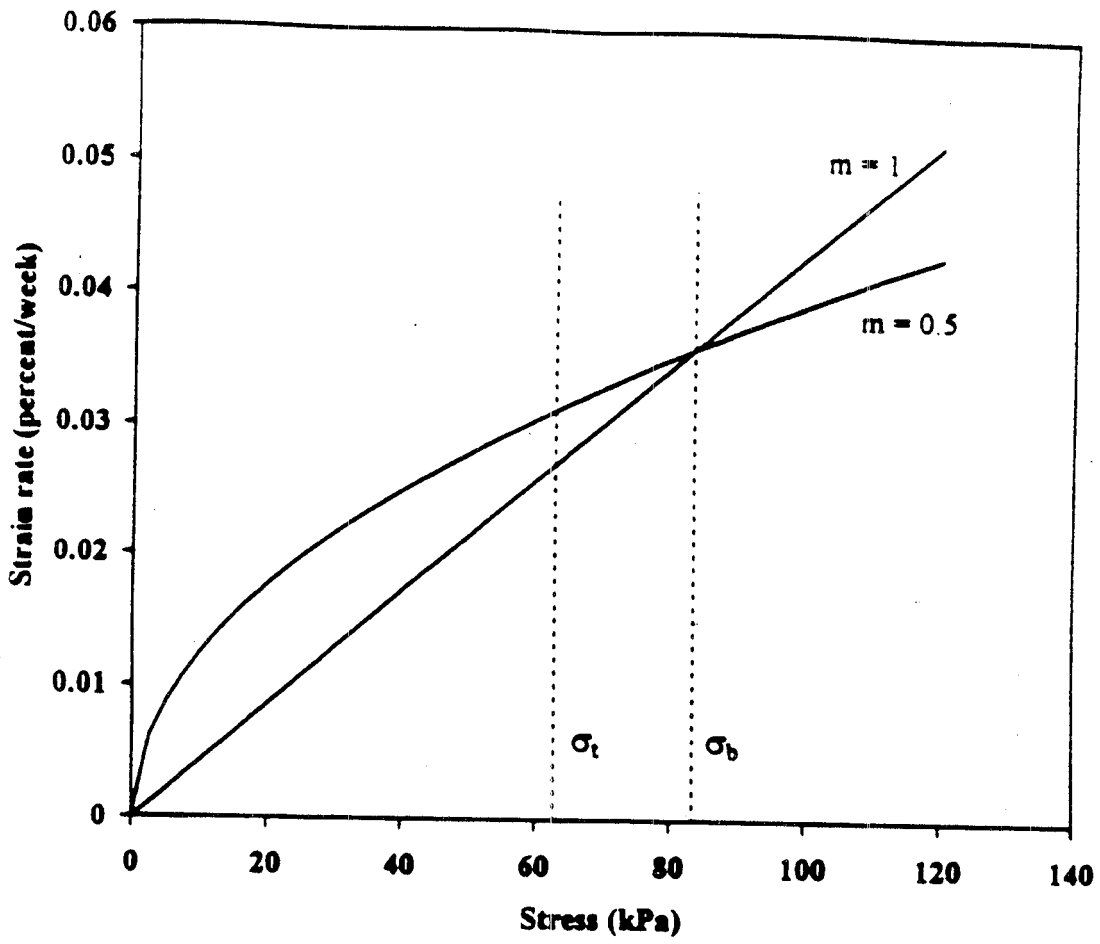


Fig. 4.11. Strain-rate as a function of stress for material in center of embankment

shredded tire layer, the settlement due to creep in the middle of the embankment is 4.02 cm/year (1.6 in/year) for $m = 1$, and 4.3 cm/year (1.7 in/year) for $m = 0.5$.

A similar calculation can be made for material near the edge of the embankment shown in Fig. 4.10, where the stress at the bottom of the shredded tires layer is 50 kPa as in the unconstrained test. The constant B in (4.5) is found as $B = 0.00467$ for $m = 0.5$ and, $B = 0.00066$ for $m = 1$ using a stress of 50 kPa and a corresponding strain rate of 0.033% per week. With $\sigma_t = 29$ kPa (4.2psi) and $\sigma_b = 50$ kPa (7.2psi), the average strain rate calculated from (4.7) is used for the whole layer of shredded tires. The settlement due to creep near the edge of the embankment is calculated as 5.9 cm/year (2.3 in/year) for $m = 1$, and 6.7 cm/year (2.63 in/year) for $m = 0.5$. Even though these calculations are approximate, they demonstrate the order of magnitude of creep settlements of shredded tire fills. These calculations have been summarized in table 4.2.

Table 4.2. Application of Results Summary

	Constrained Case		Unconstrained Case	
M	0.5	1	0.5	1
B	0.00219	0.00024	0.00467	0.00066
σ_t	63 KPa		29 KPa	
σ_b	83 KPa		50 KPa	
$\dot{\epsilon}_{av}$	4.3 cm/yr (1.7 in/yr)	4.02 cm/yr (1.6 in/yr)	6.7 cm/yr (2.63 in/yr)	5.9 cm/yr (2.3 in/yr)

One year creep results are presented in Heimdahl and Drescher, 1998.

CHAPTER 5

ANISOTROPY EXPERIMENTS

INTRODUCTION

In most road constructions utilizing shredded tire pieces, the material is brought in place by hauling tracks and dumped freely. This produces a more or less random and loose structure of the material. The action of compacting equipment, e.g., a bulldozer, causes the shredded tire pieces to rearrange, leaving most of them aligned horizontally. This is clearly visible when large shredded tire pieces are used, and results in a layered structure of the fill.

With the increase of the thickness of the shredded tire fill, or with the covering of the fill by a thick layer of soil, the resulting high overburden pressure may cause the originally curved large pieces to flatten. Figure 5.1 demonstrates this schematically. The two unloaded pieces are like opposing arches, with facing concave surfaces. Once weights are applied, the arches nearly collapse, and two flat layers result. This effect enhances the formation of the layered structure discussed above. In a fill, shredded tire material that is subject to overburden stress forms layers that are not necessarily horizontal, but slightly inclined, with curved or s-shaped pieces, as shown in Fig. 5.2. However, due to the random orientation of the pieces, the bulk material behaves as if it were comprised of horizontal layers.

Materials that are layered tend to display different load response in different directions. For example, plywood has several layers of wood pressed together with alternating directions of wood grain between layers, Fig. 5.3. A close view of a layered material is shown in Fig. 5.4. The stiffness through the layers (z-direction) is different

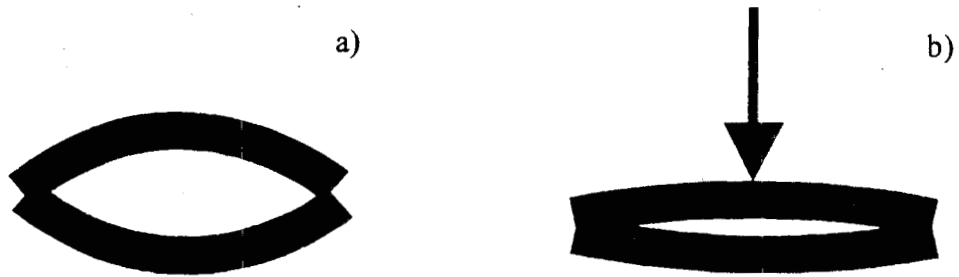


Fig. 5.1. Flattening of shredded tire pieces
a) before loading
b) after loading

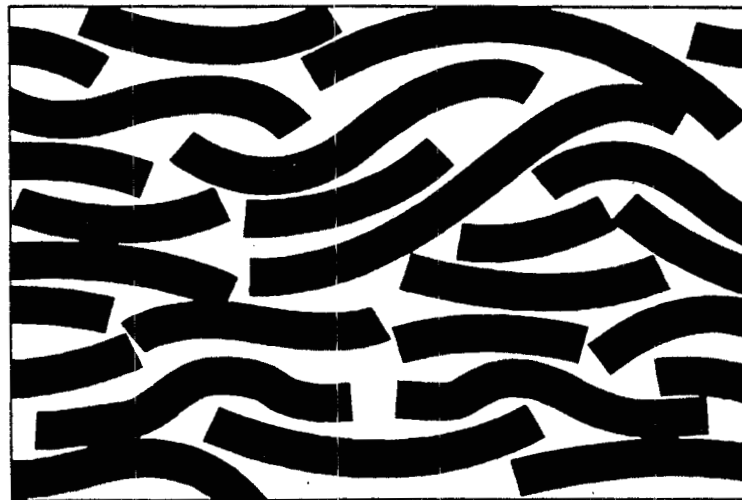


Fig. 5.2. Overlapping layers in shredded tire material

than the stiffness in directions parallel to the x,y-plane. In compacted shredded tire material, the overlapping layers may produce a similar effect. A material with different response in different directions is termed anisotropic, as opposed to isotropic for materials whose response is the same in all directions. A particular type of anisotropy relevant for the shredded tire fill is termed transverse isotropy: in all directions parallel to a plane the response is the same, and in all other directions it is different.

In the design of roads, shredded tire material is currently modeled as isotropic. This assumption may lead to errors in calculating settlements of roads with fills displaying layered structures. As no data are available regarding the anisotropic properties of compacted and stressed shredded tires, no assessment can be made as to the magnitude of these errors. Thus, exploratory laboratory experiments on samples of shredded tires were conducted in this project with the aim of investigating the response to load in two directions: parallel and perpendicular to the direction of compaction. The tests were carried out in a novel testing apparatus termed the biaxial apparatus.

TESTING APPARATUS

Principle of Biaxial Apparatus

If a uniaxial compression test is performed on a shredded tire sample, measuring the lateral displacement in a direction with no confinement is problematic. The irregularity of the exposed surfaces makes it difficult to establish a reference plane or point from which to determine displacements. Thus, true strains cannot be found, and it is necessary to find another means by which the elastic parameters can be found. Experiments in which rigid lateral confinement is provided allow for the measurement of

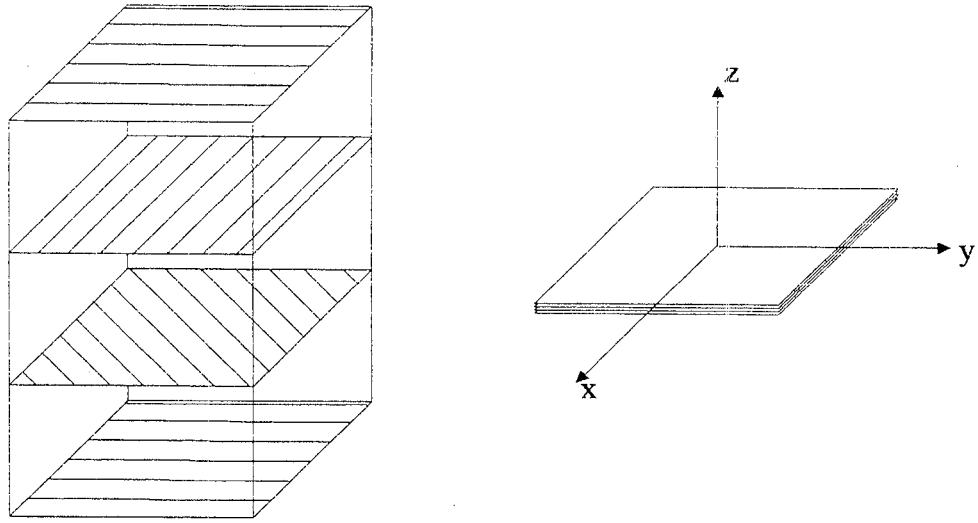


Fig. 5.3. Plywood

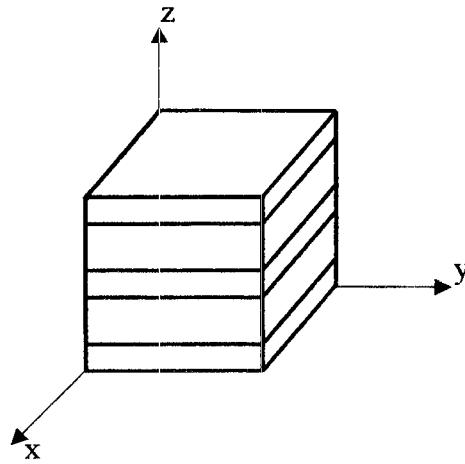


Fig. 5.4. Layered material

force in directions opposite to loading. Thus, corresponding normal stresses may be determined for a sample of known dimensions. Also, displacements in the confining directions may be measured and strains may be calculated accordingly. Suitable for compression tests on shredded tire material, tests performed with the biaxial apparatus involve the confinement of at least four sides of a six-sided prismatic test sample.

The biaxial apparatus developed for this project is designed to apply compression to a shredded tire sample in two perpendicular directions. Measurements of force and displacement in these two directions are possible. By initially compacting a shredded tire sample in one direction and by applying subsequent forces in both directions, compaction and in-situ stresses as well as stress changes in the shredded tire material can be simulated. From forces and displacements the stresses and strains can be deduced, thereby allowing for the examination of the anisotropy that may exist in shredded tire material.

Figure 5.5 shows a schematic of the biaxial apparatus. A prismatic sample of shredded tires is confined by six rigid walls, four of which are shown in the figure. The two remaining walls not represented in Fig. 5.5 are parallel to the plane of the page. Two of the four walls shown in Fig. 5.5 (3 and 4) and the two walls parallel to the page are fixed, whereas the two remaining walls (1 and 2) can move horizontally and vertically, respectively. If no friction exists between the sample and the walls, biaxial or one-dimensional compression can be induced in the material, with the directions of principal stresses and strains fixed in space. When the two walls parallel to the page are removed, a plane-stress condition is induced.

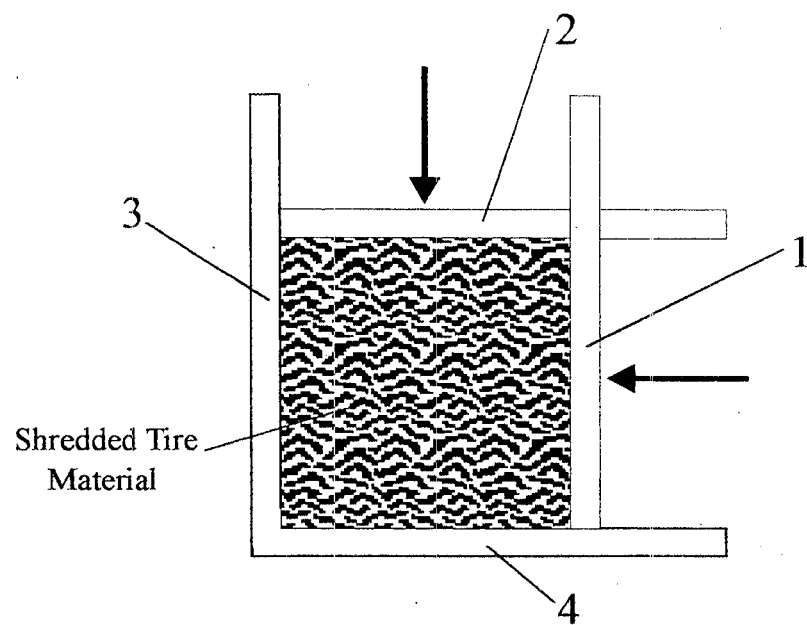


Fig. 5.5. Schematic of Biaxial Apparatus

Design of the Biaxial Apparatus

In Fig. 5.6, the biaxial apparatus is depicted. The frame of the apparatus consists of four walls constructed from 10 or 11 steel bars which are 1370 mm (54 in.) long and 12.5 mm by 50 mm (0.5 in. by 2 in.) in cross-section. In each wall, the bars are parallel and separated by washers and the adjacent bars of perpendicular walls, producing gaps slightly wider than the thickness of the bars, Fig. 5.7a; the resulting arrangement can be termed bar/gap-stacked. The bars are connected by tie rods and bolted threaded rods, and the corners of the frame are stiffened by steel truss-like struts. The outside dimensions of the rectangular frame with supporting legs are 1370 mm (54 in.) in width, 760 mm (30 in.) in depth, and 1830 mm (72 in.) in height.

The frame of the apparatus provides support for the two moving walls: one horizontal and one vertical. These are made of the same long steel bars as the frame, bar/gap-stacked by spacers and washers, and tied by rods and bolts, Fig. 5.7b. The alternating bar/gap arrangement of bars allows for the walls to move independently in two directions, with no interference with the frame walls, Fig. 5.8. The two moving walls are guided by THK SR-30W linear glides that move on stainless steel tracks attached to the frame, Fig. 5.6. The vertically moving wall is raised and lowered by winches, which have cables attached to either end of the wall.

A prismatic sample of shredded tires of approximate dimensions 330 mm (13 in.) in height, 370 mm (14.5 in.) in width, and 300 mm (12.0 in.) in depth, is placed inside the space created by two of the fixed walls of the frame and the two moving walls. Samples can be compacted to as small as 190 mm (7.5 in.) in height and 230 mm (9 in.) in width. The material may be confined on the remaining two sides by two 13 mm- (0.50 in.-) thick

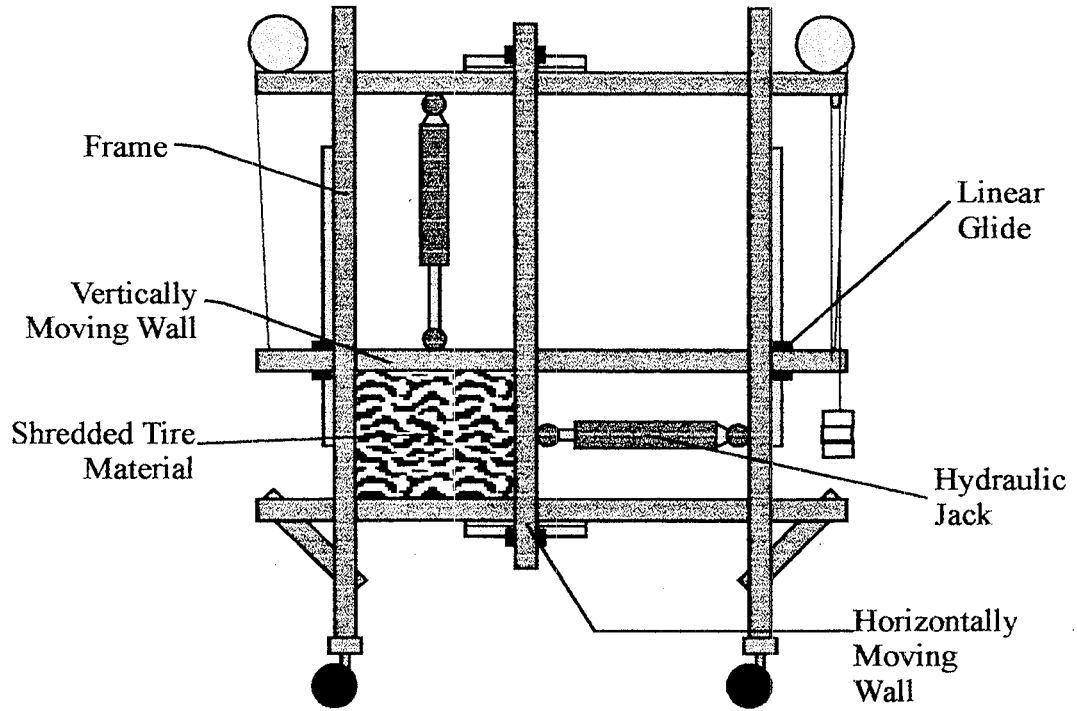
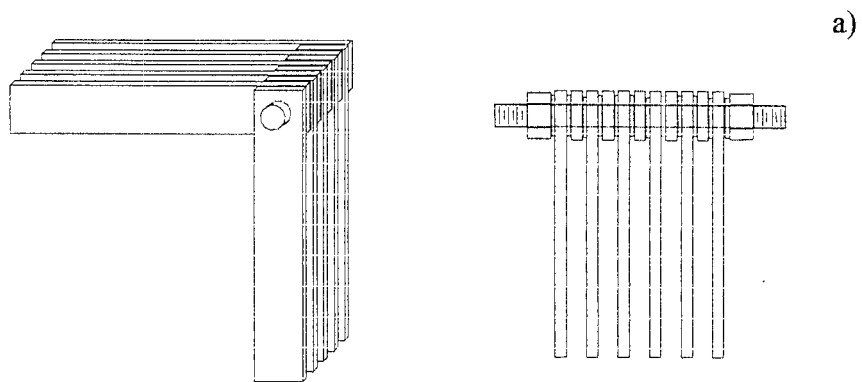
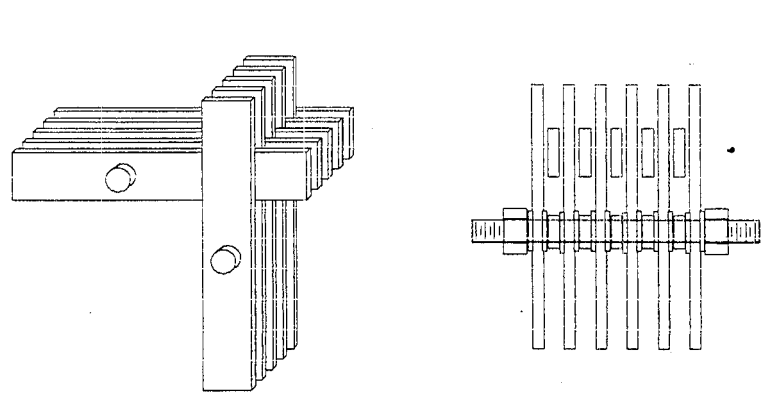


Fig. 5.6. Biaxial Apparatus Schematic



a)



b)

Fig. 5.7. Bar/gap-stacked arrangement
a) corner of frame
b) intersection of moving walls

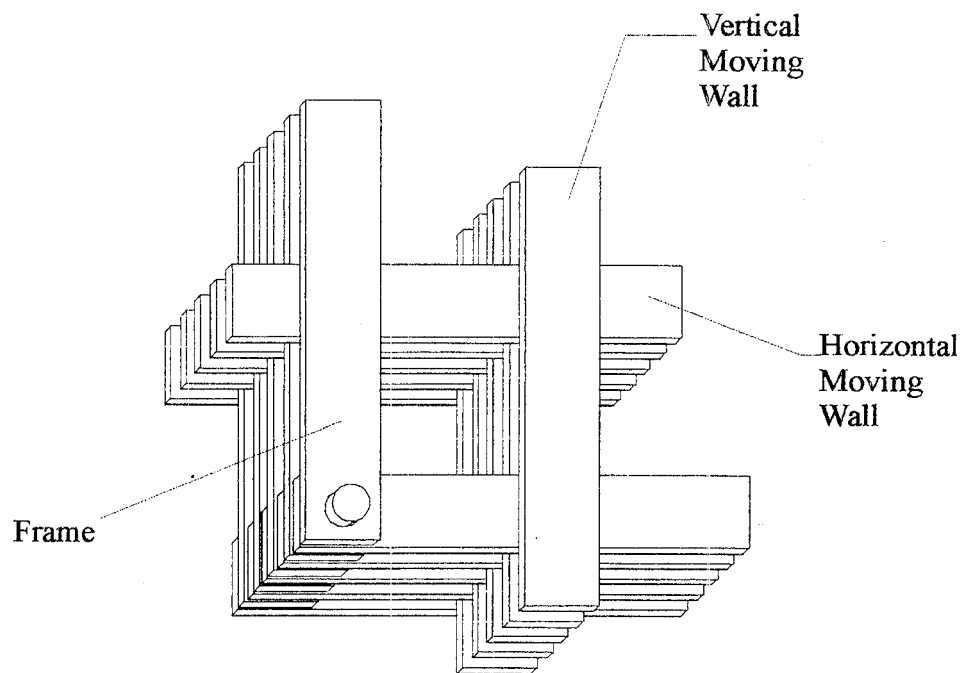


Fig. 5.8. Bar/gap-stacked arrangement: intersection of moving walls and frame

solid steel plates that are 610 mm (24 in.) square. These two plates are connected to each other by four threaded steel rods, three of which are supported by the main framework; to produce a plane-stress condition, the plates can be removed. The vertically moving wall is in contact with shredded tires only over 330 mm (13 in.) of its length. To counterbalance possible moment due to the wall weight, an upward force is applied at the unsupported end by means of a cable that runs through a pulley and is attached to a hanging dead weight.

The horizontal and vertical compressive forces are induced by means of 34 kN (7600 lb.) capacity hydraulic jacks attached to the each moving wall and the frame. The location of the jacks is approximately half-width and half-height of the prismatic sample, and their maximum travel is 200 mm (8 in.). Hoses connect each hydraulic jack to a pump, which is operated manually. Force on the hydraulic jacks is obtained by converting pressure readings of the hydraulic fluid into calibrated load. Fluid pressure is indicated by dial gages. The jacks were calibrated using an MTS-858 Table Top System load frame.

The displacement of each wall is measured by dial-face calipers, with the accuracy of ± 0.025 mm (± 0.001 in.). The jaws of each caliper are attached to two separate brackets, which run adjacent to the hydraulic jacks and are connected to the frame and moving wall.

Gage pressure and caliper displacement readings were both taken manually.

MATERIAL AND TEST PROGRAM

The anisotropy tests were conducted on the 200-mm shredded tire pieces. It was expected that the larger pieces would display the most prominent anisotropic properties.

To minimize friction between the pieces and the walls of the biaxial apparatus, all walls were lubricated before preparing a sample. After the vertically moving wall was raised and held by winch cables to provide clearance, the material for testing was placed in the space created by the five remaining walls. To simulate conditions of fill material, the pieces were arranged with alternating curvature, Fig. 5.9. For plane stress tests, the rigid square plates were removed, and the material was stacked in the space created by the three remaining walls.

In order to compare the performance of the apparatus in the vertical and horizontal loading directions, the pieces were oriented in either horizontal or vertical layers. For tests with vertically oriented pieces, the pieces were initially stacked in horizontal layers in a metal enclosure outside the apparatus. The metal enclosure was turned on its side, placed in the test space of the apparatus, and removed from the sample, leaving vertically oriented pieces in the test space. For tests on both vertically- and horizontally-oriented pieces, the vertically moving wall was lowered by the winches until it came in contact with the shredded tires.

To simulate the in-situ compaction of the shredded tire material, all samples were first appropriately compacted. For vertical compaction, the weight of the vertically moving wall was allowed to bear on the sample immediately, and the required compaction load was applied in three loading/unloading cycles. For horizontal compaction, the vertically moving wall was held by the winch cables. As in the vertical



Fig. 5.9. Stacking shredded tire pieces with alternate curvature

compaction tests, load that simulated compaction was then applied in three loading/unloading cycles, but in the horizontal direction.

Upon completion of the compaction sequence, overburden pressure was simulated by applying load in the horizontal and vertical directions simultaneously until desired stresses were achieved. During this time, in tests with horizontal compaction, the vertically moving wall was released to aid in the application of vertical stress.

From one-dimensional compression tests performed on shredded tire material by Humphrey and Sandford (1993) and Newcomb and Drescher (1994), it was found that horizontal stress, σ_h , that develops as a result of vertical stress, σ_v , can be approximated by

$$\sigma_h = K\sigma_v \quad (5.1)$$

where K is the coefficient of lateral earth pressure and has experimental values between 0.4 and 0.6. This relation was used to determine the level of horizontal stress for a given vertical stress.

Once simulated overburden stress was attained, additional load was applied alternately in the vertical and horizontal directions to cause incremental changes in stress. From stress-strain curves of Chapter 3 (e.g., Fig. 3.7), it is evident that the material response in the reloading region of repeated load tests is different than that in the virgin loading region. In actual fills, shredded tire material subject to traffic loads can be expected to display similar behavior, assuming a history of loads due to construction and traffic. Therefore, in the anisotropy tests, the shredded tire sample was first subject to

stress increments corresponding to virgin loading above overburden stress. This virgin loading was applied simultaneously in the vertical and horizontal directions, and the material experienced stress levels that were slightly above anticipated reloading stress levels. Upon unloading from the virgin loading stress to overburden stress, the tested material was assumed to be similar in terms of load response to in situ material with no traffic load placed upon it. Subsequent load increments were then applied to the shredded tire samples in the vertical and horizontal directions alternately, with stress levels such that the material was always within the reloading region.

Figure 5.10 depicts the target stress path for a test with horizontally aligned pieces (vertical compaction). The three cycles of vertical compaction shown are followed by an increase in stress corresponding to overburden stress. In this case, vertical stress is 52 kPa (7.5 psi) and horizontal stress is 24 kPa (3.5 psi) at simulated overburden stress. The virgin loading above the overburden stress is applied to both directions simultaneously, and an unloading to the overburden stress follows. Load is then applied in the vertical direction and a vertical stress increment results. Following a decrease in the vertical load to the simulated overburden stress level, load is applied in the horizontal direction such that the resulting horizontal stress increment is equal in magnitude to the previous vertical stress increment. The load in the horizontal direction is decreased to the overburden stress level, and the alternation of vertical and horizontal stress increments is repeated several times. The magnitude of stress increments is increased periodically, and increased virgin loading is applied accordingly.

In most tests, simulated overburden stress in the direction of compaction was about 52 kPa (7.5 psi). This corresponds to stress in the middle of a 3.6-m (11.8-ft.) layer

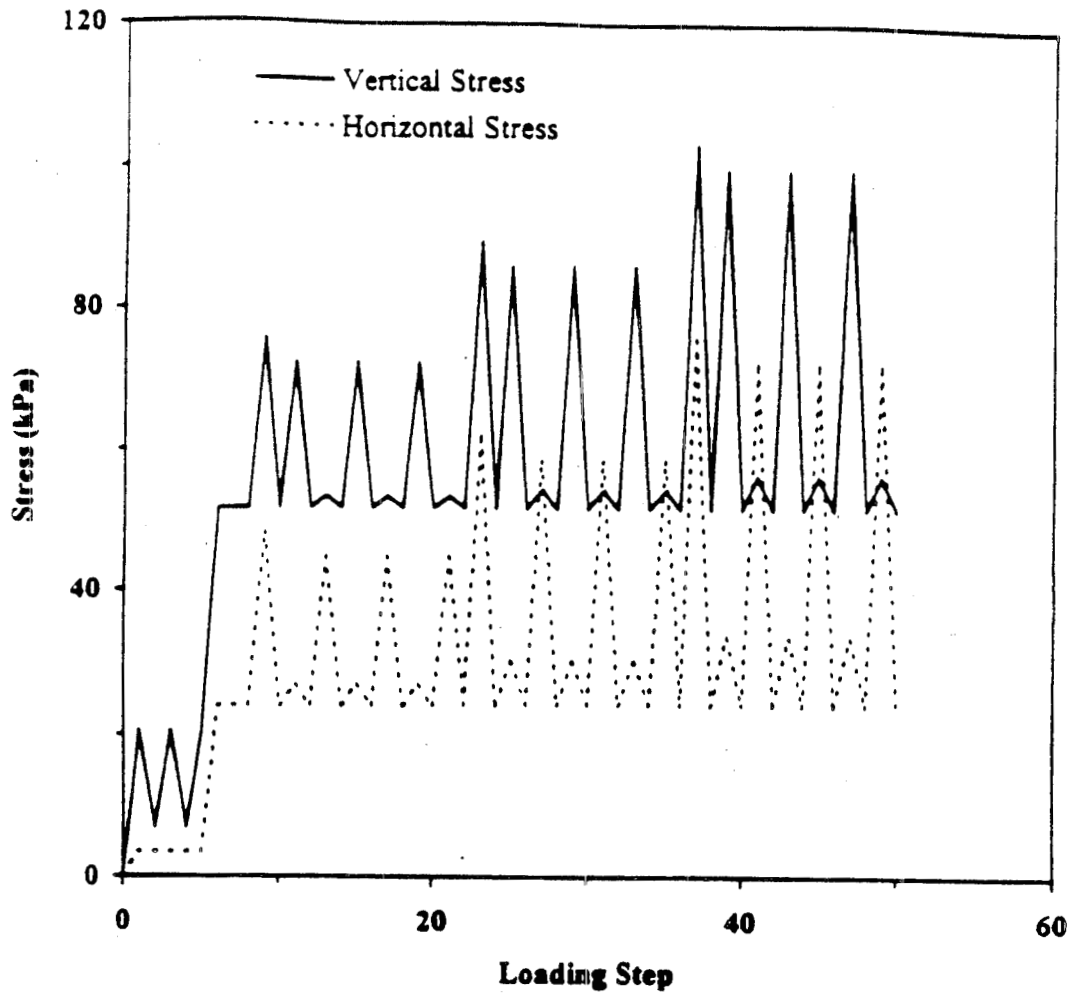


Fig. 5.10. Target stress path for test with vertical compaction

of shredded tires, which is overlain by a 2.2 m (7.2 ft.) layer of soil (Fig. 3.3). For comparison, a test was conducted at a lower level of overburden stress, where stress in the direction of compaction was about 21 kPa (3.0 psi). This corresponds to stress in the middle of a 1.2-m (3.9-ft.) layer of shredded tires, which is covered by a 0.92-m (3-ft.) layer of soil. Stress increments in tests ranged from 21 to 48 kPa (3.0 to 7.0 psi).

The test matrix, Table 5.1, presents typical tests that were conducted in the investigation of shredded tire material anisotropy.

TEST RESULTS

Data Evaluation

Gage pressure and caliper displacement readings were collected for the vertical and horizontal directions. Using pressure gage readings, the vertical and horizontal forces applied by the jacks, F_v and F_h , respectively, are calculated by

$$\begin{aligned} F_v &= C_v p_v \\ F_h &= C_h p_h \end{aligned} \tag{5.2}$$

where p_v and p_h are vertical and horizontal gage pressure, and C_v and C_h are calibration constants for the jacks corresponding to the vertical and horizontal directions of loading, respectively. The depth dimension of the sample is assumed constant (x-direction in Fig. 5.4) since it depends on the size of the walls and frame, which do not change. The height, h , and width, w , of the sample measured in the z- and y-directions, respectively, are given by

Table 5.1. Biaxial Loading/Unloading Test Matrix

Test #	Type of Test	Horizontal Stress level kPa (psi)	Vertical Stress level kPa (psi)	Stress Increments kPa (psi)	Number of Tests Performed
1.	Plane stress	24.1 (3.5)	51.7 (7.5)	20.7 to 48.3 (3 to 7)	8
2.	Plane stress	11.0 (1.6)	24.1 (3.5)	20.7 to 48.3 (3 to 7)	1
3.	One-dimensional constrained compression	11.0 (1.6)	24.1 (3.5)	20.7 to 48.3 (3 to 7)	1
4.	One-dimensional constrained compression	-	144.8 (21.0)	-	2

$$\begin{aligned} h &= h_0 + \Delta h \\ w &= w_0 + \Delta w \end{aligned} \tag{5.3}$$

where h_0 and w_0 are the initial height and width of the sample upon contact of the vertical wall with the sample, and Δh and Δw are the changes in the height and width of the sample, respectively. Using the dimensions of the sample, contact areas of the prismatic sample with the walls are given by

$$\begin{aligned} A_v &= w d \\ A_h &= h d \end{aligned} \tag{5.4}$$

where d is the depth dimension, and A_v and A_h correspond to contact areas of the vertically and horizontally moving walls, respectively,

The average vertical stress, σ_v , and average horizontal stress, σ_h , on the sample are calculated from

$$\begin{aligned} \sigma_v &= \frac{F_v + F_{wall} + F_{st}}{A_v} \\ \sigma_h &= \frac{F_h}{A_h} \end{aligned} \tag{5.5}$$

where F_{wall} is the estimated force due to the weight of the vertically moving wall, and F_{st} is the resultant force at the midheight of the sample due to the small self-weight of the shredded tire material. Knowing the weight of the wall and the force acting in the cable

attached to the hanging counterbalance dead weight, F_{wall} could be determined. F_{st} was estimated using a bulk unit weight of 4.7 kN/m^3 (30 lbs/ft^3).

The corresponding average vertical strain, ϵ_v , and average horizontal strain, ϵ_h , are calculated as

$$\begin{aligned}\epsilon_v &= -\frac{\Delta h}{h_0} \\ \epsilon_h &= -\frac{\Delta w}{w_0}\end{aligned}\tag{5.6}$$

For the purpose of determining parameters that reveal the level of anisotropy in layered shredded tire material, linear elasticity is assumed. Thus, material parameters are assumed to be constant for small increases in stress and strain even though they are most likely varying with changes in stress for shredded tire material. Also, in actual tests, load was applied in both the y- and z-directions at a rate of about 0.5 kN/sec. , meaning incremental loads above the overburden stress were applied over a period of 5-10 seconds. Due to the fast loading rate, the effects of time dependent settlement were assumed to be negligible.

Under the assumptions of linear elasticity and time independent settlement, the Hooke's law equations for an anisotropic-transversely isotropic material are

$$\begin{aligned}
\varepsilon_{xx} &= \frac{1}{E} \sigma_{xx} - \frac{\nu}{E} \sigma_{yy} - \frac{\nu'}{E'} \sigma_{zz} \\
\varepsilon_{yy} &= -\frac{\nu}{E} \sigma_{xx} + \frac{1}{E} \sigma_{yy} - \frac{\nu'}{E'} \sigma_{zz} \\
\varepsilon_{zz} &= -\frac{\nu'}{E'} \sigma_{xx} - \frac{\nu'}{E'} \sigma_{yy} + \frac{1}{E'} \sigma_{zz} \\
\gamma_{xy} &= \frac{2(1+\nu)}{E} \tau_{xy}, \quad \gamma_{xz} = \frac{1}{G'} \tau_{xz}, \quad \gamma_{yz} = \frac{1}{G'} \tau_{yz}
\end{aligned} \tag{5.7}$$

where, in reference to Fig. 5.4, ε_{xx} , ε_{yy} , and ε_{zz} are normal strains, σ_{xx} , σ_{yy} , and σ_{zz} are normal stresses, γ_{xy} , γ_{xz} , and γ_{yz} are engineering shear strains, τ_{xy} , τ_{xz} , and τ_{yz} are shear stresses, and E , E' , ν , ν' , and G' are material parameters. (Lekhnitskii, 1981).

Four of the five independent material parameters in (5.7) are obtainable in tests with the biaxial apparatus. Two of these parameters are the Young's modulus E and Poisson's ratio ν in the x,y -plane of isotropy, Fig. 5.4, and two are the Young's modulus E' and Poisson's ratio ν' in planes perpendicular to the x,y -plane. The fifth parameter is the shear modulus, G' , which relates shear stresses and strains in planes perpendicular to the x,y -plane. The determination of this modulus requires sophisticated torsion tests, which cannot be performed with the biaxial apparatus.

In Section 5.2, it was mentioned that the biaxial apparatus had large plates that provided confinement in the x -direction. These plates are removable to give freedom in the choice of 4 sides or 6 sides of rigid confinement. To find the parameters E , E' , ν , and ν' using the biaxial apparatus, two types of tests were performed on the shredded tire samples: a) tests with the plates removed (plane stress) and b) tests with the plates attached.

In tests with the plates removed, the plane stress condition results. Confinement is

present in both the y- and z-directions and the material is free to move in the x-direction. In the plane stress condition, with unidirectional stress applied in the z-direction, (5.7b) and (5.7c) become, for incremental stresses and strains,

$$\begin{aligned} d\varepsilon_{yy}^z &= \frac{1}{E} d\sigma_{yy}^z - \frac{\nu'}{E'} d\sigma_{zz}^z \\ d\varepsilon_{zz}^z &= -\frac{\nu'}{E'} d\sigma_{yy}^z + \frac{1}{E'} d\sigma_{zz}^z \end{aligned} \quad (5.8)$$

where the superscript z denotes loading in the z-direction of compaction. For loading in the y-direction, (5.7b) and (5.7c) become

$$\begin{aligned} d\varepsilon_{yy}^y &= \frac{1}{E} d\sigma_{yy}^y - \frac{\nu'}{E'} d\sigma_{zz}^y \\ d\varepsilon_{zz}^y &= -\frac{\nu'}{E'} d\sigma_{yy}^y + \frac{1}{E'} d\sigma_{zz}^y \end{aligned} \quad (5.9)$$

where the superscript y denotes loading in the y-direction.

From (5.8b) and (5.9b), E' may be expressed as

$$\begin{aligned} E' &= \frac{d\sigma_{zz}^z - \nu' d\sigma_{yy}^z}{d\varepsilon_{zz}^z} \\ E' &= \frac{d\sigma_{zz}^y - \nu' d\sigma_{yy}^y}{d\varepsilon_{zz}^y} \end{aligned} \quad (5.10)$$

Equating (5.10a) and (5.10b) and solving for ν'

$$v' = \frac{d\sigma_{zz}^z d\varepsilon_{zz}^y - d\sigma_{zz}^y d\varepsilon_{zz}^z}{d\sigma_{yy}^z d\varepsilon_{zz}^y - d\sigma_{yy}^y d\varepsilon_{zz}^z} \quad (5.11)$$

Then, by inserting the value for v' from (5.11) into (5.10a) or (5.10b), E' may be obtained. From (5.8a), E may be expressed as

$$E = \frac{d\sigma_{yy}^z}{d\varepsilon_{yy}^z + \frac{v'}{E'} d\sigma_{zz}^z} \quad (5.12)$$

In the other type of tests, with the plates in place, confinement is present in the x-, y- and z-directions. If no movements are allowed in the x or y-directions, one-dimensional compression in the z-direction can be performed. In this condition, with axial load applied in the z-direction, the incremental normal stresses in the x,y-plane are equal, or $d\sigma_{xx} = d\sigma_{yy}$. Eq. (5.7b) becomes, for incremental stresses and strains,

$$d\varepsilon_{yy} = \frac{1-v}{E} d\sigma_{yy} - \frac{v'}{E'} d\sigma_{zz} = 0 \quad (5.13)$$

which can be written as

$$v = 1 - \frac{E v' d\sigma_{zz}}{E' d\sigma_{yy}} \quad (5.14)$$

In actual tests, once the simulated overburden stress was reached and the virgin loading was performed, load was applied alternately in the directions parallel and perpendicular to the direction of compaction. Measurements of displacement and force were obtained for the y- and z-directions. Knowing the dimensions of the sample, stress and strain changes were calculated. Eqs. (5.10), (5.11), (5.12), and (5.14) were then used to estimate the material parameters E' , ν' , E , and ν , respectively.

Experimental Anisotropic Parameters

Fig. 5.11 shows the actual stepwise vertical and horizontal stress paths for a typical plane stress test with compaction in the vertical direction; each step represents a loading or unloading. At overburden stress, vertical and horizontal stresses were about 52 kPa (7.5 psi) and 24 kPa (3.5 psi), respectively. The stress increments ranged from about 20.7 to 48.3 kPa (3 to 7 psi).

The stress-strain relationships for the same test are shown in Figs. 5.12 and 5.13 for the vertical and horizontal directions, respectively.

In Fig. 5.14, the variation of vertical and horizontal stresses is depicted for the above test. Three stress increments of varying magnitude with subsequent unloading are shown for loading in both the vertical and horizontal directions. This graph demonstrates that the response in the horizontal direction to load in the vertical direction is greater than the response in the vertical direction to load in the horizontal direction.

Typical values of the elastic parameters from tests are $E = 5.86$ MPa (849 psi), $E' = 2.19$ MPa (318 psi), and $\nu' = 0.11$, Table 5.2. It is evident that the Young's modulus in the horizontal direction, E , is about 2.5 to 3 times more than the value for the vertical

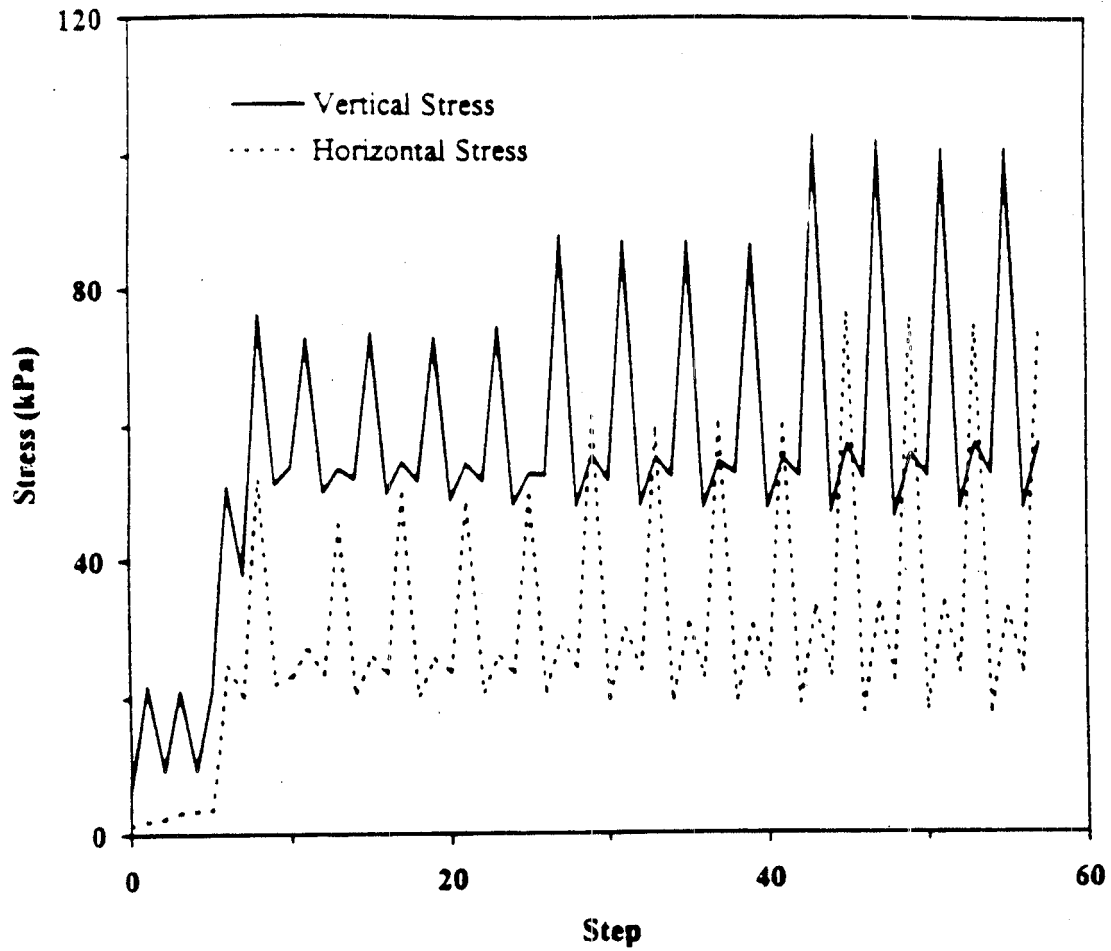


Fig. 5.11. Stress paths in a typical anisotropy test

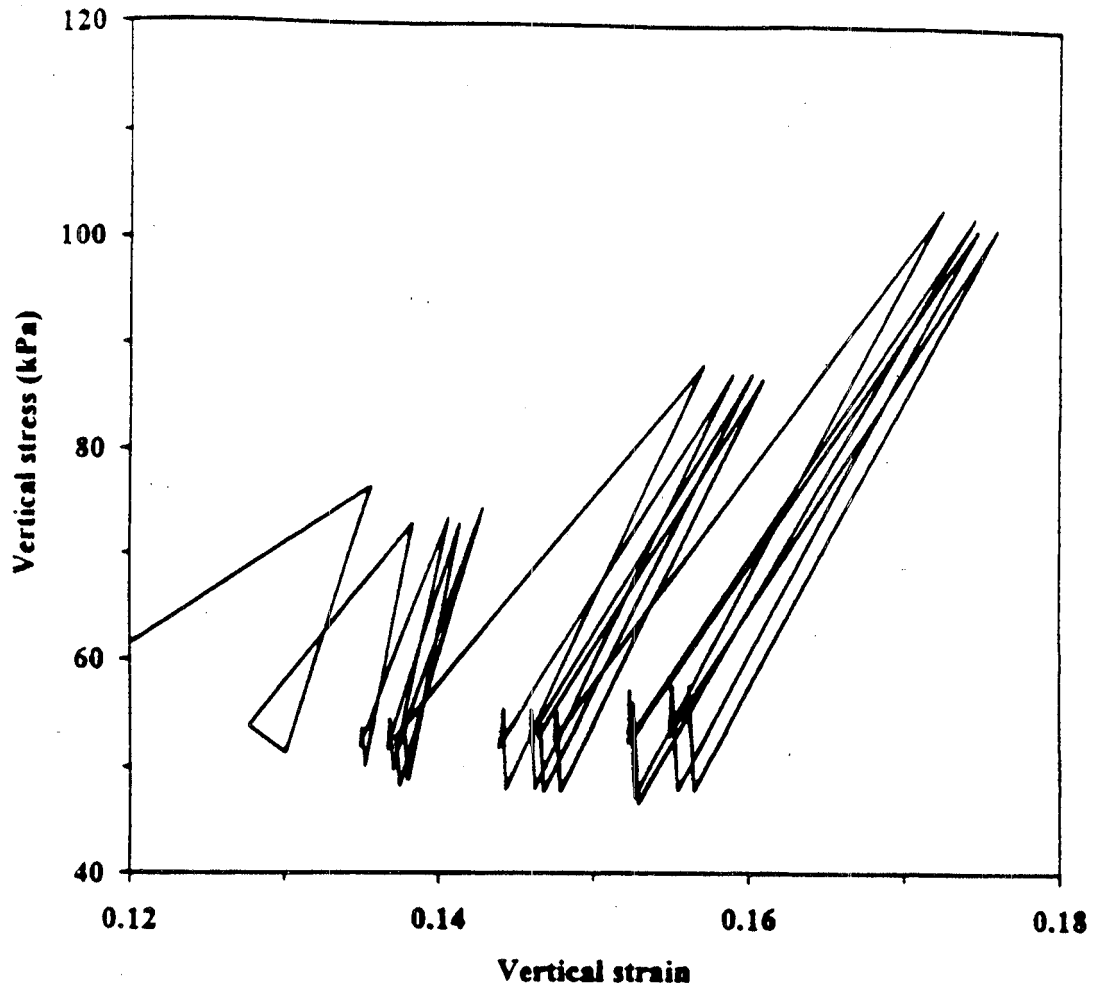


Fig. 5.12. Vertical stress vs. vertical strain

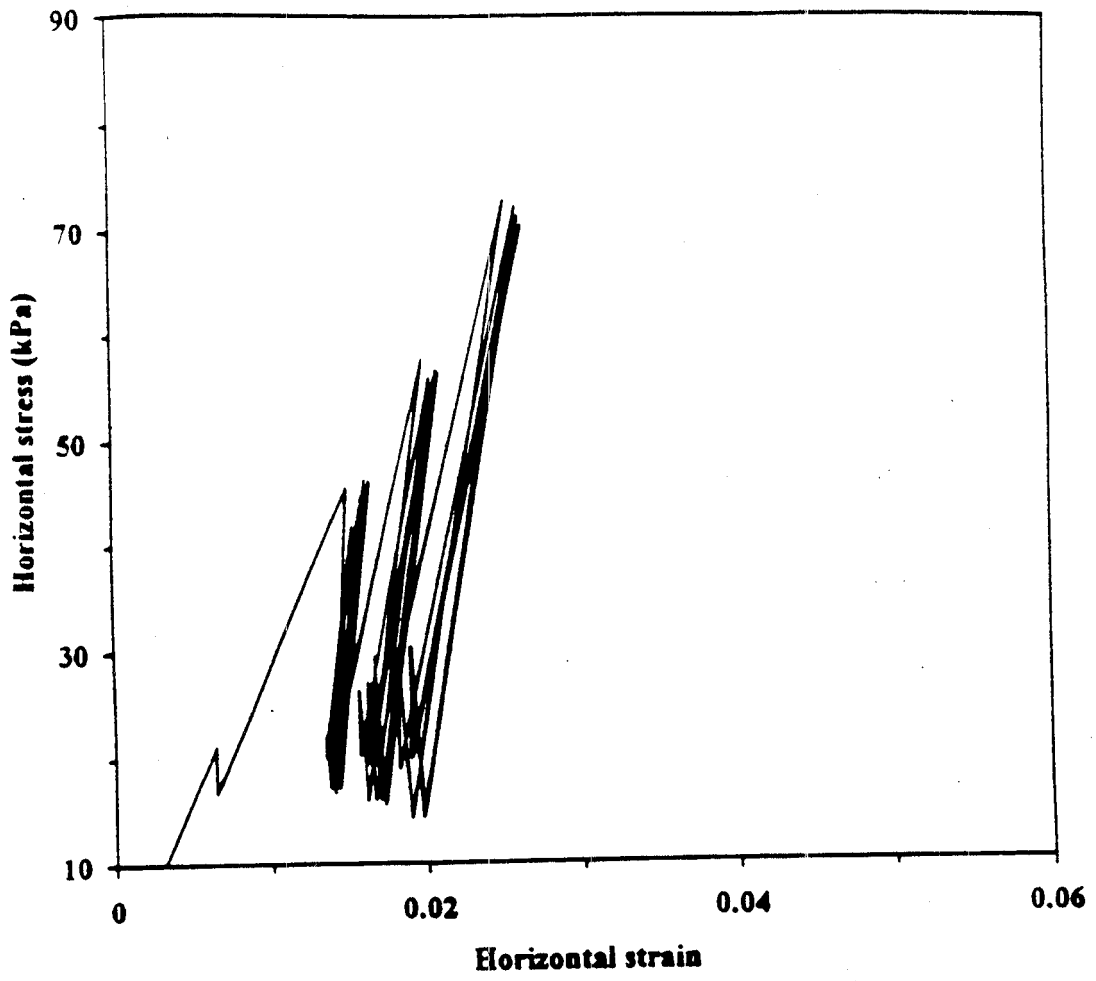


Fig. 5.13. Horizontal stress vs. horizontal strain

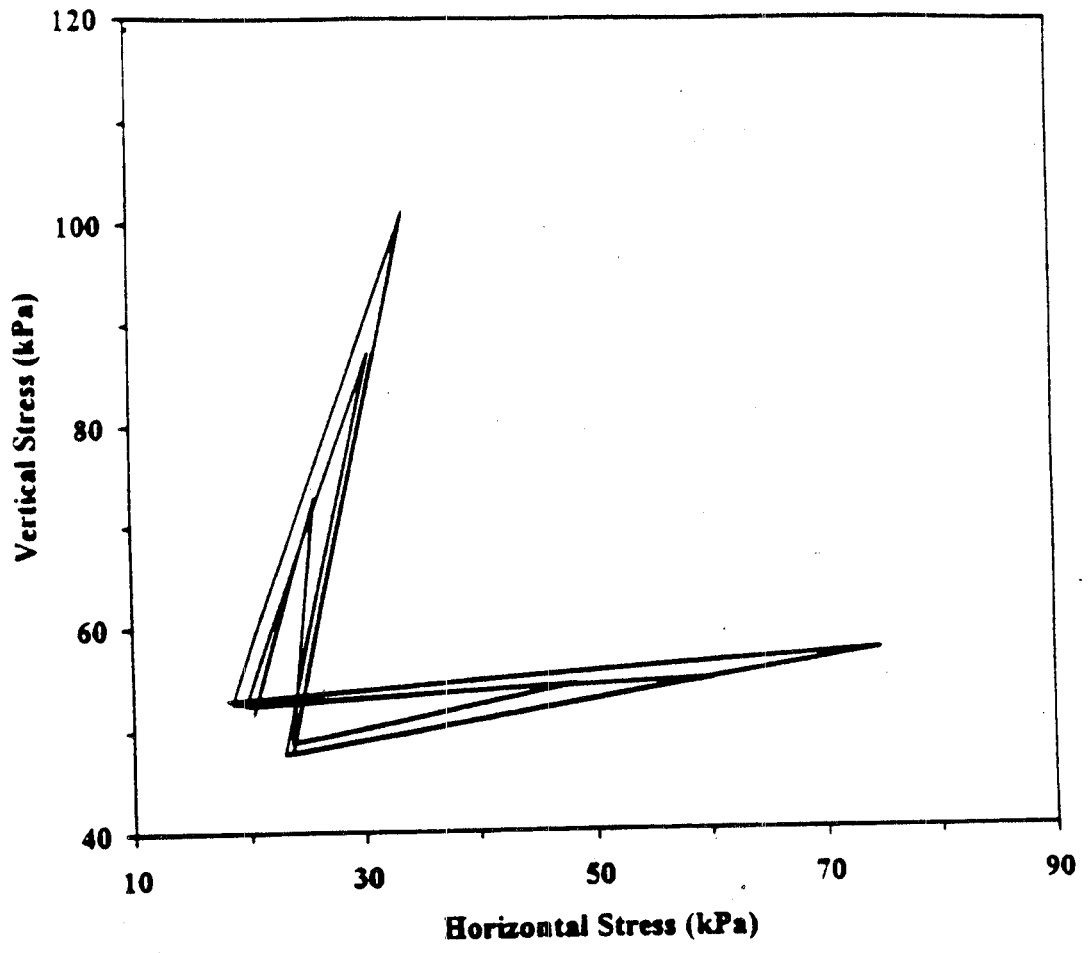


Fig. 5.14. Vertical stress vs. horizontal stress

Table 5.2. Experimental Anisotropic Parameters

Vertical Young's Modulus	E	5.9 MPa (850 psi)
Horizontal Young's Modulus	E'	2.2 MPa (320 psi)
Vertical Poisson's Ratio	ν'	0.11
Horizontal Poisson's Ratio	ν	0.1 to 0.45
Shear Modulus	G'	unobtainable

direction, E' . This indicates strong anisotropy. The calculated value of the in-plane Poisson's ratio, ν , in Eq. (5.11) is extremely sensitive to experimental error. For this reason, the values ranged widely, and a distinct value was not found.

Isotropic Parameters

In general, a body consisting of layers with different material properties, as in Fig. 5.4 is anisotropic. If shredded tire material is structured this way, it can be modeled as an anisotropic-transversely isotropic material. Five elastic parameters are necessary to fully describe the stress-strain relationships, as expressed in Eqs. (5.7). However, in considering the response of shredded tires to load, it is customary to assume the material to be isotropic. In other words, the actual anisotropic properties of the material are disregarded and the material is treated as purely isotropic. Under this assumption, stress-strain relations are given by the generalized Hooke's law equations for a linearly elastic isotropic material as follows

$$\begin{aligned}
 \varepsilon_{xx} &= \frac{1}{E_i} \sigma_{xx} - \frac{\nu_i}{E_i} \sigma_{yy} - \frac{\nu_i}{E_i} \sigma_{zz} \\
 \varepsilon_{yy} &= -\frac{\nu_i}{E_i} \sigma_{xx} + \frac{1}{E_i} \sigma_{yy} - \frac{\nu_i}{E_i} \sigma_{zz} \\
 \varepsilon_{zz} &= -\frac{\nu_i}{E_i} \sigma_{xx} - \frac{\nu_i}{E_i} \sigma_{yy} + \frac{1}{E_i} \sigma_{zz} \\
 \gamma_{xy} &= \frac{2(1+\nu_i)}{E_i} \tau_{xy}, \quad \gamma_{xz} = \frac{2(1+\nu_i)}{E_i} \tau_{xz}, \quad \gamma_{yz} = \frac{2(1+\nu_i)}{E_i} \tau_{yz}
 \end{aligned} \tag{5.15}$$

where the isotropic Young's modulus, E_i , and isotropic Poisson's ratio, ν_i , are the only independent parameters (Lekhnitskii, 1981).

In past research, estimates for E_i and ν_i , were most often obtained using results from one-dimensional compression tests in which shredded tire material is placed in a cylindrical mold, with confinement in the x,y -plane, and loaded in the z -direction. The parameters E_i and ν_i were derived from the measurements of axial strains, axial stresses, and hoop stresses (Manion and Humphrey, 1992; Newcomb and Drescher, 1994). By combining the Hooke's law equations in (5.7) and (5.15), E_i and ν_i can be derived as functions of $E, E', \nu,$ and ν' for a one-dimensional compression in the z -direction as follows.

Considering $\varepsilon_{xx} = 0$ and $\sigma_{xx} = \sigma_{yy}$ in Eq. (5.15a), ν_i becomes

$$\nu_i = \frac{\sigma_{yy}}{\sigma_{yy} + \sigma_{zz}} \quad (5.16)$$

Eq. (5.15c) becomes

$$E_i = \frac{\sigma_{xx} - 2\nu_i\sigma_{yy}}{\varepsilon_{zz}} \quad (5.17)$$

By solving (5.7a) for σ_{zz} and substituting the expression into (5.16), the following equation results

$$\nu_i = \frac{E\nu'}{E\nu' + E'(1 - \nu)} \quad (5.18)$$

Upon solving (5.7c) for ε_{zz} and substituting the expression into (5.17) along with the equation for ν_i in (5.18), the following relation may be formulated

$$E_i = \frac{E'^2(1-\nu)[Ev' + E'(1-\nu)] - 2E'E^2\nu'^2}{[Ev' + E'(1-\nu)][E'(1-\nu) - 2E\nu'^2]} \quad (5.19)$$

To illustrate the dependence of the values of E_i and ν_i on the test used to obtain them, other tests may be considered. For uniaxial compression in the z-direction

$$E_i = E' \quad (5.18)$$

$$\nu_i = \nu' \quad (5.19)$$

and for uniaxial compression in the y-direction

$$E_i = E' \quad (5.20)$$

$$\nu_i = \nu' \quad (5.21)$$

As shown by the above equations, significantly different values of E_i and ν_i are obtained from different tests.

Using the parameters E' , ν' , and E obtained from tests, and by assuming reasonable values for ν , (5.18) and (5.19) are used to express fictitious values for E_i and ν_i correspond to values obtained by performing a one-dimensional compression test. These are summarized in Table 5.3 for several values of ν .

Table 5.3. Elastic Constants

Anisotropic Material, Measured	E'	ν'	E
	2.19 MPa	0.11	5.86 MPa

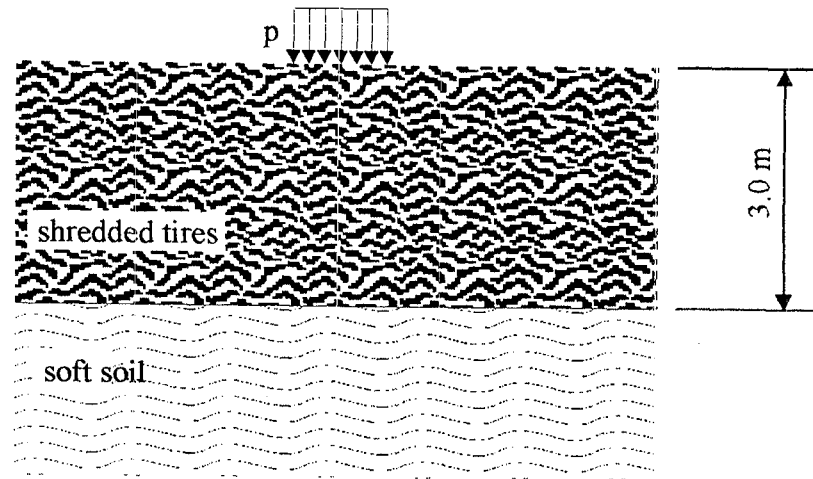
Isotropic Material One-Dimensional Compression, z-axis	Value of anisotropic ν	Isotropic parameters Eqs. (5.18, 5.19)	
		E _i (MPa)	ν _i
	0.1	1.98	0.25
	0.15	1.95	0.26
	0.2	1.91	0.27
	0.25	1.87	0.28
	0.3	1.81	0.30
	0.35	1.75	0.31
	0.4	1.66	0.33
	0.45	1.56	0.35

APPLICATION OF RESULTS

To evaluate the difference in settlements of fills for shredded tire material regarded as either isotropic or anisotropic, two test cases were considered. The first case is a layer of shredded tires 3.0 m (9.8 ft.) thick overlying a soft soil, which is subjected to surface stresses (tractions) simulating a single-axle load, Fig. 5.15a. The layered system in this case is similar to a shredded tire fill under construction before the placement of an overlay, with low-volume traffic loading. The second case, shown in Fig. 5.15b, is a multilayered pavement system in which a 0.1 m (3.9 in.) thick asphalt concrete layer and an underlying 1.0 m (3.3 ft.) layer of soil are placed on top of the 3.0 m shredded tire layer and layer of soft soil in the first case. This case may be considered as a completed road subjected to low-volume traffic loading. The single-axle load that is assumed to act on the surface of the road is represented in calculations by a uniform pressure of 566 KPa (82 psi) acting over a circular area 750 mm (30 in.) in diameter.

The numerical code CIRCLY (Wardle, 1976) was used to calculate settlements for the above cases. This code has been developed specifically for modeling the response of multilayered isotropic and anisotropic elastic systems to static traffic-related loads. Two sets of anisotropic material parameters for the shredded tire fill that were selected in each of the two study-cases used in the numerical analysis, as shown in Table 5.4. The first set comprises E' , ν' , and E measured in the tests, two chosen values of ν , and two values of G' selected as follows. The isotropic parameters corresponding to measured anisotropic parameters (Table 5.3) can be used to find an isotropic shear modulus, G_i , using

a)



b)

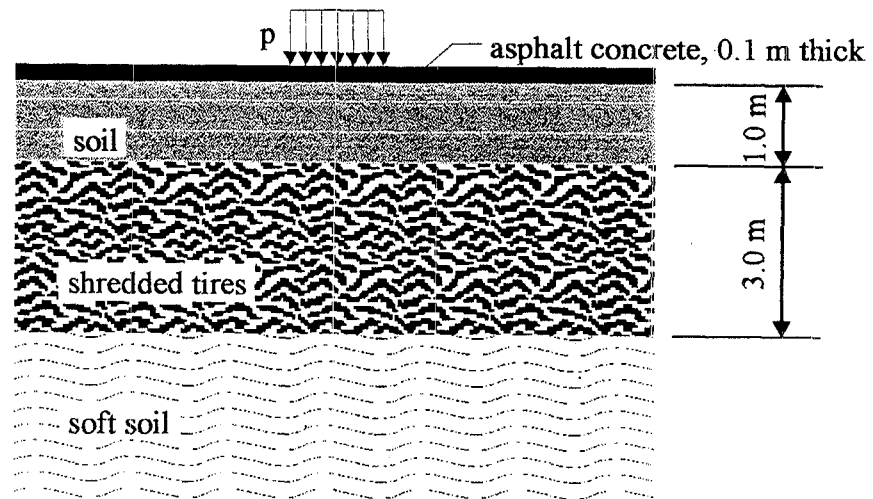


Fig. 5.15. Test-cases
a. 2-layer system
b. 4-layer system

Table 5.4. Material and Layer Characteristics for Study Cases

Material properties of shredded tires				
Set 1. Measured E, E', ν' , assumed ν and G'				
	E (MPa)	E' (MPa)	ν'	G' (MPa)
a. $\nu = 0.15, G' = 0.5 G_i$	5.86	2.19	0.11	0.387
b. $\nu = 0.15, G' = 1.5 G_i$	5.86	2.19	0.11	1.162
c. $\nu = 0.35, G' = 0.5 G_i$	5.86	2.19	0.11	0.333
d. $\nu = 0.35, G' = 1.5 G_i$	5.86	2.19	0.11	0.998
Set 2. Reduced E, E', E/E', measured ν' , assumed ν and G'				
	E (MPa)	E' (MPa)	ν'	G' (MPa)
a. $\nu = 0.15, G' = 0.5 G_i$	1.6	0.8	0.11	0.157
b. $\nu = 0.15, G' = 1.5 G_i$	1.6	0.8	0.11	0.472
c. $\nu = 0.35, G' = 0.5 G_i$	1.6	0.8	0.11	0.143
d. $\nu = 0.35, G' = 1.5 G_i$	1.6	0.8	0.11	0.429
Assumed material properties				
Material	Assumed material properties		Thickness (m)	
	E (MPa)	ν	Case-one	Case-two
asphalt concrete	5000	0.35	-	0.1
base soil	70	0.25	-	1.0
shredded tires	see above	see above	3	3
soft clay	10	0.5	30	30

$$G_i = \frac{E_i}{2(1 + \nu_i)} \quad (5.22)$$

which can be considered as a rough estimate of the anisotropic out-of-plane shear modulus, G' . The selected values of G' correspond to values $\pm 50\%$ of the isotropic shear modulus from (5.22). In the second set of anisotropic parameters used for analysis, the values of the in-plane and out-of-plane moduli were reduced as was their ratio, and the values of G' were adjusted according to (5.22), but the Poisson's ratios were the same as in the first set. These reduced values were chosen as more representative of those found in a real shredded tire fill, where the placement of the pieces is more random than in the biaxial tests conducted, in which the layered structure was deliberately enhanced by manually stacking the pieces. The two sets of parameters, along with relevant isotropic shear moduli, are shown in Table 5.4. All other layers in the systems shown in Fig. 5.15 were assumed to be isotropic elastic, with the corresponding parameters also listed in Table 5.4.

Computations of settlements at the center of the loaded area were performed for the above layered systems, and the results are presented in Table 5.5. It is evident that Young's moduli have the greatest effect on settlements. Settlements are increased by reducing the values of E' and E , whereas changing the value of ν had less effect on settlements. The influence of G' on settlements in case-two (4-layer case), is relatively small, but in case-one (2-layer case), its significance warrants further study. To better evaluate the sensitivity of settlements to the out-of-plane shear modulus, computations

Table 5.5. Results of Settlement Analysis, Anisotropic Material

2-Layer System						
	E (MPa)	E' (MPa)	ν'	ν	G' (MPa)	Settlement (mm)
Set 1a.	5.86	2.19	0.11	0.15	0.387	87.1
Set 1b.	5.86	2.19	0.11	0.15	1.162	62.8
Set 1c.	5.86	2.19	0.11	0.35	0.333	88.6
Set 1d.	5.86	2.19	0.11	0.35	0.998	64.9
Set 2a.	1.6	0.8	0.11	0.15	0.157	239
Set 2b.	1.6	0.8	0.11	0.15	0.472	172
Set 2c.	1.6	0.8	0.11	0.35	0.143	240
Set 2d.	1.6	0.8	0.11	0.35	0.429	173

4-Layer System						
	E (MPa)	E' (MPa)	ν'	ν	G' (MPa)	Settlement (mm)
Set 1a.	5.86	2.19	0.11	0.15	0.387	2.02
Set 1b.	5.86	2.19	0.11	0.15	1.162	1.86
Set 1c.	5.86	2.19	0.11	0.35	0.333	2.04
Set 1d.	5.86	2.19	0.11	0.35	0.998	1.89
Set 2a.	1.6	0.8	0.11	0.15	0.157	2.78
Set 2b.	1.6	0.8	0.11	0.15	0.472	2.63
Set 2c.	1.6	0.8	0.11	0.35	0.143	2.78
Set 2d.	1.6	0.8	0.11	0.35	0.429	2.64

were repeated for a wide range of G' and two values of ν for the second set of parameters (reduced values) in the 2-layer case. The results are depicted in Fig. 5.16, and this plot indicates that for G' within $\pm 30\%$ of the corresponding isotropic shear modulus, settlements differ by at most $\pm 12\%$ from the settlement for $G' = G_i$.

To assess the validity of the customary settlement analysis of shredded tire fills in which the shredded tire material is modeled as isotropic elastic, computations similar to those above were performed using the code CIRCLY, but isotropic parameters were used. The isotropic parameters E_i and ν_i corresponding to the above selected anisotropic parameters for case-one and case-two were calculated according to (5.18) and (5.19), and are listed in Table 5.6 with the resulting computed settlements. These settlements may be compared with those in Table 5.5. A further comparison of settlements is illustrated by Fig. 5.17, which depicts the isolines of vertical displacement for the anisotropic fill and the fill considered as isotropic for the 4-layer case using experimental parameters. Table 5.5, Table 5.6, and Fig. 5.17 indicate that Young's modulus in the vertical direction has a direct effect on settlements. Also, the maximum and minimum settlements are 31% larger and 13% smaller than those calculated assuming the fill to be isotropic in the 2-layer case, and 7.4% larger and 1.8% smaller in the 4-layer case. If the design criteria in road construction are based on the maximum settlement allowed, the only unsafe estimate is one in which settlement for an isotropic fill is less than settlement for a corresponding anisotropic fill. If this is true, using the isotropic fill results in an unconservative estimate for maximum settlement. If maximum settlement is greater for the isotropic fill, then the estimate is conservative when compared to the settlement for the anisotropic fill. The settlements of the isotropic fill in the 2-layer case are at most 13% unconservative, and

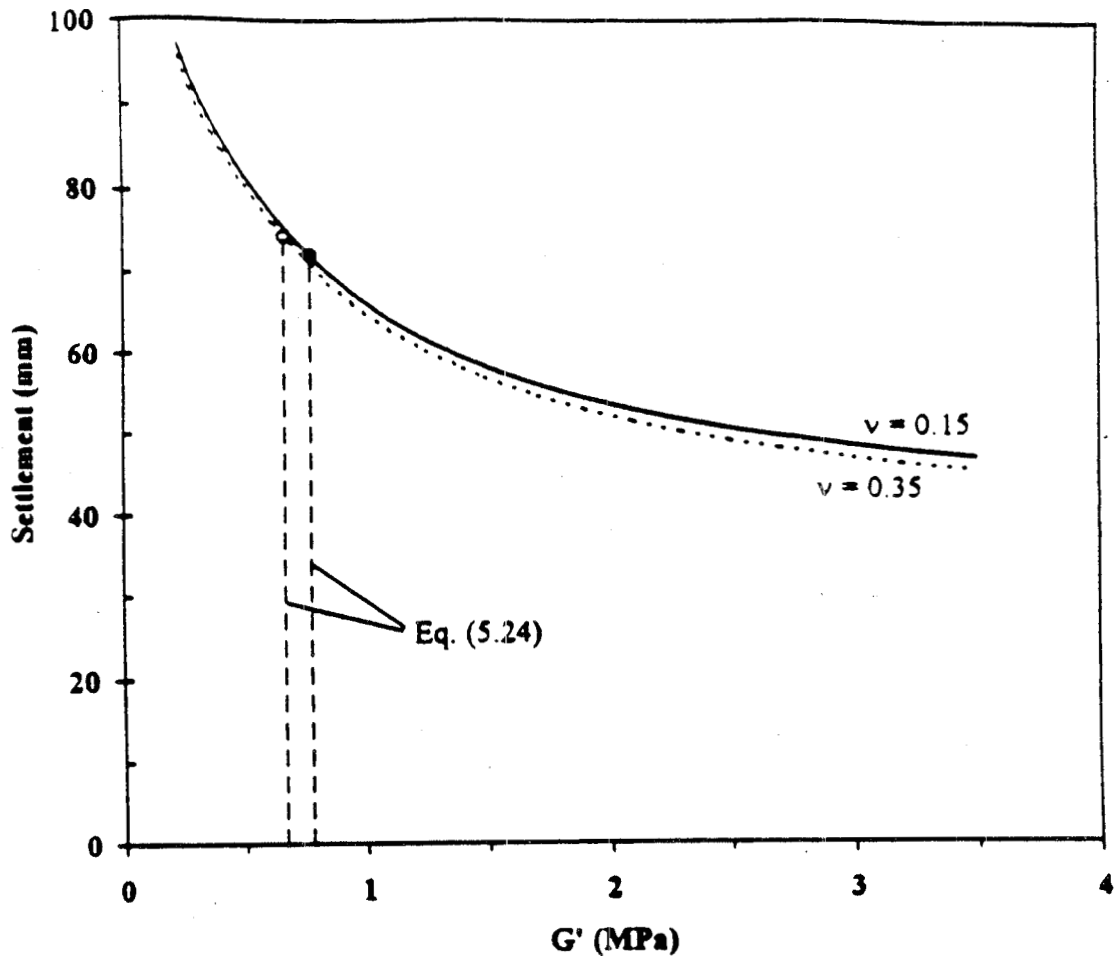


Fig. 5.16. Settlement as a function of G'

Table 5.6. Results of Settlement Analysis, Isotropic Material

2-Layer System

	E_i (MPa)	ν_i	Settlement (mm)
Sets 1a and 1b	1.95	0.26	79.2
Sets 1c and 1d	1.75	0.31	85.2
Sets 2a and 2b	0.76	0.21	208
Sets 2c and 2d	0.72	0.25	215

4-Layer System

	E_i	ν_i	Settlement (mm)
Sets 1a and 1b	1.95	0.26	1.99
Sets 1c and 1d	1.75	0.31	2.03
Sets 2a and 2b	0.76	0.21	2.73
Sets 2c and 2d	0.72	0.25	2.75

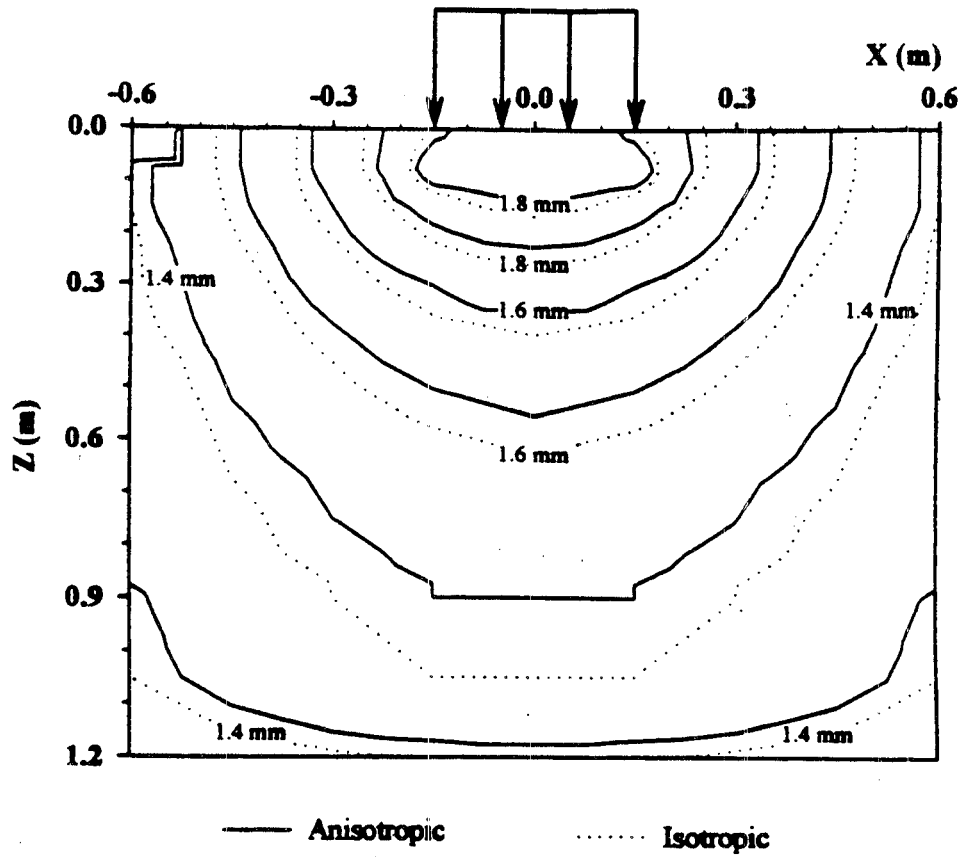


Fig. 5.17. Settlement isolines - vertical component of displacement

may be acceptable considering that no road will be constructed with an exposed layer of shredded tires. In the 4-layer case, the most unconservative value of settlement is 7.4% for the isotropic fill, and can very well be regarded as negligible for design purposes when measured against the error involved in the analysis. Thus, the assumption of isotropic elasticity in current settlement analysis of shredded tire fills seems to be validated for the layer cases studied. In other words, consideration of the anisotropic properties of material consisting of large-size pieces may be unnecessary for practical purposes. However, only two test cases were investigated using a limited number of parameters, and further studies should be conducted.

A more detailed analysis of anisotropic parameters of shredded tires is given in Heimdahl and Drescher (1999).

CHAPTER 6

CONCLUSIONS AND RECOMMENDATIONS

CONCLUSIONS

Based on the experiments that were conducted in this project and the subsequent analyses of results, the following conclusions can be made:

Behavior Under Repeated Load

1. Compression tests were conducted on small-size (50 mm (2 in.)) shredded tires. The confining conditions imposed in constrained and unconstrained tests were selected to provide lower and upper bounds to settlements of a fill, respectively. Samples were first compacted, and then subjected to cyclic load, with typical maximum stresses of about 90 kPa and 130 kPa (13 and 19 psi) in the unconstrained and constrained compression tests, respectively. In tests on both constrained and unconstrained samples, the material exhibited a non-linear response to load, such that the material became stiffer with increasing stress.
2. Shredded tire material under constrained compression, in general, undergoes less plastic strain per cycle with successive load cycles, ranging from 8% strain for the first cycle to 0.03% strain for the 80th cycle. A similar trend is observed for the first 5 to 10 cycles of load in unconstrained compression tests. Generally, plastic strain is less in tests performed on constrained samples. For load cycles 12 through 20, the average

plastic strain per cycle was about 6 times higher for unconstrained compression tests than that found for constrained compression tests.

3. Primarily due to the effects of creep, using a slower loading rate in repeated load tests will, in general, cause more strain for a given load than if a faster rate were used.
4. The master curve for constrained compression tests, which results from eliminating the effect of wall friction, indicates that constrained material is stiffer than that found in unconstrained compression tests, where the master curve accounts for the effects of plate friction. Again, these curves should provide lower and upper bounds to settlements of a fill for the loading range selected.

Behavior Under Constant Load

1. In creep tests, compacted samples of small-size (50 mm (2 in.)) shredded tire pieces were subjected to constant loading in both constrained and unconstrained conditions similar to those used for the repeated load tests. Stresses in tests on unconstrained material ranged from 28 to 70 kPa (4.0 to 10 psi) and on constrained material ranged from 48 to 97 kPa (7.0 to 14 psi). Based on the results of these tests, it was determined that the material exhibits progressive yet sharply decreasing creep settlement with time in both constrained and unconstrained confining cases.
2. The creep settlement that occurred in constrained tests averaged 0.02% strain per week for the period 60-630 days after loading, which is less than that in unconstrained tests, where settlement averaged 0.033% per week. As in the repeated load tests, but

with regard to creep settlement, the results of the creep tests for the constrained and unconstrained tests should provide lower and upper bounds to settlements of a fill.

3. By assuming a constant rate of creep for the period 60-630 days after application of load, settlements in the shredded tire layer of a representative embankment fill can be predicted. Material in the center of the embankment will settle about 4 cm (1.6 in) in one year, and material near the edge of the fill will settle about 6 cm (2.3 in) per year for a layer of shredded tires 4.4 m thick.

Anisotropic Properties

1. Anisotropy tests were conducted on masses of large-size (200 mm (8 in.)) shredded tire pieces in which the material was placed in overlapping layers, compacted, and subjected to load in two directions. Tests were performed on material under simulated overburden stresses of about 52 kPa (7.5 psi) parallel to the layers and 24 kPa (3.5 psi) perpendicular to the layers. Stress increments ranged from 21 to 48 kPa (3.0 to 7.0 psi). Neglecting the viscoelasticity of the material and assuming that the masses of shredded tires exhibit linear elastic anisotropic-transversely isotropic properties, material parameters were calculated. From these calculations, it was found that compacted shredded tire material exhibits mechanical anisotropy, as evidenced by a horizontal modulus that is 2-3 times the vertical modulus. The in-plane and out-of-plane Poisson's ratios also appear to differ, but to an extent that is not discernable from tests.

2. A numerical analysis using the code CIRCLY was performed to compare elastic settlements of a fill comprised of a layer of anisotropic shredded tire material with those of a fill with a shredded tire layer regarded as isotropic. Two cases of fills were considered: a) shredded tires overlying a soft soil layer and b) pavement and overburden soil situated above the shredded tires and soft soil in the first case. As a general observation, the vertical Young's modulus had the greatest influence on the settlements of fills.
3. For the case in which pavement and soil lie above the shredded tires, it was found that the difference in maximum settlements of an anisotropic fill and one considered isotropic is relatively small. Results for the case in which the shredded tire layer surface is exposed to the applied load indicate that, for practical purposes, little difference exists between these maximum settlements. Thus, if roads are designed on the basis of maximum settlement under single-axle traffic loads, the current assumption of isotropic shredded tire material appears to be valid.

RECOMMENDATIONS

1. The existence of creep in shredded tire fills should be accounted for in the design of roads and embankments. The growth of constrained and unconstrained creep settlements can be approximated by power law relationships as seen in figures 4.7 and 4.8. In unconstrained conditions the strains are approximately two times larger than constrained conditions (Fig. 4.6).
2. The settlement due to creep may be considered negligible after a period of two years subsequent to loading (Fig. 4.9).
3. The design of roads utilizing shredded tire fills should follow the existing elastic, isotropic design procedures. The anisotropic properties of the material may be regarded as inconsequential in design. Therefore, currently used layered-elastic computer programs such as WESLEA or ELSYM5 may be used to predict settlement in designs incorporating shredded tire fills.

REFERENCES

- Beatty, J.R., "Physical Properties of Rubber Compounds", *Mechanics of Pneumatic Tires*, S.K. Clark, ed., United States Department of Transportation, National Highway Traffic Administration, Washington, D.C., 1981.
- Bosscher, P.J., Edil, T.B., and Eldin, N.N., "Construction and Performance of a Shredded Waste Tire Test Embankment", *Transp. Res. Rec. No .1345*, 44-52, Transportation Research Board, Washington, D.C., 1992.
- Bosscher, P.J., Edil, T.B., and Kuraoka, S., "Design of Highway Embankments Using Tire Chips", *J.Geot.Geoenv.Eng. ASCE*, Vol. 123, No. 4, 295-304, 1997.
- Das, B.M., "Principles of Geotechnical Engineering", Third Edition, PWS Publishing Co., Boston, 1994.
- Das, B.M., "Principles of Foundation Engineering", Third Edition, PWS Publishing Co., New York, 1995.
- Drescher, A., and Newcomb, D., "Development of Design Guidelines for Use of Shredded Tires as a Lightweight Fill in Road Subgrade and Retaining Walls", Mn/DOT, Report MN/Rc-94/04, 1994.
- Edil, T.B., and Bosscher, P.J., "Development of Engineering Criteria for Shredded Waste Tires in Highway Applications", Research Report GT-92-9, Wisconsin Department of Transportation, Madison, WI, September 1992.
- Geisler, E., Cody, W.K., and Nieme, M.K., "Tires for Subgrade Support," Presented at the Annual Conference on Forest Engineering, Coeur D'Alene, Aug. 1989.
- Heimdahl, T., and Drescher, A., "Deformability Parameters of Shredded Tire Lightweight Fills", Proceedings of the 9th International Conference on Cold Regions Engineering, Duluth, MN, 1998.
- Heimdahl, T., and Drescher, A., "Elastic Anisotropy of Tire Shreds", *J.Geot.Geoenv.Eng. ASCE*, (in print).
- Humphrey, D.N., and Nickels, W.L. Jr., "Tire Chips as Subgrade Insulation and Lightweight Fill", Presented at the: 18th Annual Meeting of the Asphalt Recycling and Reclaiming Association, Pompano Beach, Florida, February 1994.

Humphrey, D.N., and Sandford, T.C., "Tire Chips as Lightweight Subgrade Fill and Retaining Wall Backfill", Submitted to: Symposium on Recovery and Effective Reuse of Discarded Materials and By-Products for Construction of Highway Facilities, Denver, CO, October 19-22, 1993.

Humphrey, D.N., Sandford, T.C., Cribbs, M.M., Gharegrat, H.G., and Manion, W.P., "Tire Chips as Lightweight Backfill for Retaining Walls – Phase 1 (Draft), A Study for the New England Transportation Consortium, August 1992.

Lekhnitskii, S.G., "Theory of Elasticity of an Anisotropic Body", English Translation, Mir Publishers, Moscow, 1981.

Manion, W.P., and Humphrey, D.N., "Tire Chips as Lightweight and Conventional Embankment Fill, Phase 1-Laboratory", A Study for the Maine Dept. of Transportation, 1992.

Minnesota Pollution Control Agency, "Environmental Study of the Use of Shredded Waste Tires for Roadway Sub-grade Support", by Twin City Testing Corp., St. Paul, MN, for Andy Ronchak, Waste Tire Management Unit, Site Response Section, Groundwater and Solid Waste Division, Minnesota Pollution Control Agency, St. Paul, MN, 1990.

National Asphalt Pavement Association, "Scrap Tire Utilization Technologies", February 1993.

Newcomb, D.E., and Drescher, A., "Engineering Properties of Shredded Tires in Lightweight Fill Applications", *Transp.Res.Rec.*, 1437, 1-7, National Academy Press, Washington, DC, 1994.

Read, J., Dodson, T., and Thomas, J., "Experimental Project Use of Shredded Tires for Lightweight Fill", Oregon Department of Transportation, Prepared for Federal Highway Administration, Washington, DC, February 1991.

Soupir, S.P., "Use of Alternative Backfill Designs for Integral Abutment Bridge End Treatment", Proceedings of the 46th Annual Geotechnical Engineering Conference, St. Paul, MN, 1998.

Upton, R.J., Thomas, J., and Kobernik, R., "Experimental Project Use of Shredded Tires for Lightweight Fill", FHWA Experimental Project No. 1, DTFH-71-90-501-OR-11, Final Monitoring Report, Oregon Department of Transportation, Prepared for Federal Highway Administration, Washington, DC, September 1992.

Wardle, L.J., "Program CIRCLY - A Computer Program for the Analysis of Multiple Complex Circular Loads on Layered Anisotropic Media - User's Manual", Geomechanics Computer Program No. 2, CSIRO Division of Applied Geomechanics, 1976.

Wu, W.Y., Benda, C.C., and Cauley, R.F., "Triaxial Determination of Shear Strength of Tire Chips", *J. of Geotech. and Geoenv. Engrg., ASCE*, Vol. 123, No. 5, May 1997.



Office of Research Services
395 John Ireland Blvd., Mail Stop 330
Saint Paul, Minnesota 55155



(651) 282-2274